SYNTHESIS AND PHOTOCHEMISTRY OF PT(IV) HYDROXO COMPLEXES

A Dissertation

presented to

the Faculty of the Graduate School

at the University of Missouri – Columbia

In Partial Fulfillment

of the Requirements for the Degree

Doctor of Philosophy

---

by

LASANTHA ANURANGANA WICKRAMASINGHE

Prof. PAUL R. SHARP, Dissertation Supervisor

May 2015

The undersigned, appointed by the dean of the Graduate School, have examined the dissertation entitled

SYNTHESIS AND PHOTOCHEMISTRY OF PT(IV) HYDROXO COMPLEXES

presented by Lasantha A Wickramasinghe,

a candidate for the degree of doctor of philosophy,

and hereby certify that, in their opinion, it is worthy of acceptance.

Prof. Paul R. Sharp

Prof. Timothy E Glass

Prof. Justin R. Walensky

Prof. Sheila Baker

To my dear academic parents

who encouraged me throughout my life

ACKNOWLEDGEMENTS

I wish to express my gratitude to Prof. Paul. R. Sharp. I would wholeheartedly thank him for giving me an opportunity to become one of this graduate students. Since I met Prof. Sharp in Sri Lanka, I have been given enormous support and the guidance to uplift my carrier in science. His notable enthusiasm in science and research inspired me to picture myself as a future scientist. He helped us throughout these years by making himself always availability for discussions and learning. Thank you very much for supporting me with research assistantship.

I would like to thank all my thesis committee membsers; Prof. Timothy E Glass, Prof. Justin R. Walensky and Prof. Sheila Baker for their guidance and useful ideas. Thank you very much for giving your precious time for discussions and feedback. The support and the guidance you all and Prof. Sharp gave me on my future carrier is highly appreciated.

I am also thankful to Dr. Charles Barnes X-ray crystallography for obtaining numerous crystal structures and giving me opportunity to learn X-ray crystallography. I am also thankful to Dr. Wei Wycoff NMR support and her guidance. I am very grateful to the Department of Chemistry and the University of Missouri-Columbia for giving me this great opportunity to peruse my graduate studies in a wonderful research atmosphere. Among others, I'd like to thank present and former Sharp group members, Dr. Robert Robinson, Dr. Morgan Moody, Dr. Malathi Nandita Weliange, Dr. Alice Raphael, Dr. Andreas Ross, Tharushi Perera, Lakshmi Nilakantan and Yang Li for their friendship and support.

Above all I would like to thank my family and friends, finally my loving wife Thameesha and son Oneth for their patients and dedication. At last I would like to pay my heartfelt gratitude to every single advice be given in my life.

TABLE OF CONTENTS

LIST OF TABLES

LIST OF FIGURES

LIST OF SCHEMES

ABBREVIATIONS

TPP	*meso*-tetraohenylporphyrin

TME	2,3-dimethyl-2-butene
DF	2,5-dimethylfuran
SET	single-electron transfer
MeTHF	2-methyltetrahydrofuran
THF	Tetrahydrofuran
CH_2Cl_2	Methylene chloride
tft	trifluoromethylphenyl
DFT	Density Functional Theory
TDDFT	Time-Dependent Density Functional Theory
NTO	Natural Transition Orbitals
PCM	Polarizable Continuum Model
hν	Photon
UV-Vis	Ultraviolet-visible
DOSY	Diffusion-Ordered Spectroscopy

LIST OF COMPLEXES

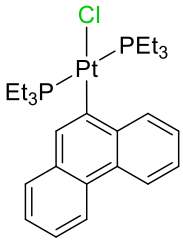

1

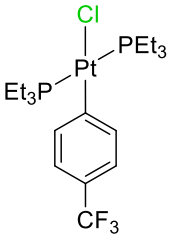

2

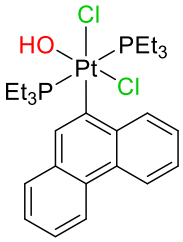

3

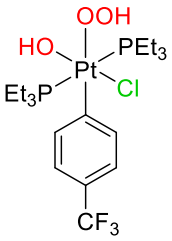

4

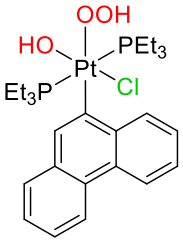

5

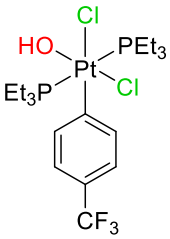

6

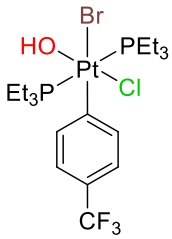

7

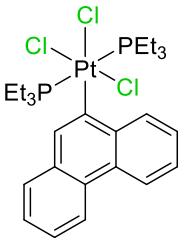

8

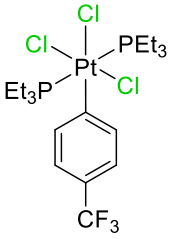

9

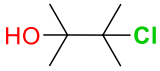

10

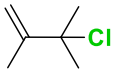

11

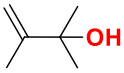

12

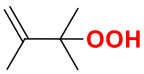

13

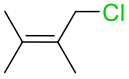

14

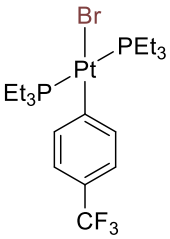

15

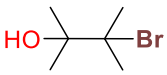

16

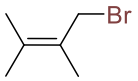

17

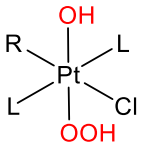

18

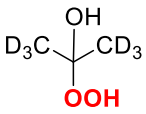

19

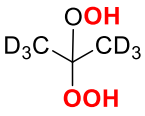

20

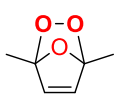

21

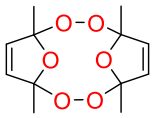

22

23

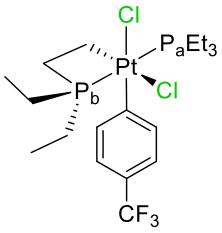

24

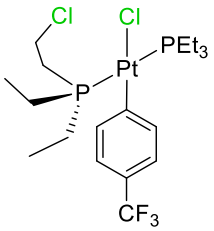

25

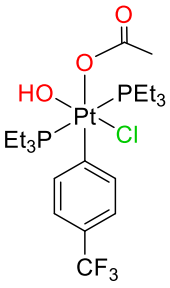

26

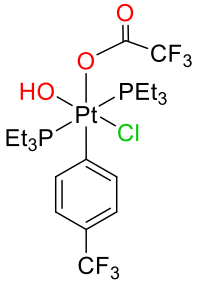

27

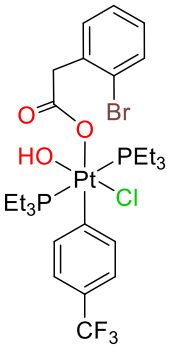

28

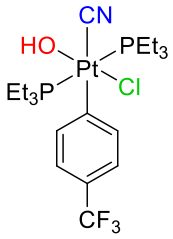

29

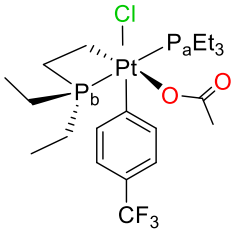

30

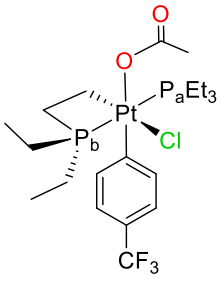

30'

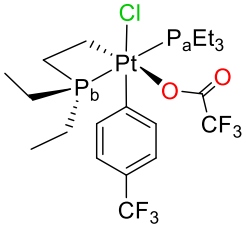

31

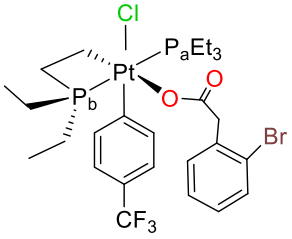

32

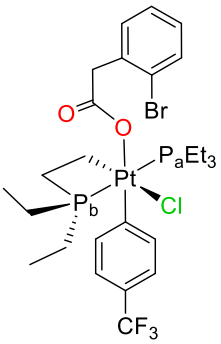

32'

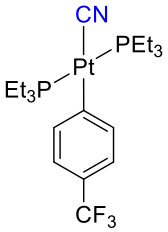

33

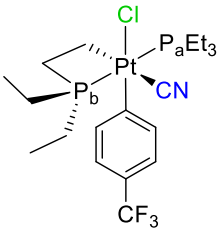

34

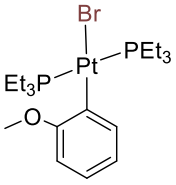

35

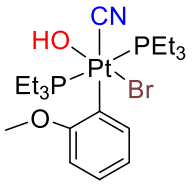

36

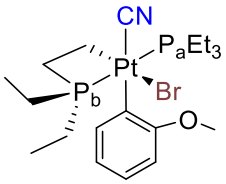

37

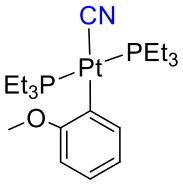

38

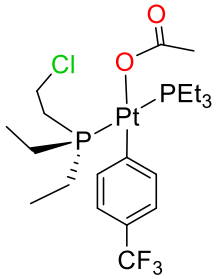

39

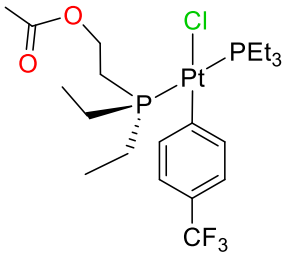

40

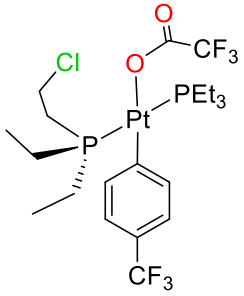

41

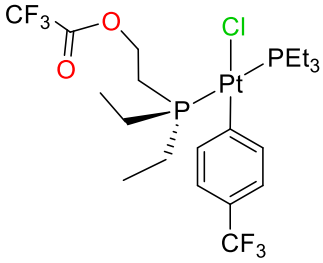

42

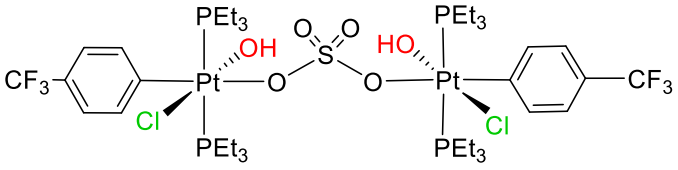

43

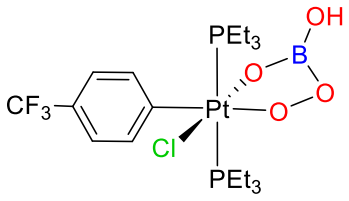

44

LIST OF COMPUTATIONAL MODEL COMPLEXES

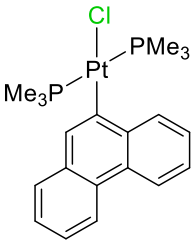

1'

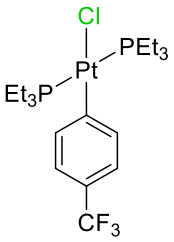

2'

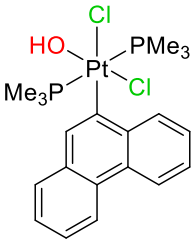

3'

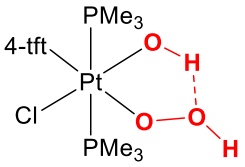

4a'

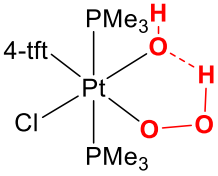

4b'

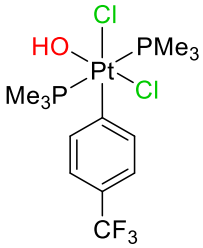

6'

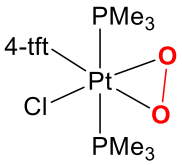

9'

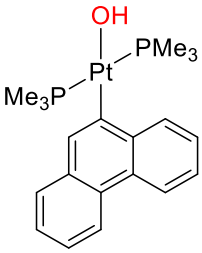

18'

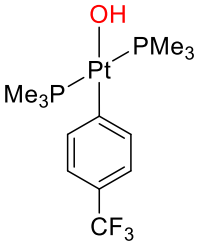

19'

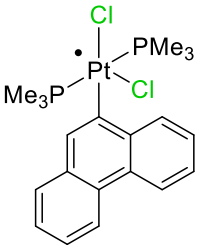

20'

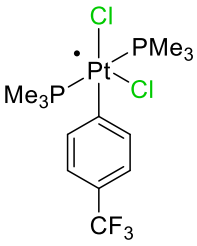

21'

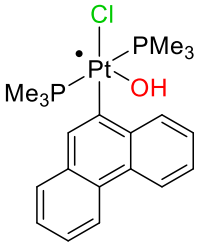

22'

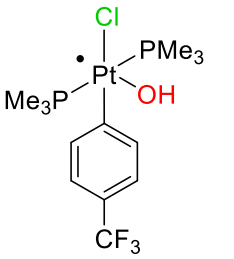

23'

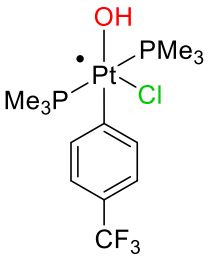

23a'

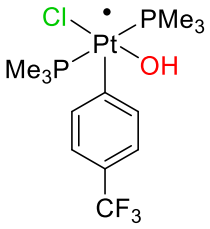

23b'

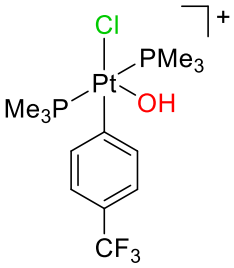

24'

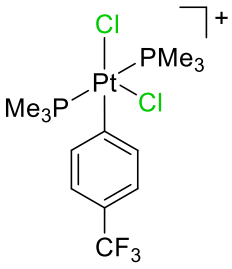

25'

SYNTHESIS AND PHOTOCHEMISTRY OF PT(IV) HYDROXO COMPLEXES

Lasantha A Wickramasinghe

Prof. Paul R. Sharp, Dissertation Supervisor

ABSTRACT

Global energy consumption and the production of clean renewable energy have become greater challenges. Sunlight-induced splitting of water into H_2 and O_2 is one of the leading strategies to achieve clean and renewable energy. Transition metal photochemistry has considerable potential for making this task more viable. Along with water splitting, hydrohalic acid (HX) splitting is being thoroughly investigated. HX splitting is a more facile two electron process whereas water splitting is a relatively difficult four electron oxidation process. Light driven HX splitting and endergonic elimination of X_2 (Br_2 and Cl_2) have received more attention as a potentially more economical and promising solar energy conversion process than water splitting.

Apart from Br_2 or Cl_2 elimination, hydrogen peroxide elimination is of interest and the synthesis of Pt(IV)-dihydroxo complexes was attempted. Concentrated hydrogen peroxide addition to *trans*-$Pt(PEt_3)_2ClR$ yielded hyroxo-hydroperoxo complexes trans-$Pt(IV)Cl(OH)(OOH)R(PEt_3)_2$ [**5** (R = 9-phenanthryl), **4** (R = 4-tft)]. Complex **5** is unstable and reacts with solvent CH_2Cl_2 to give *trans,cis*-$Pt(PEt_3)_2(Cl)_2$(OH)(9-phenanthryl) (**3**). Protonation of OOH ligand in **4** by HCl gives *trans,cis*-$Pt(PEt_3)_2(Cl)_2$(OH)(4-tft) (**6**) and HBr gives analogous *trans*-$Pt(PEt_3)_2$(Br)(Cl)(OH)(4-tft) (**7**). The characterization of above complexes was done by NMR spectroscopy and X-ray crystallography. Photoelimination of hypohalous acid was studied in detail along with

DFT and TDDFT calculations. Direct detection of HOCl was not successful. Photolysis of **3** or **6** at 313 or 380 nm in the presence of 2,3-dimethyl-2-butene (TME) yields the chlorohydrin (2-chloro-2,3-dimethyl-3-butanol), 3-chloro-2,3-dimethyl-1-butene, and acetone. Expected products from HOCl trapping in TME were tested separately using an authentic sample of HOCl. The results obtain from photolysis of **7** are consistent with cis elimination of HOBr and bromohydrin is detected from the TME reaction. Computational studies of related model complexes suggest a dissociative triplet excited state reaction pathway leading to HOCl elimination.

Photolysis (380 nm) of **4** at -78℃ in acetone-d_6 or toluene-d_8 yields HOOOH (16-20%) and *trans*-$Pt(PEt_3)_2Cl(4\text{-tft})$ (**2**). The direct detection of HOOOH is done by ^1H NMR spectroscopy. Several other products are observed in acetone-d_6; H_2O_2, $(CD_3)_2C(OH)(OOH)$ and $(CD_3)_2C(OOH)_2$. Thermal decomposition or room temperature photolysis gives **2**, O_2 (not detected) and water. 2,5-dimethylfuran is used as a reagent for chemical detection of $^1O_2$. Thermodynamics and kinetics were studied for the thermal decomposition reaction of **4**. Computational studies indicate the importance of intramolecular hydrogen-bonding which may control the photolysis and thermolysis pathways.

Photolysis of **6** at 77 K in 2-methyltetrahydrofuran gives platinum(III), hydroxo radical and emission from a triplet excited state. The triplet emission is further confirmed by emission lifetime (phosphorescence) and λ_{max} comparable to the calculated triplet energy. The photolysis in toluene gives benzyl radical via OH radical mediated hydrogen atom abstraction. Warming the photolyzed solutions of **6** gives phospha-platinacycle *trans*-$Pt(CH_2CH_2PEt_2)(PEt_3)Cl_2(4\text{-tft})$ (**24**) by hydrogen atom abstraction from PEt_3, where

abstraction possibly occurs at 77 K. The complex 24 undergoes thermal reductive elimination at room temperature or photolytic reductive elimination even at 77 K.

Reactions of carboxylic acids with the OOH ligand in **4** gives Pt(IV)hydroxo-carboxylate complexes *trans*-$Pt(PEt_3)_2(Cl)(OH)(X)(4\text{-tft})$ [**26** (X = acetate), **27** (X = trifluoroacetate) and **28** (X = 2-bromophenylacetate)]. These complexes introduce strong hydrogen bonding between the hydroxo and carboxylate ligands. Photolysis of the carboxylate complexes at room temperature gives phospha-platinacycles analogous to **24** in high yield. DFT calculations showing much shorter hydrogen bonding in the triplet excited state suggest photo-generated hydroxyl radicals are tethered and directed to a hydrogen atom abstraction from the PEt_3 group.

CHAPTER 1: INTRODUCTION

1.1 Importance of solar energy.

Photosynthesis is one of the most important chemical processes to sustain and balance life on earth. In this process, plants capture radiant energy (solar energy) to convert carbon dioxide and water from the environment to glucose (food) while giving off oxygen as a byproduct.[1] The vast expanses of forest coverage helps to harness solar energy in order to sustain the life we claim. Solar energy is a renewable and continuous source of energy on earth. Thus, it has caught more attention than other renewable energy sources such as wind and ocean wave power.[2] However, global energy consumption and the production of clean renewable energy have become a great challenge to every single nation.[3] Environmental concerns such as emission of CO_2 and other pollutants by fossil fuel combustion also drives us towards finding renewable energy sources. As a result, modern day scientists have put their thoughts on the viable use of solar energy in the field of science.[4]

The use of photovoltaics (solar panels) to generate electricity is one of the modern applications of solar energy.[5] Moreover, conversion of solar energy into more productive form via storing it in chemical bonding has been considered as the key to achieve the goal of renewable energy.[6] Sunlight induced (photocatalytic) splitting of water into molecular hydrogen (H_2) and oxygen (O_2) has been studied extensively.[7,8] Recombination of H_2 and O_2 can be implemented in a fuel cell generating thermal or electrical energy. Water splitting is a difficult and complex four-electron four-proton process. In contrast,

hydrogen halide (HCl and HBr) splitting has been highlighted as a much simpler two-electron two-proton process. The knowledge gained from such adaptable systems can be readily used in the development of this chemistry.

1.2 Relevance of transition metal photochemistry.

In recent years transition metal photochemistry has received a lot of attention toward the development of efficient photocatalysts suitable for water/HX splitting. Synthesis and photochemistry of mono and bi metallic complexes of late transition metals have been rewarded towards the development of photocatalysts.[9,10] Theoretical studies involving computational modelling have been extensively used along with experimental data to understand the mechanistic and thermodynamic behavior.[8] Density functional theory (DFT) calculations could be highly acknowledged in transition metal photochemistry for their contribution. DFT calculations have been used extensively to look at the transition states and their properties such as electronics and thermodynamics pertaining to redox reactions.[11,12]

In the field of transition metal chemistry, reductive elimination has been well explored and understood for many years. When reductive elimination is induced by absorption of a photon this can be termed as photo reductive elimination or more simply photoelimination (eq 1). If elimination is endergonic the photoelimination process accomplishes conversion and storage of solar energy into chemical bonds.

$$L_nM(Y)(X) \xrightarrow{h\nu} L_nM + Y\text{-}X \qquad \text{eq 1}$$

Photoelimination of a strong oxidant (Y-X) has a higher propensity toward facile re-oxidation or recombination. Such re-oxidation is crucial for engineering such systems to accomplish effective storage of solar energy. Photocatalytic conversion of HX (X= Cl, Br or OH) into H_2 and elimination of X_2 (Cl_2, Br_2 or H_2O_2) is illustrated in Scheme 1.2.1. The HX based photoelimination has a serious drawback due to recombination of X_2 (X= a halogen) with the reduced catalyst as opposed to H_2O_2 photoelimination as H_2O_2 can decompose to O_2 and H_2O. A recent paper by Milstein and co-workers provides insight for splitting of water into H_2 and O_2 in the presence of light[13]. With an outstanding enthusiasm Sharp group has discovered ample amount of information regarding the key step in the proposed catalytic cycle. Findings of molecular bromine and chlorine photoelimination were reported after extensive studies.[11,12,14] In our studies, we have further focused on the synthesis of novel mononuclear Pt(IV)-hydroxo complexes and photoelimination of hydrogen peroxide (H_2O_2) and hypochlorous acid (Scheme 1.2.1(b)). The catalytic cycle shown in Scheme 1.2.1(b) is a modification of the HX splitting cycle proposed previously (Scheme 1.2.1 (a))[9].

Scheme 1.2.1. Potential catalytic cycle for HX splitting; (a) general splitting cycle, (b) cycle for hypohalous acid (HOX) and hydrogen peroxide (H_2O_2) elimination.

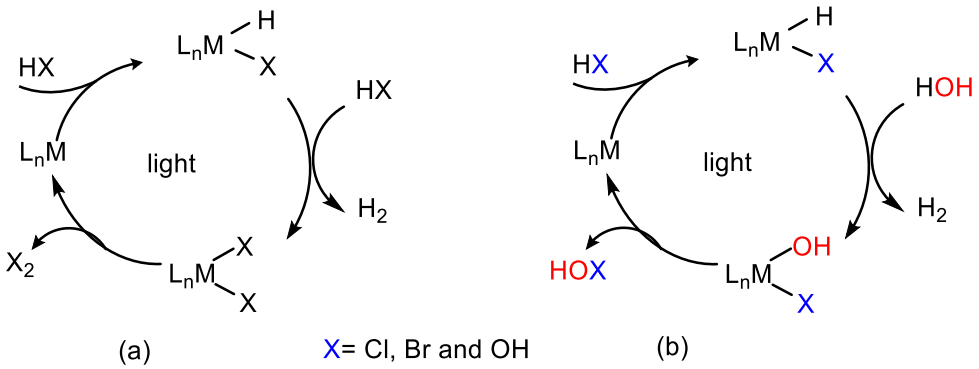

Few instances of oxidative addition of water to metal complexes are reported.[15] However, such oxidative addition of water to Pt(II) is not being reported up to date. Primarily we were interested in synthesis of Pt(IV)-dihydroxo complexes which can be applied in studies of H_2O_2 photoelimination. In addition, regeneration of catalyst via clean photoelimination of a single molecule such as H_2O_2 from a light induced excited metal complex is one of the underlying concerns. Behavior of an excited higher oxidation state metal complex is always hard to predict. For an instance, attempted net Cl_2/Br_2 photoelimination studies from triphos iridium(III) halide complexes have shown undesirable triphos arm dissociation leading to the formation of various iridium complexes (Scheme 1.2.2)[14].

Scheme 1.2.2. Tripos arm dissociation from photolysis of triphos iridium(III) halide

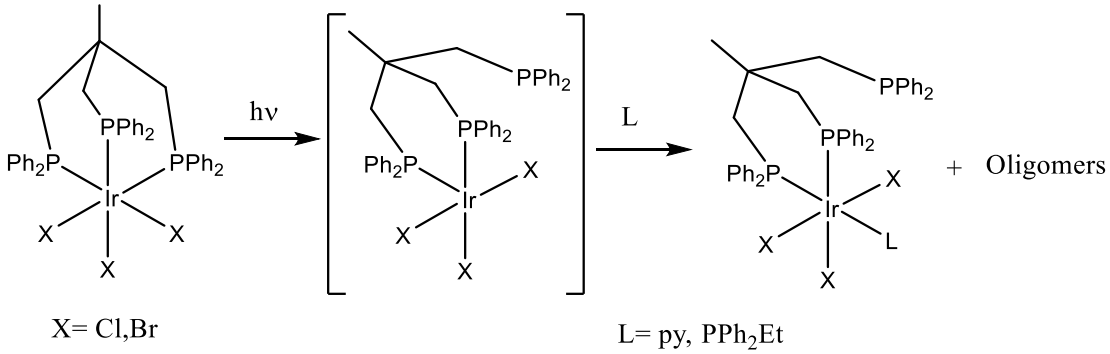

X= Cl,Br

L= py, PPh_2Et

Regeneration of a catalyst under photolysis does not always guarantee molecular photoelimination. Photoreduction of an excited state metal complex may be facilitated by foreign agents like reactive solvents or unsaturated hydrocarbons. Specially in the case of initial dissociation of a radical species which can be captured by unsaturated hydrocarbons making the photoreduction still favorable[12]. Scheme 1.2.3, shown below,

explains the possibility of such photoreduction and the involvement of halogen traps. Photoelimination does not occur in the absence of the traps implies a fast recombination of dissociated Br radical or direct reaction of the trap with the excited metal complex causing photo-reduction.[11] Photochemistry observed with our Pt(IV)hydroxo complexes exhibited diversity in chemical reactivity such as C–H activation and metal–carbon bond formation along with HOX elimination. Photochemistry of Pt(IV)hydroxo-halide complexes yielded net hypohalous acid elimination. Pt(IV)hydroxo complexes (discussed in later) are photoactive even in the absence of unsaturated hydrocarbons. Most surprisingly, photoelimination of dihydrogen trioxide (HOOOH) is observed from a Pt(IV)hydroxo-hydroperoxo complex. Furthermore, observation of C–H activation by hydroxo radical and metal-carbon bond formation creates an opportunity to explore and understand the chemistry of hyroxo radical in various environments. In order to design an ideal photocatalyst for HX/water splitting it is important to understand the salient features belong to this type of photocatalysis.

Scheme 1.2.3. Photoreduction of trans-Pt(IV)(PEt3)2Br3(1-Nap)

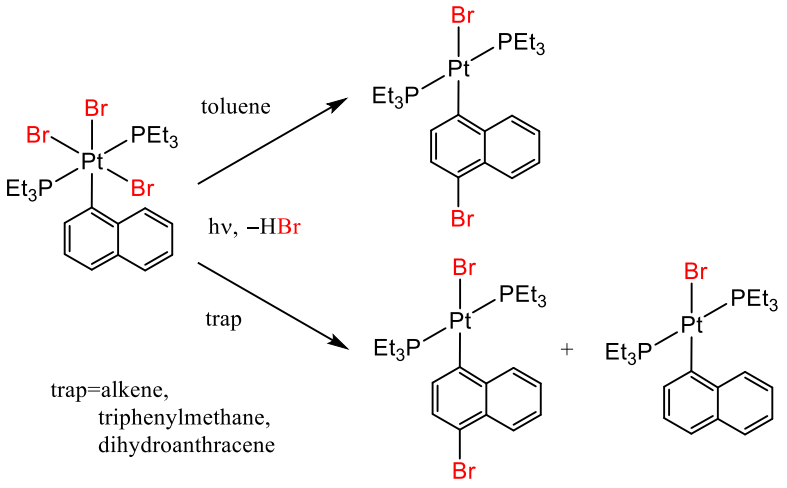

1.3 Chemistry of Platinum(IV)-hydroxo complexes.

Pt(IV) hydroxo complexes have been previously prepared mainly by oxidative addition of H_2O_2.[16] A number of di, tri, and tetra hydroxo Pt(IV) complexes can be found in peroxide mediated synthesis.[17] In general, the oxidative addition to Pt(II) yields *trans* dihydroxo complexes.[18] A detail mechanism is discussed in Chapter 2. However, an instance of *cis* oxidative addition was also found in a previous report where, the role of hydrogen bonding to stabilize the *cis* configuration was highlighted (Scheme 1.3.1).[19] Substituting the two -NH_2 groups on the 2,2′–bipyridine with either –CH_3 or –H did not yield a cis configuration indicating the role of hydrogen bonding in the *cis* addition.

Scheme 1.3.1. Formation of cis-dihydroxo Pt(IV) with the aid of hydrogen bonding.

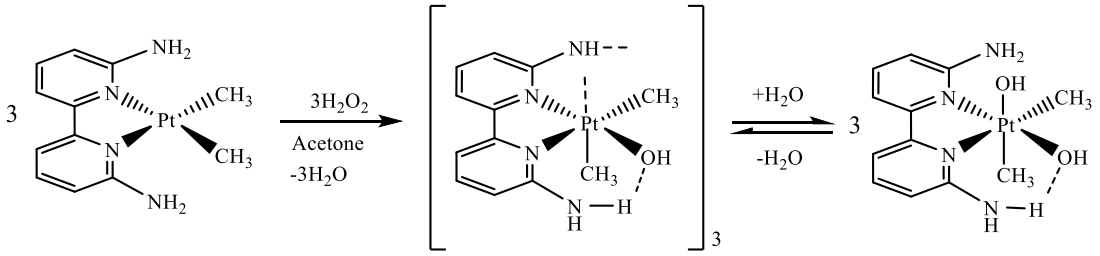

The use of O_2 as an oxidant in the presence of polar protic solvents such as methanol has been employed in the oxidation of Pt(II) to Pt(IV) hydroxo and hydroperoxo complexes.[20,21] The oxidative addition of phthaloyl peroxide[18] also caught our attention (Scheme 1.3.2). In our work, we report the synthesis and photochemistry of Pt(IV) hydroxo-carboxylate complexes (discussed in chapter 4) which shows the importance of intramolecular hydrogen bonding in hydroxo radical chemistry. The type of complex shown in Scheme 1.3.2 is analogous to our system though there is no photochemistry reported on them.

Scheme 1.3.2. Pt(IV) hydroxo carboxylate complex from phthaloyl peroxide.

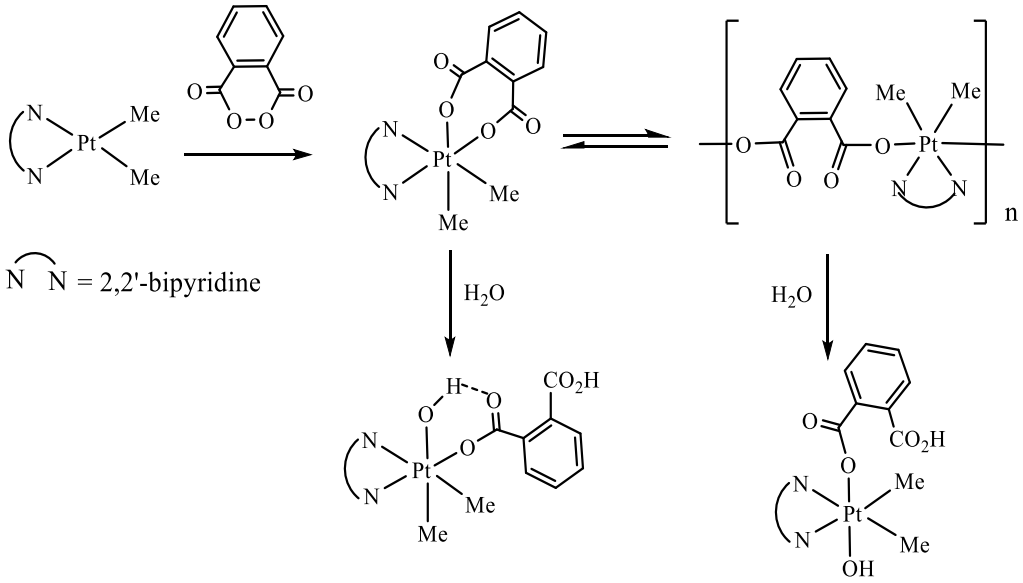

1.4 Chemistry of polyoxides (RO_nR).

Chemistry of polyoxides has not been explored and is not understood enough, though it could be highly potent in oxidation chemistry. A general formula for polyoxides can be given as RO_nR, (n > 2) where R stands for hydrogen, other atoms or alkyl/aryl groups. The simplest form of RO_nR is hydrogen peroxide (H_2O_2). Chemistry related to this simple molecule, H_2O_2 has been developed and utilized for centuries. Dihydrogen trioxide (H_2O_3) is the closest to H_2O_2 in this category. In contrast with H_2O_2, chemistry of H_2O_3 hasn't been thoroughly investigated until recently. Identification and characterization of H_2O_3 is relatively recent.[22] The existence of H_2O_3 was merely hypothetical for a long time. Studies in the early 1980s suggested H_2O_3 as a possible intermediate formed in low-temperature condensates obtained from electrodissociated hydrogen/oxygen mixture.[23] Antibody catalyze reactions of H_2O and $^1O_2$ were also believed to generate H_2O_3 as an intermediate leading to the final product of H_2O_2.[24]

However, development in this area of chemistry will surely rewrite the history of oxidation chemistry and their applications in subsequent fields such as pharmaceutical, atmospheric, environmental and biological chemistry.

H_2O_3 is less stable in solutions at room temperature, decomposing to water and singlet oxygen. Hence, synthesis and characterization need to be done at a low temperature (ex. -60℃). Characterization using ^1H and ^{17}O NMR spectroscopy has been reported in a series of organic solvents at low temperatures (around -65℃).[25] Observable chemical shift in ^1H NMR varied significantly with temperature. Laboratory synthesis of HOOOH can be mainly divided into three categories: (1) hydrogenation of ozone (O_3), and (2) decomposition of hydrotrioxides (ROOOH, R = $SiMe_3$) (Scheme 1.4.1).[25-26]

Scheme 1.4.1. Laboratory synthesis of H_2O_3.

(1) hydrogenation of ozone

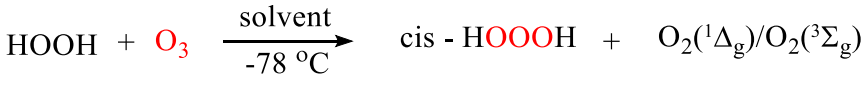

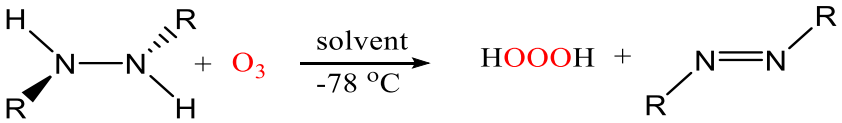

R= H, Me,Ph

(2) decomposition of hydrotrioxide

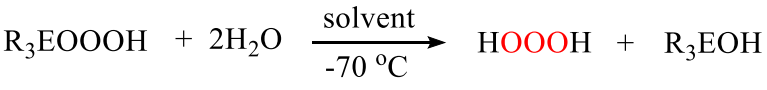

E = Si, Ge R = H, Me

1.5 Research summary.

Chemistry we describe later in chapter 2-4 will include various aspects of Pt(IV)hydroxo complexes. They are mainly in four categories; synthesis, characterization, photochemistry and computational modeling. We have been able to synthesize novel *trans*-Pt(IV)$(PEt_3)_2$(R)(OH)(X)(Y) (R=aryl; X=Cl, Br and Y= OOH, CN and acetate) complexes and study their photolchemistry. Photoelimination of HOCl and HOBr from *trans*-Pt(IV)$(PEt_3)_2$(R)(OH)$(X)_2$ complexes was studied extensively. Detection of hypohalous acid was attempted via chemical reactions such as alkene oxidation leading towards halohydrin formation. Direct detection was not successful due to instability of HOCl/HOBr in the presence of Pt species. First synthesis of Pt(IV)(OH)(OOH) complex and studies of dihydrogen trioxide (H_2O_3) photoelimination was accomplished. Direct identification of H_2O_3 was performed using ^{1}H NMR spectroscopy in two different solvent systems at low temperature (-60℃). Photolytic formation of H_2O_3 was further confirmed via chemical detection of singlet oxygen as one of its decomposition products.

Apart from conventional solution phase photolysis, frozen matrix photolysis were performed and an unusual phosphorescence (confirmed by lifetime measurement) and intramolecular C-H activation motivated us to investigate the behavior of OH radical in various systems. As an advancement of this chemistry, here we report the synthesis of *trans*-Pt(IV)$(PEt_3)_2$(R)(OH)(Cl)(acetate) analogues and intramolecular C-H activation observed in solution phase. This change can be attributed to the control gained via OH radical hydrogen bonding to the acetate ligand.

CHAPTER 2: PHOTOREDUCTION OF PLATINUM(IV) HALO-HYDROXO COMPLEXES

2.1 Introduction

Our group reported efficient molecular bromine photoelimination from the mononuclear Pt(IV) complexes *trans*-$Pt(PEt_3)_2(R)(Br)_3$ (R = Br, aromatic carbyl ligand).[11] These reactions suffer from back reaction of Br_2 with co-product, *trans*-$Pt(PEt_3)_2(R)(Br)$, and hence bromine traps must be added.[11] With the idea of H_2O_2, instead of Br_2, photoelimination we targeted to prepare the analogous dihydroxo complexes *trans*-$Pt(PEt_3)_2(R)(X)(OH)_2$ (X = Cl, Br). Simple oxidative addition of hydrogen peroxide to *trans*-$Pt(PEt_3)_2(R)(X)$ type complexes was aimed as a potential route for making dihydroxo complexes. Even though peroxide-assisted oxidation of Pt(II) with different R groups was achieved, the desired dihydroxo complexes were not observed, instead, we isolated monohydroxo complexes. While not the desired complexes, they are also highly photochemically active to net elimination, surprisingly of hypohalous acid (HOX, X = Cl, Br).[27] Their synthesis and photochemistry is reported herein.

2.2 Complex synthesis and characterization.

Pt(II) complexes *trans*-$Pt(PEt_3)_2Cl(R)$ [**1** (R = 9-phenanthryl), **2** (R = 4-trifluoromethylphenyl (4-tft)] are resistant to oxidation by hydrogen peroxide and solutions (CH_2Cl_2, THF, acetone) of the complexes remain unchanged when stirred with excess 30% aqueous hydrogen peroxide. However, slow oxidation does occur with concentrated diethyl ether solutions of hydrogen peroxide (Scheme 2.2.1). The reactions

are accompanied by extensive decomposition of the hydrogen peroxide and can require multiple additions to complete. The final product depends on the R group. With R = 9-phenanthryl, the product is *trans,cis*-Pt(PEt_3)$_2$(Cl)$_2$(OH)(9-phenanthryl) (**3**). The source of the additional chloride is unknown, but as the isolated yield (68%) exceeds 50%, at least a portion of the chloride must originate from the CH_2Cl_2 solvent. However, both bromo and chloro of *trans*-Pt(PEt_3)$_2$(2-trifluoromethylphenyl)(X) were not able to oxidize by H_2O_2 under above condition. It could be explained due to steric crowding cause by CF_3 group.

Scheme 2.2.1 Synthesis of Pt(IV) hydroxo complexes.

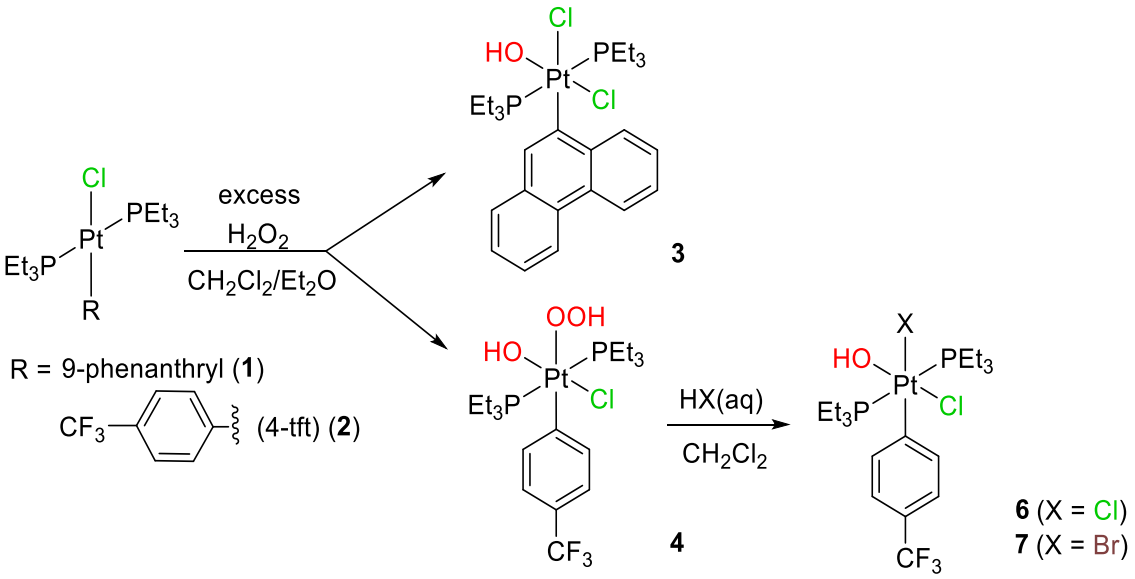

The reaction is more rapid with **2** than with **1**. However, the product is now the hydroxo-hydroperoxo complex *trans*-Pt(PEt_3)$_2$(Cl)(OH)(OOH)(4-tft) (**4**). Complex **4** is the first Pt(IV)-hydroxo-hydroperoxo to be observed. The NMR properties of **4** are similar to

those of an intermediate (**5**), observed in the preparation of **3** and assigned as the 9-phenanthryl analog of **4**. Complex **4** is readily converted to *trans,cis*-$Pt(PEt_3)_2(Cl)_2(OH)$(4-tft) (**6**), an analog of **3**, simply by the addition of aqueous HCl (X = Cl). The same reaction with HBr(aq) yields the mixed bromo-chloro-hydroxo complex *trans*-$Pt(PEt_3)_2$(Br)(Cl)(OH)(4-tft) (**7**).

Complexes **3**, **4**, **6**, and **7** gave crystals suitable for X-ray analysis. The solid-state structures of **3, 4** and **6** are shown in Figure 2.2.1, Figure 2.2.2 and Figure 2.2.3. Complex **7** is isomorphous and isostructural with **6** and also co-crystallized with ~20% **6** that was present as an impurity in the reaction mixture. Although the presence of a Br atom *trans* to the 4-trifluoromethylphenyl group is confirmed, the co-crystallization with **6** and disorder make the metrical parameters unreliable and the structure of **7** will not be discussed. Selected metrical parameters for the other complexes are listed in Table 2.2.1 and have been averaged where chemically equivalent parameters are present.

Complexes **3** and **4** crystallized as hydrogen-bonded dimers. In the case of **3**, the dimer is asymmetric and only one of the hydroxo-group hydrogen atoms participates in the hydrogen bonding. In contrast, a centrosymmetric dimer is observed for **4** and both the hydroxo and the hydroperoxo groups are involved in hydrogen bonding. However, only the hydroperoxo group participates in the intermolecular hydrogen bonding and forms a 6-membered ring through head-to-tail dimerization of the OOH group. Meanwhile, the hydroxo group is intramolecularly hydrogen bonded to the β-O of the hydroperoxo group. A similar hydrogen bonding arrangement is found in the dimer structure of Tp*Pt(OOH)$(CH_3)_2$ (Tp* = hydrotris(3,5-dimethylpyrazolyl)borate).[28]

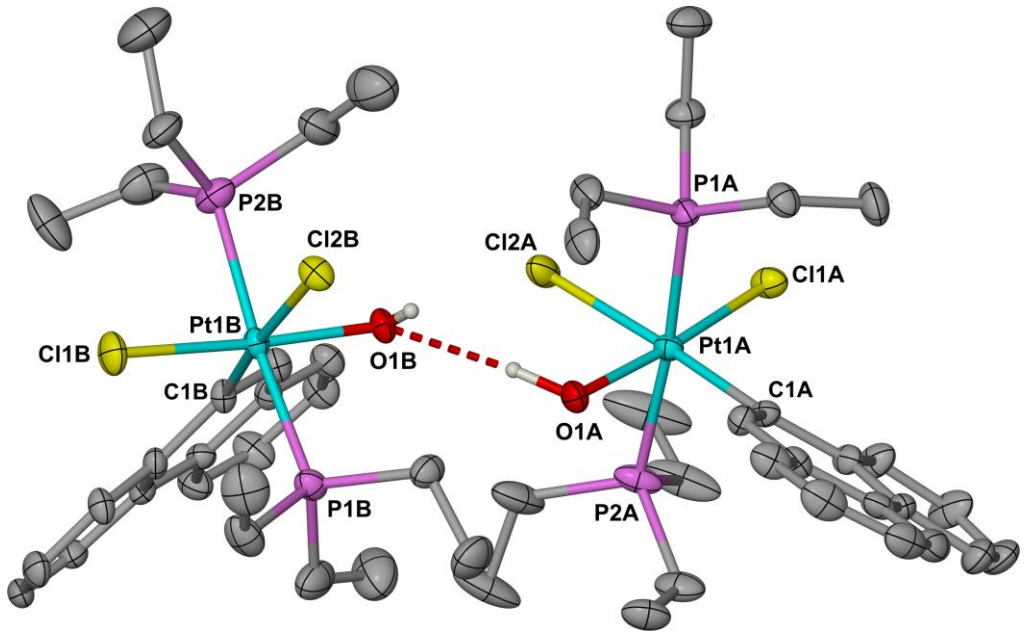

Figure 2.2.1. Solid-state structure of the hydrogen-bonded dimer of **3** (30% probability ellipsoids, hydrogen atoms omitted except for the OH-group hydrogen atoms which are represented as arbitrary spheres).

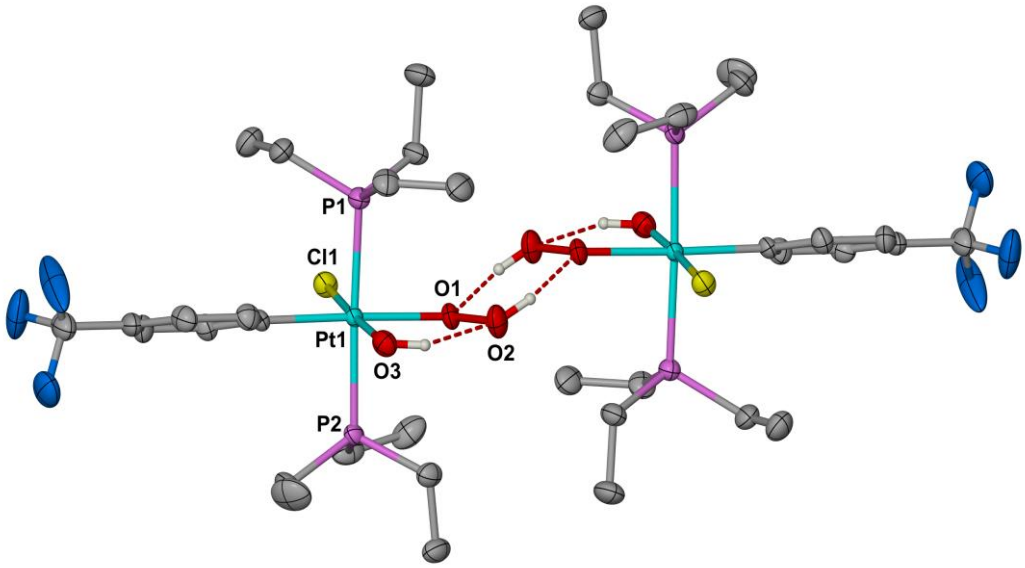

Figure 2.2.2. Solid-state structure of the centrosymmetric hydrogen bonded dimer of **4** (50% probability ellipsoids, hydrogen atoms omitted except for the OH and OOH group hydrogen atoms which are represented as arbitrary spheres).

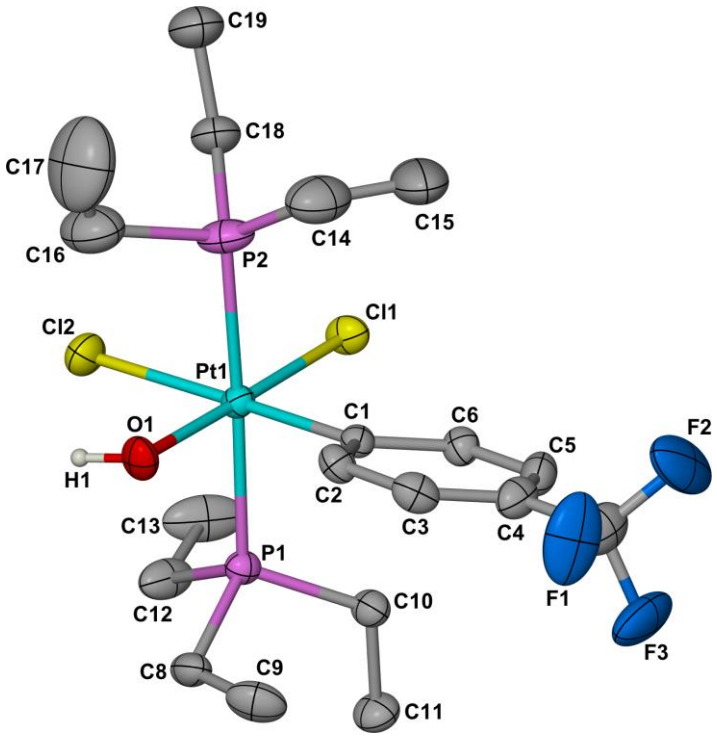

Figure 2.2.3. Solid-state structure of **6** (one of two independent molecules, 50% probability ellipsoids, hydrogen atoms omitted, except for the OH ligand hydrogen atom which is represented as an arbitrary sphere). Rotational disorder in the CF_3 group is not shown

.

Table 2.2.1. Selected mean[a] metrical parameters for chloro-hydroxo complexes **3** and **6**, and hydroperoxo-hydroxo complex **4**.

	3	**6**	**4**
Pt-Cl1	2.356(6)	2.349(1)	2.3541(11)[b]
Pt-Cl2	2.444(2)	2.442(9)	--
Pt-P	2.374(4)	2.371(6)	2.36(1)
Pt-OH	2.018(2)	2.028(5)	2.032(3)[b]
Pt-OOH	--	--	2.104(3)[b]

Pt-C	2.088(6)	2.050(1)	2.040(4)[b]
O-O	--	--	1.472(4)[b]
Cl1-Pt-Cl2	88.98(3)	92.0(6)	--
Cl1-Pt-P	87.5(8) 95.6(4)[c]	90(1)	88.23(4)[b] (P1) 93.05(4)[b] (P2) mean = 91(3)
Cl2-Pt-P	87(1) 89(1)[c]	89(3)	--
Cl1-Pt-OH	175(1)	178.2(6)	176.47(9)[b]
Cl1-Pt-OOH			84.98(9)[b]
Cl2-Pt-OH	86(1)	86(1)	--
Cl1-Pt-C1	98(1)	93.3(1)	94.96(13)[b]
Cl2-Pt-C1	172(1)	174(1)	--
P-Pt-P	174.7(4)	177.8(1)	177.51(4)[b]
P-Pt-OH	91(1) 85.4(5)[c]	90(2)	89(3)
P-Pt-OOH			92.11(9)[b] (P1) 85.87(9)[b] (P2)
P-Pt-C1	90.9(6) 92.8(5)[c]	90.8(6)	91(2)
HO-Pt-C1	86.5(4)	88.4(4)	88.54(15)[b]

HO-Pt-OOH	--	--	91.54(12)[b]
C1-Pt-OOH	--	--	178.14(14)[b]
Pt-O1-O2	--	--	110.4(2)[b]

[a] Mean of chemically equivalent parameters with standard deviation in parenthesis. [b] Single value with estimated error in parenthesis. [c] P atom of PEt_3 ligand near phenanthryl *peri*-hydrogen atom.

Metrical parameters for the complexes are much as expected with essentially identical Pt-P and Pt-Cl distances for all three complexes. The Pt-OH and Pt-C distances in the phenanthryl complex (**3**) differ slightly from those in the CF_3-phenyl complexes (**4** and **6**). The Pt-C distance is longer in **3**, possibly due to steric interactions of the *peri*-hydrogen atom of the phenanthryl group with the *cis*-PEt_3 and -Cl ligands, although electronic factors may also be involved. The steric effect of the *peri*-hydrogen atom is evident in the angles around the Pt center, which deviate more from the ideal 90^o and 180^o angles in **3** than in **6**. (For examples of *peri*-hydrogen steric interaction in Pt(IV) organometallic complexes see reference 9.) Larger deviations are also seen in **4** and may be associated with the hydrogen bonding.

Complex **4** is preceded by two crystallographically characterized Pt(IV) η^1-hydroperoxo complexes: Pt(tmeda)(OOH)(OCH_3)(CH_3)$_2$[29] and Tp*Pt(OOH)(CH_3)$_2$ (Tp* = hydrotris (3,5-dimethylpyrazolyl)borate).[28] Crystallographic problems with the tmeda structure make the metrical parameters unreliable. Comparison of the O-O bond distance and the Pt-O-OH angle in the Tp* complex to those in **4** shows that they are essentially identical, however, the Pt-OOH distances differ markedly being longer by ~0.1 Å in **4**. This is likely due to a difference in the donor *trans* to the OOH ligand. In **4**, it is a strong *trans*-

influence aryl ligand, while in the Tp* complex it is a weaker *trans*-influence pyrazolyl group of the Tp* ligand.

The hydroxo complexes **3** and **6** are new members of a very small group of structurally characterized Pt(IV) hydroxo complexes containing a phosphine ligand. While there are many structurally characterized Pt(IV) hydroxo complexes with a variety of ligands,[30] only *fac*-Pt(dppbz)Me_3(OH) (dppbz = *o*-bis(diphenylphosphino)benzene)[31] and [Pt(PCN)$(OH)_2(H_2O)$]BF_4 (PCN = $C_6H_3[CH_2P(t\text{-}Bu)_2](CH_2)_2N(CH_3)_2$)[32] contain a phosphine ligand. Unfortunately, the hydroxo and aqua ligands were not differentiated in the PCN complex. In the dppbz complex, the OH group is *trans* to a strong *trans*-influence methyl group and the Pt-OH distance, 2.116(7) Å, is consequently longer than the 2.018(2) and 2.028(5) Å distances observed in **3** and **6**.

The stereochemistry of the Pt centers in **3**, **4, 6** and **7** is established by the X-ray structures and places the phosphine ligands *trans* to each other and the hydroxo group *cis* to the R group. While less definitive, the NMR data for the complexes is consistent with the solid-state results. A single phosphine ^{31}P NMR resonance with ^{195}Pt satellites is observed. The J_{PPt} values are typical of similar Pt(IV) complexes (1700-1800 Hz) with *trans* PEt_3 ligands and, as expected, are reduced from the parent Pt(II) complexes **1** and **2**.[11] Separate signals are observed for the phenyl ring protons in the ^1H NMR spectra of **4**, **6**, and **7**. This signifies a non-rotating phenyl ring on the NMR time scale and an asymmetric environment for the aryl ligand. For **6**, this would only be consistent with the OH ligand and a Cl ligand being *cis* to the phenyl ring, as observed in the solid-state structure.

The complexes also show evidence of hydrogen bonding and exchange in their solution NMR spectra. ^{31}P NMR chemical shifts for **3** are sensitive to the presence of H_2O such that there are slight differences in the shift (δ ~1) observed for the isolated complexes and those for the reaction mixtures that contain water from H_2O_2 decomposition. In addition, an OH signal (δ -0.13) is not observed in the ^{1}H NMR spectrum of **3** unless protic impurities are removed by treatment of the NMR sample with base. For **4**, **6**, and **7**, ^{1}H NMR spectra in $CDCl_3$ show peaks for the OH ligand at δ 0.20 (**4**), -0.48 (**6**), and -0.6 (**7**). The OOH ligand of **4** is found at δ 6.42. The OH and OOH signals are concentration dependent for **4** and **6**. (This is presumably also true of **7**, but this was not investigated.) With increasing concentration the signals broaden and the OH signals, which have ^{195}Pt satellites (40 Hz), begin to lose their coupling to the Pt center. In C_6D_6, the OH signal for **6** lacks satellites, even in dilute solutions, suggesting more rapid exchange than in $CDCl_3$, probably resulting from a greater tendency to form hydrogen-bonded dimers.

The UV-Vis absorption spectra for **3** and **6** are given in Figure 2.2.4. As expected from their pale yellow color the spectra show only a tail-off from the UV into the visible. The spectrum of **3** is much more intense in the UV than that for **6** and is likely dominated by absorptions associated with the phenanthryl moiety. In particular, the vibronically coupled π-π* transitions are usually located in the 300 nm region and the bands in this region in the spectrum of **3** can be thus assigned. In contrast, the higher energy aryl group π-system in **6** will shift such bands to higher energy exposing more Pt centered transitions. As we are more interested in the Pt centered transitions we will focus on the spectrum of **6**.

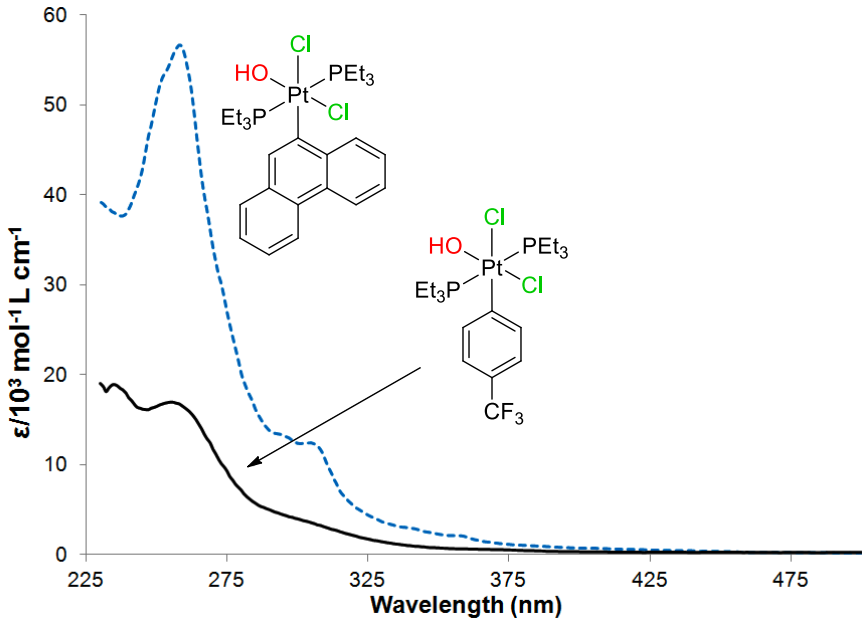

Figure 2.2.4. UV-Visible absorption spectra of 3 and 6 in dichloromethane.

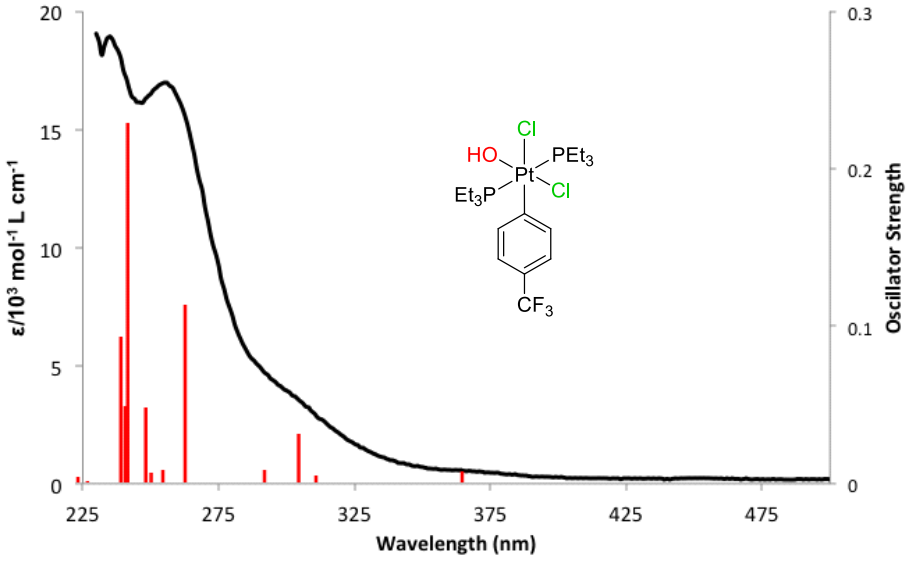

Figure 2.2.5. UV-Visible absorption spectrum of **6** in dichloromethane with TDDFT (CAM-B3LYP, pcm) vertical transitions for **6'** (red vertical lines with the height corresponds to the oscillator strength).

Table 2.2.2. Vertical singlet transitions for 6' in dichloromethane (CAM-B3LYP, pcm).

Transition	Wavelength	Osc. Strength	Contributions (>3%)
1	365	0.0082	H-3->LUMO (56%) HOMO->LUMO (20%) H-1->LUMO (17%)
2	311	0.0054	H-4->LUMO (40%) H-7->LUMO (15%) HOMO->LUMO (12%) H-5->LUMO (8%)
3	304	0.0313	HOMO->LUMO (49%) H-3->LUMO (19%) H-4->LUMO (12%) HOMO->L+1 (7%) H-6->LUMO (5%)
4	292	0.009	H-1->LUMO (65%) H-3->LUMO (13%) H-1->L+1 (4%)

To help in the assignment of the low-UV bands in **6**, a TDDFT (CAM-B3LYP, pcm) study was undertaken with model complex *trans,cis*-$Pt(PMe_3)_2(Cl)_2(OH)$(4-trifluoromethylphenyl) **6'** where the PEt_3 ligands of **6** are replaced by PMe_3 ligands. The calculated vertical singlet transition energies and oscillator strengths (Table 2.2.2) over the region of the experimental spectrum are displayed in Figure 2.2.5 along with the experimental spectrum. A good fit of the calculated transitions for **6'** to the experimental spectrum of **6** is observed, especially in the lower-energy region. The obtained orbital contributions to the transitions are fairly complex (Table 2.2.2) and a natural transition orbital (NTO) analysis[33] was applied for the five lowest-energy transitions. This yielded one dominant (eigenvalue $\geq$ 0.96) contributing orbital set for each transition. The NTO set for the first (lowest-energy) transition is graphically presented in Figure 2.2.6. In common with the other three sets, the arrival orbital for the first transition is an e_g*-type

(pseudo-octahedral symmetry) orbital with strong antibonding interactions between the Pt and the OH and Cl ligands along the HO-Pt-Cl axis. The departure orbital is largely composed of an OH lone-pair and a matching t_{2g}-type Pt orbital, with minor P, C and Cl components. The departure orbitals for the other three transitions are various combinations of Cl lone-pair, t_{2g}-type Pt, P, and π-aryl orbitals. The first five triplet excited-state transitions were also calculated and the compositions and energies of the two lowest match closely to those of the corresponding singlets, suggesting facile singlet-triplet intersystem crossing at this level. Also possible is direct excitation into the triplet excited states at lower energies.

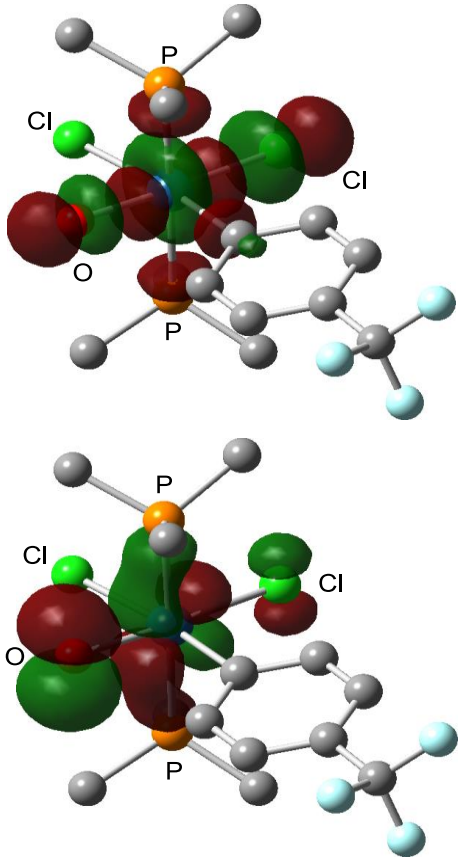

Figure 2.2.6. Natural transition orbital (NTO) set for the first singlet excited state of **6'** (isovalue = 0.04). The "arrival" orbital is on the top and the "departure" orbital is on the bottom (H atoms omitted).

Photochemistry. Complexes **3** and **6** are photosensitive to light in the blue and UV regions. In C_6D_6 (λ = 313 nm), clean conversion of **3** to Pt(II) complex **1** is observed (eq 2) as indicated by ^1H and ^{31}P NMR spectroscopy and by the observation two isobestic points when the reaction is monitored by UV-vis absorption spectroscopy. Two Pt products are obtained for **6** in C_6D_6 and for both **3** and **6** in $CDCl_3$ and CD_2Cl_2. The major products (60-80% yield) are again **1** and **2** but significant amounts (10-35% yield) of the Pt(IV) complexes *trans,mer*-$Pt(PEt_3)_2(Cl)_3R$ [R = 9-phenanthryl (**8**), R = 4-trifluoromethylphenyl (**9**)] are also obtained (eq).

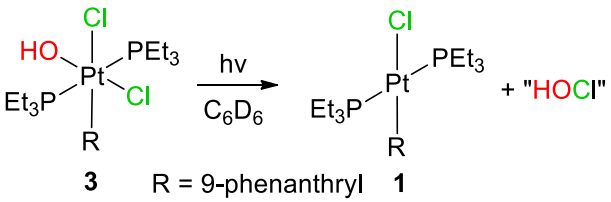

3 R = 9-phenanthryl **1** eq 2

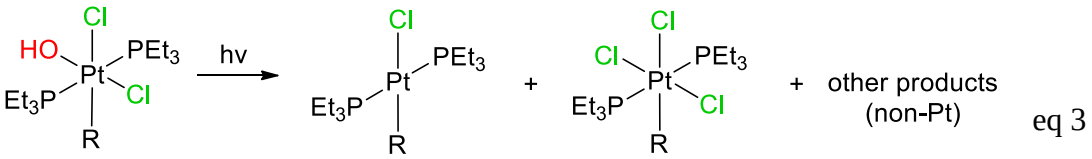

3 in $CDCl_3$ or CD_2Cl_2 **1**
6 in $CDCl_3$, CD_2Cl_2, or C_6D_6 **2**
8, R = 9-phenanthryl
9, R = 4-trifluoromethylphenyl
eq 3

By stoichiometry, the formation of **1** and **2** implies that **3** and **6** photoeliminate HOCl. To test for the possible presence of HOCl, PPh_3 was added to C_6D_6 solutions of **3** immediately after photoconversion (313 nm) to **1**. A 22% yield (based on **3**) of $OPPh_3$ (eq 4) was indicated by ^{31}P NMR spectroscopy. No $OPPh_3$ is observed for the $CDCl_3$ and

CD_2Cl_2 photoreaction mixtures. To help identify the oxidant in the photolyzed C_6D_6 solutions, 2,3-dimethyl-2-butene (TME) was added to a photolyzed solution of **3** in place of PPh_3. The expected HOCl oxidation product, chlorohydrin **10**, is not observed, nor are other possible oxidation products (see below).

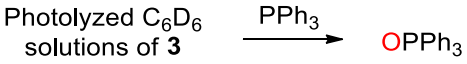

eq 4

As reaction conditions typically used to generate chlorohydrins from an alkene employ a large excess of HOCl in aqueous acid,[34] very different from our potential reactions conditions of low HOCl concentration and non-protic solvents, we studied HOCl reactions with TME under conditions similar to ours. Gaseous HOCl was generated by treating solid $Ca(OCl)_2$ with acid (H_2SO_4 or HCl)[35] and was vacuum transferred into solution. Alternatively, HOCl solutions were prepared by the reaction of HgO and Cl_2 in water-saturated solvents.[36] HOCl formation was confirmed by UV-Vis absorption spectroscopy after transfer to water (Figure 2.2.7). Approximately 10 mol % ClO_2 was also detected in the HOCl from $Ca(OCl)_2$.

TME reactions with HOCl solutions were analyzed by ^{1}H NMR spectroscopy and showed that chlorohydrin **10** is formed along with 3-chloro-2,3-dimethyl-1-butene (**11**) and acetone in about a 1:2:0.2 ratio (Char1). Thus, the oxidant in the photolyzed solutions of **3** and **6** (eq 3) is not HOCl but probably a solvent derived species. Attempts to detect ^{1}H NMR signals for this species in photolyzed C_6H_6 solutions were not successful, although chlorobenzene was detected in 50% yield (relative to **2**). Photolysis of HOCl solutions in C_6H_6 also produced chlorobenzene.

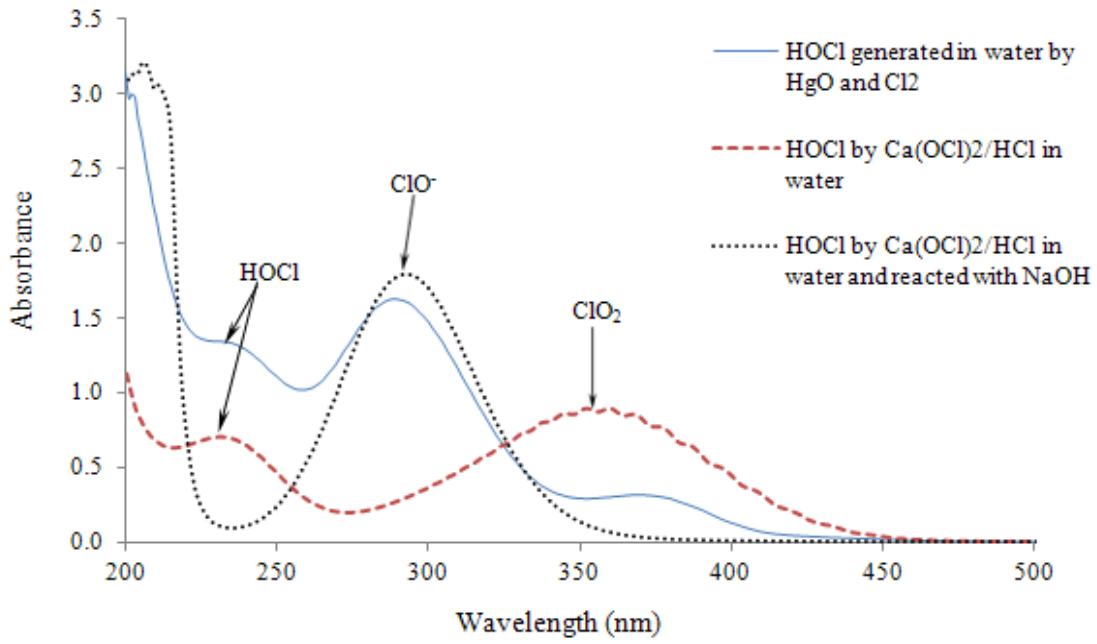

Figure 2.2.7. UV-Visible spectra confirming formation of HOCl from $Ca(OCl)_2$/H+ and HgO/Cl_2. Relative amount of ClO_2 (12%) determined from extinction coefficients. (Note remarkably well defined vibronic coupling on ClO_2 band.)

Chart 1. TME-HOCl reaction products (HOCl from H_2SO_4 and $Ca(OCl)_2$).

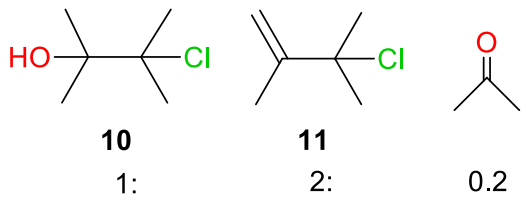

The absence of HOCl in photolyzed solutions of **3** and **6** is consistent with the low stability of HOCl in the presence of Pt complexes and under photolysis.[37] Fresh benzene solutions of HOCl start out a characteristic yellow color, but become colorless within 15 min and lose their ability to oxidize TME. Dichloromethane and chloroform solutions appear to be more stable (hours), but quickly decolorize under irradiation (313 or 380

nm) and the resulting solutions do not oxidize PPh_3. Addition of *trans*-$Pt(PEt_3)_2Cl$(4-trifluoromethylphenyl) (**2**) to a fresh benzene solution of HOCl results in the immediate formation of trichloro Pt(IV) complex **9** and subsequent TME addition does not give oxidation products indicating that HOCl has been consumed. Thus, HOCl photoelimination from **3** and **6** may occur, but the HOCl would not survive the reaction conditions.

To further investigate the role of **2** in the possible decomposition of photoeliminated HOCl, the photolysis of **6** in the presence of an equimolar amount of **2** was examined. Photolysis proceeds as without added **2** (similar time scale), but the yield (based on **6**) of trichloro Pt(IV) complex **9** increases to 48%. From the amount of chlorine in **6**, the maximum possible yield of **9** is 50%. If this represents capture of photoeliminated HOCl by **2**, the capture efficiency is 96%.

TME was used as a possible HOCl trap. Photolysis of **3** and **6** proceeds as without added trap, but now the amount of **8** and **9** formed in $CDCl_3$ and CD_2Cl_2 is reduced to just traces. TME oxidation is observed and products from the CD_2Cl_2 and C_6D_6 reactions are listed in Table 2.2.3 (**3**) and Table 2.2.4 (**6**). In common with HOCl, **11** and acetone are observed for **3**, but only small amounts of chlorohydrin (**10**) are detected and several new products (**12-14**) are formed. Another product, formed in low yield, has a single ^1H NMR signal and could be triacetone triperoxide,[38] but this was not confirmed. In contrast to **3**, photolysis of **6** with TME in $CDCl_3$ and CD_2Cl_2 produces chlorohydrin **10** as a major product in addition to **11**, **12**, **14**, and acetone. Chlorohydrin **10** is the only detected TME product for **6** in C_6D_6, but the yield is only 5%.

Table 2.2.3. TME (0.1 M) product yieldsa from photolysis of 3 (10 mM).

TME	CD_2Cl_2 (% yield)[a]		C_6D_6 (% yield)[a]			
Products	**380 nm[b]**	**313 nm**	**380 nm[b]**	**380 nm,[b] O_2 saturated**	**313 nm**	**313 nm,[b] O_2 saturated**
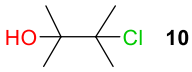 **10**	<1	7	2	2	0	2
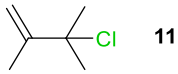 **11**	7	8	5	12	10	9
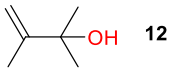 **12**	4	5	<1	<1	5	<1
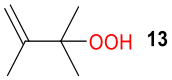 **13**	20	10	21	65	26	90
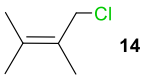 **14**	4	5	2	<1	<1	<1
Acetone	9	7	0	0	0	0
O atom yield[c]	45	34	24	133	57	183
Cl atom yield[c]	12	20	9	14	10	11

[a] Yields are relative to the molar amount of **2** with an estimated error of 1%. [b] Short (< 6 min) high-intensity irradiations. [c] O atom yield = **10** yield + **12** yield + 2(**13** yield) + acetone yield, Cl atom yield = **10** yield + **11** yield + **14** yield.

Table 2.2.4. TME product yields[a] from photolysis of 6 (18 mM, 313 nm).

TME Products	[TME] in $CDCl_3$		[TME] in CD_2Cl_2	
	0.13 M	1.8 M	0.21 M, O_2 saturated[c]	0.44 M
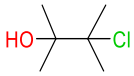 **10**	18 %	26 %	13%	28 %
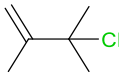 **11**	7 %	9 %	5%	11 %
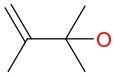 **12**	3 %	23 %[b]	5%	7 %
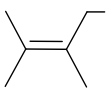 **14**	8 %	25 %	7%	18 %
Acetone	<1 %	5 %	10%	4 %
O atom yield[d]	22	54	31	39
Cl atom yield[d]	33	60	25	57

[a] Yields are relative to the molar amount of **2** with an estimated error of 1%. [b] TME impurities at this high concentration are significant and may interfere. [c] 13 mM **6** (3% epoxide also formed). [d] O atom yield = **10** yield + **12** yield + acetone yield, Cl atom yield = **10** yield + **11** yield + **14** yield.

Hydroperoxide **13** is reported to be the major product of the TME reaction with singlet oxygen.[39] Its formation in the photolysis of **3** (Table 2.2.3) suggests triplet sensitization of O_2 with formation of singlet oxygen.[40] To investigate this possibility, the photolysis of **3** and TME was conducted in O_2-saturated C_6D_6 solutions. (All other photolyses were conducted in vacuum-degassed solutions backfilled with Ar.) The yield of **13** increased

greatly such that the total yield of oxygen-containing products exceeds that possible from **3** alone, clearly indicating the involvement of the added O_2 in product formation. Photolysis of an O_2-saturated TME C_6D_6 solution does not produce **13**. Thus, if **13** is produced from singlet oxygen in the degassed solutions of **3**, the source of the O_2 must be **3,** possibly from decomposition of photoeliminated HOCl into O_2 and HCl. Photolysis of **6** with TME in O_2-free and O_2-saturated solutions (Table 2.2.4) does not produce **13**, indicating a difference in the photochemistry of **3** and **6**.

Complex **7** is also photochemically active. Photolysis of a mixture of **6** (17%) and **7** (83%) gives predominately **2** (69%) with lesser amounts of *trans*-Pt(PEt_3)$_2$(Br)(4-trifluoromethylphenyl) **15** (31%), both in the presence and in the absence of TME (eq 5). Seventeen percent of the yield of **2** is from **6** with the remaining 52% coming from **7.** Thus, the photolysis of **7** produces **2** and **15** in a 1:0.6 ratio suggesting that the reaction is primarily a net *cis*-photoelimination of the Br and OH groups. Consistent with HOBr photoelimination, TME products are primarily (21%) bromohydrin **16** (Chart 2) with no detectable chlorohydrin **10**.

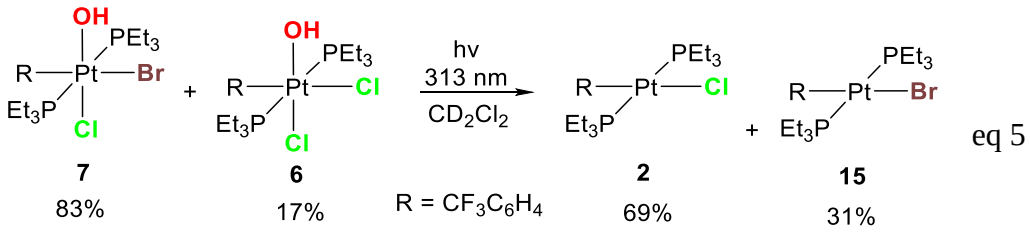

7 83% **6** 17% R = $CF_3C_6H_4$ **2** 69% **15** 31% eq 5

Chart 2

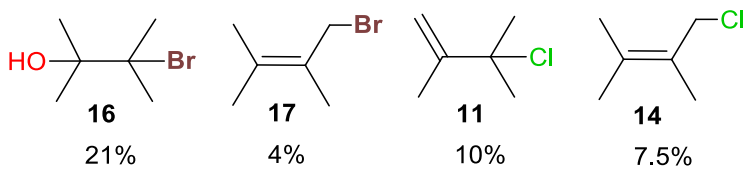

16 21% **17** 4% **11** 10% **14** 7.5%

Computational modeling. Previously, we found that the M06 functional gave gas-phase thermodynamic estimates for Br_2 oxidative-addition to *trans*-$PtL_2Br(R)$ complexes that matched well with toluene solution experimental measurements.[11] Extending these calculations to the current system using PMe_3 model complexes gave the free energies for reductive elimination of HOCl and Cl_2 in Scheme 2.2.2 (L = PMe_3).

Scheme 2.2.2. DFT gas-phase reductive elimination free energies (25°C, 1 atm).

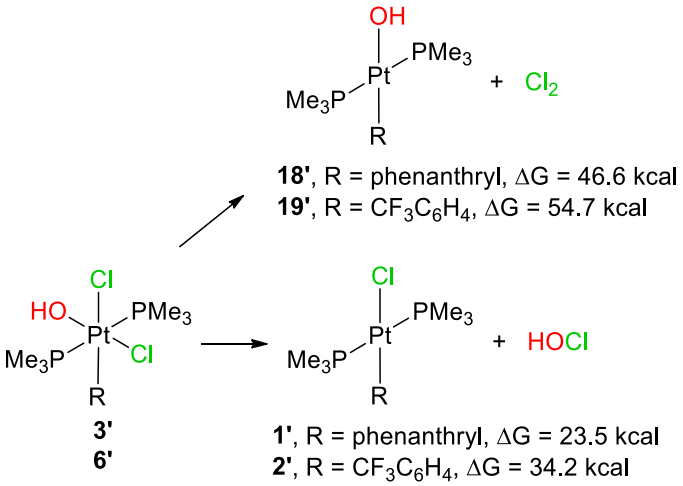

As expected, the reductive-elimination free energies for HOCl and Cl_2 from *trans,cis*-$Pt(PMe_3)_2(Cl)_2(OH)$(9-phenanthryl) (**3'**) and *trans,cis*-$Pt(PMe_3)_2(Cl)_2(OH)$(4-trifluoromethylphenyl) (**6'**) are positive, indicating thermodynamically unfavorable reactions but favorable reverse oxidative-addition reactions. Chlorine elimination is disfavored over HOCl elimination by ~20 kcal. The Cl-Cl bond enthalpy is ~2 kcal/mol greater than the HO-Cl bond enthalpy, slightly favoring Cl_2 elimination.[41] A Pt-OH bond that is significantly weaker than the Pt-Cl bond must be invoked to explain the favored HOCl elimination. Indeed, the calculated (M06) Pt-OH and Pt-Cl (*trans* to OH) gas-phase bond dissociation enthalpies for **3'** and **6'** are 63.6 and 55.6, repectively for the Pt-

OH bond and 78.9 and 69.8, repectively for the Pt-Cl bond. Thus, the Pt-Cl bond (*trans* to OH) in **3'** and **6'** is stronger than the Pt-OH bond by 14-15 kcal/mol.

The relaxed triplet structures for the Pt(IV) complexes were also explored. Two triplet structures (**3'^{T1}** and **3'^{T2}**) from **3'** and one (**6'^{T2}**) from **6'** were located at 40 to 45 kcal above the singlets (gas phase). Drawings of **3'^{T1}** and **3'^{T2}** are given in Figure 2.2.8. That for **6'^{T2}** is given in the SI (Figure S35). The structures **3'^{T2}** and **6'^{T2}** are similar and only **3'^{T1}** and **3'^{T2}** will be discussed. Triplets **3'^{T1}** and **3'^{T2}** have distorted octahedral geometries and can be viewed as Jahn-Teller structures resulting from single occupancy of an e_g-type orbital. The two structures differ primarily in the extent of OH and Cl dissociation along the HO-Pt-Cl1 axis in the distorted octahedron. Both the Pt-OH and Pt-Cl1 distance increase by ca 0.3 Å on going from **3'** to **3'^{T1}**. These distances also increase in **3'^{T2}** but the increase is dominated by the Pt-Cl1 distance which increases by nearly 0.4 Å. Accompanying the Pt-Cl1 distance increase is a bending of the PMe_3 ligands in the direction of Cl1 such that the P1-Pt-P2 angle decreases from near linearity in **3'** to 159.6^o in **6'^{T2}**. Changes in the Pt-C and Pt-Cl2 distances are less than 0.1 Å. Both triplets appear to have weak hydrogen bonding between the OH group and Cl2.

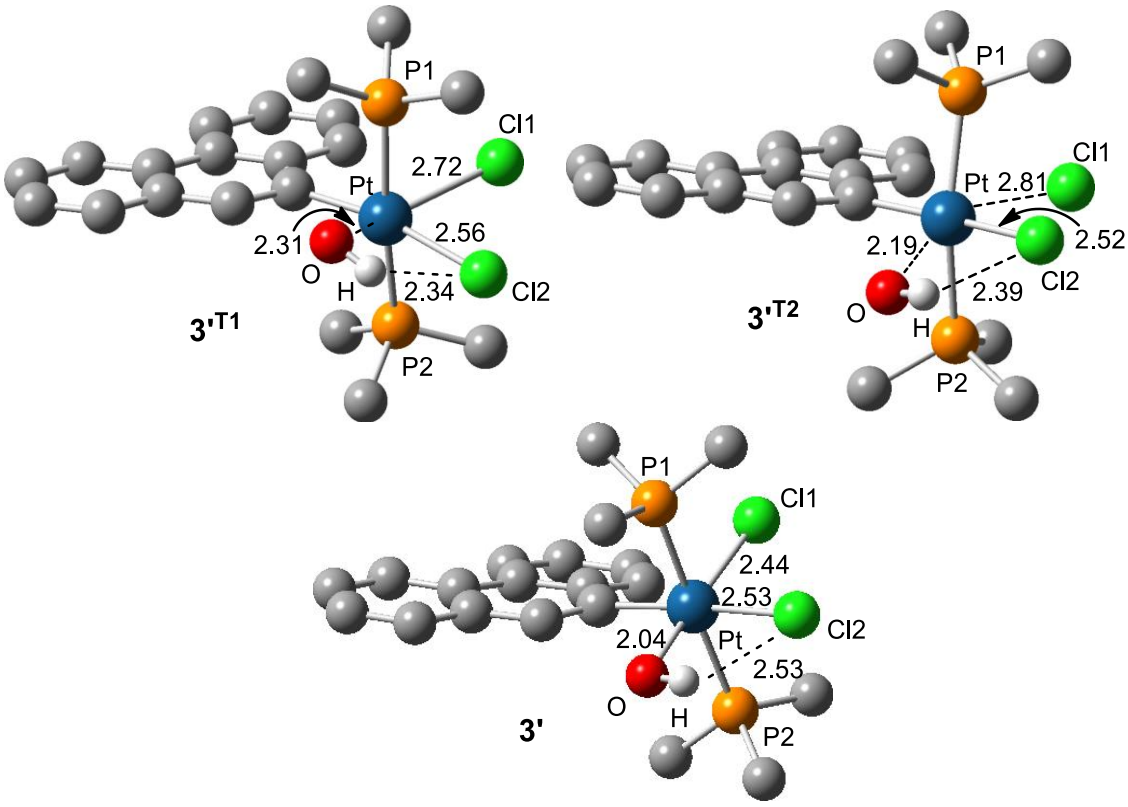

Figure 2.2.8. Triplet **3'**^{T1} and **3'**^{T2} and singlet **3'** structures (distances in Å, carbon-bonded H atoms omitted for clarity).

Dissociative triplet excited states are a common feature of d^6-octahedral metal complexes and can result in ligand dissociation reactions, either with heterolytic or homolytic bond cleavage.[42] The loss of an OH and a Cl radical from the triplets was examined by optimizing the Pt(III) doublets $Pt(PMe_3)_2(Cl)_2(R)$ (**20'**, R = 9-phenanthryl; **21'**, R = 4-trifluoromethylphenyl) and $Pt(PMe_3)_2(Cl)(OH)(R)$ (**22'**, R = 9-phenanthryl; **23'**, R = 4-trifluoromethylphenyl) derived from OH or Cl1 removal from **3'** and **6'**. The resulting structures for R = 4-trifluoromethylphenyl are displayed in Figure 2.2.9. The optimized structures retain the parent configuration and are square pyramidal with a chloro or an hydroxo ligand in the axial position, although facile isomerization is expected for a

square-pyramidal complex. Atomic spin density values reveal spin density on the axial OH (0.3 e-) and Cl (0.5 e-) ligands suggesting substantial radical character for these ligands. (This is consistent with the first excited state NTO set in Figure 2.2.6.) Energetically, the loss of an OH group from either triplet, **3'^{T1}** or **3'^{T2}**, is nearly energetically neutral, while that from **6'^{T2}** is slightly (6 kcal) endergonic. Loss of a Cl atom from the triplets is unfavorable being ~18 kcal endergonic for **3'^{T1}** or **3'^{T2}** and 22 kcal endergonic for **6'^{T2}**.

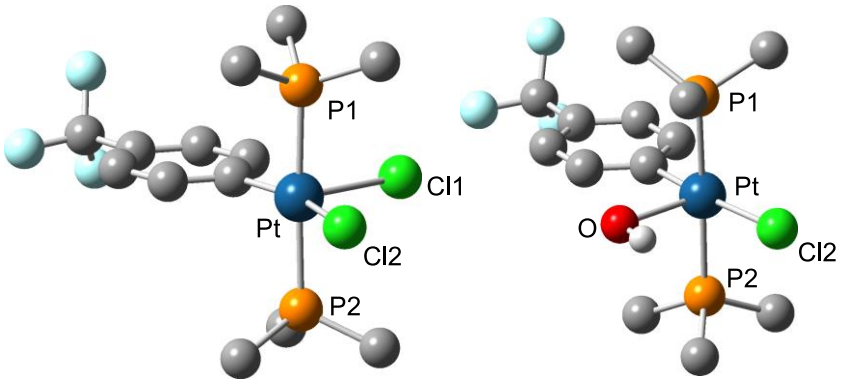

Figure 2.2.9. Doublet structures 21' and 23' (carbon-bonded H atoms omitted for clarity).

Heterolytic bond cleavage with chloride and hydroxide ion dissociation was examined by optimization of the cations $[Pt(PMe_3)_2(Cl)(OH)(4\text{-trifluoromethylphenyl})]^+$ (**24'**) and $[Pt(PMe_3)_2(Cl)_2(4\text{-trifluoromethylphenyl})]^+$ (**25'**), derived from $Cl1^-$ and OH^- removal from **6'**. The gas-phase free energies to dissociate an OH^- from **6'** to give **24'** and a Cl^- to give **25'** are, of course, very high (>100 kcal) due to charge separation without solvation. Applying a dichloromethane solvent correction (pcm model) lowers the free energies to 90.2 (**24'**) and 24.2 (**25'**) kcal. Relative to triplet **6'^{T2}**, the energies are 46.5 and -19.5

kcal. Clearly, hydroxide ion dissociation to **24'** is not favorable and unlikely to occur in this system. On the other hand, chloride ion dissociation appears favorable, at least in dichloromethane. However, with benzene as the solvent, an unfavorable energy of 60.4 kcal relative to **6'** (15.9 kcal relative to **6'^{T2}**) is obtained, indicating that even chloride ion dissociation is probably unfavorable in benzene.

2.3 Discussion.

Syntheses. Pt(IV)-hydroxo complexes have been previously prepared by oxidative addition of H_2O_2 to Pt(II) complexes.[43] However, this has been mostly restricted to Pt(II) complexes with amine or diimine ligands, research driven largely by the anti-tumor activity of Pt amine complexes. These reactions generally occur at, or slightly above, room temperature with 30% aqueous H_2O_2 to give dihydroxo complexes. The resistance of **1** and **2** to oxidation by 30% H_2O_2 was therefore unexpected but could be overcome with higher H_2O_2 concentrations. The Pt(II) oxidative addition mechanism for H_2O_2 has been proposed to be a 3-centered concerted process[44] similar to C-H oxidative addition or to follow an ionic process similar to that for halogen oxidative addition; (a) oxidant electrophilic attack at an axial position with heterolytic cleavage of the oxidant, and then (b) capture of the 5-coordinate Pt(IV) cation by the oxidant anion or another available anion or ligand (Scheme 2.3.1).[18, 43f, 45] The capturing anion or ligand may also participate in the oxidation step by interaction with the Pt center opposite to the attacking oxidant, thereby bypassing the 5-coordinate Pt(IV) cation. In addition, isomerization can occur such that the final product does not contain a *trans* disposition of the added ligands.

Scheme 2.3.1. General mechanism for H_2O_2 oxidative addition.

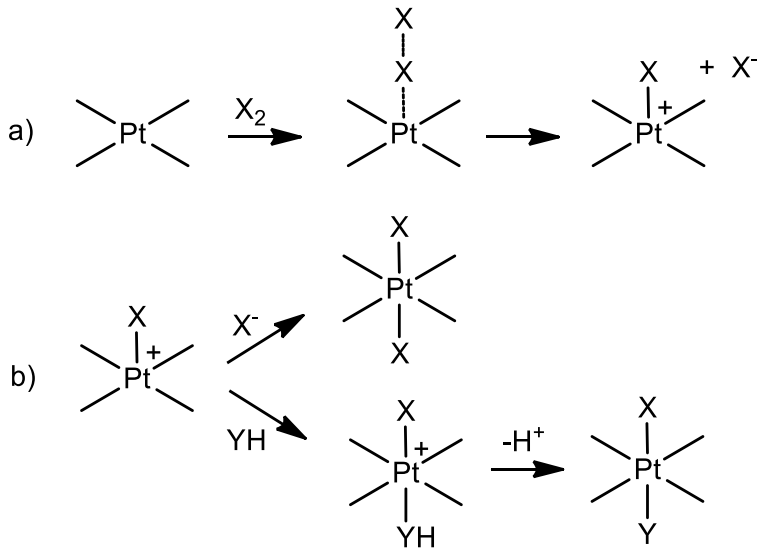

Applying the ionic mechanism to the current system gives the proposed pathway to **3** and **4** given in Scheme 2.3.2. Here, capture of the 5-coordinate cation (or assistance in the oxidation) is by high-concentration H_2O_2, giving first *trans*-hydroperoxo-hydroxo **18**, which then isomerizes to **4** or **5**. Complex **5** is unstable, possibly due to the strong labilizing effect of the *trans*-9-phenanthryl group, and reaction of the hydroperoxo ligand with CH_2Cl_2 yields chloride ion for formation of **3**. A relatively strong basic character for the hydroperoxo group is indicated by its selective protonation over the hydroxo group in the synthesis of **6** and **7** from **4** (Scheme 2.2.1). Since large excess H_2O_2 being used in the synthesis, capture of five-coordinate cation by H_2O_2 in the axial position has received more attention. An alternative mechanism for this has shown in Scheme 2.3.3. Coordination of H_2O_2 gives an ionic Pt(IV) complex, the subsequent reaction of hydroxyl ion with the free/coordinated H_2O_2 can yield hydroperoxo-hydroxo complex.

Scheme 2.3.2. Proposed oxidation of *trans*-Pt(PEt_3)$_2$RCl without H_2O_2 coordinated intermediate.

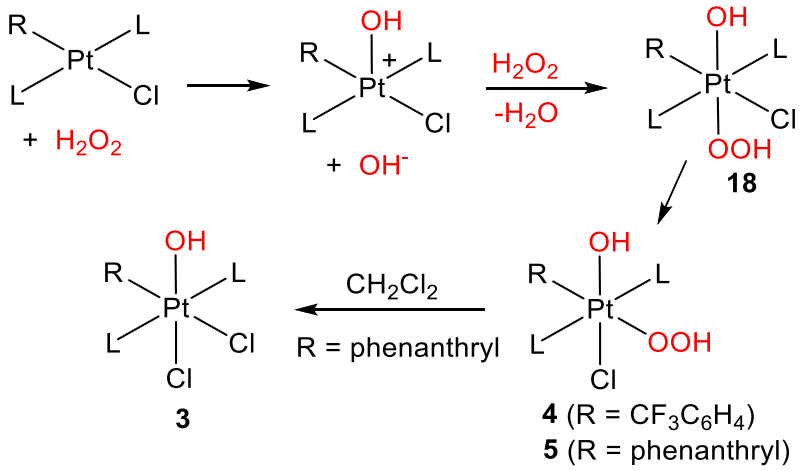

Scheme 2.3.3. Proposed oxidation of *trans*-Pt(PEt_3)$_2$RCl via H_2O_2 coordinated intermediate.

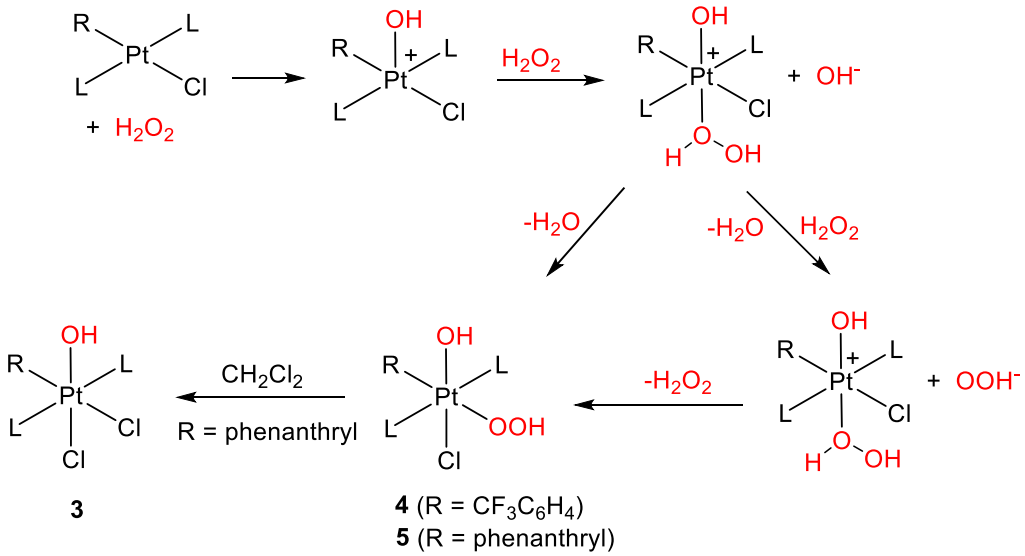

Photochemistry. Understanding the photoreduction of **3** and **6** is challenging. Stoichiometry indicates HOCl elimination, but without direct detection of HOCl other possibilities exist that could give the final stoichiometry without HOCl ever being formed. (A previous report of HOCl photoelimination from prolonged irradiation of

Pt(IV) complexes assumes HOCl elimination by stoichiometry and bleaching of a dye.[46]) Unfortunately, HOCl is not stable in the presence of Pt(II) complexes **1** and **2**, making direct detection difficult. Clearly, a strong oxidant is photochemically produced that oxidizes solvent benzene to chlorobenzene and other unidentified products, which retain some oxidizing power and oxidize added PPh_3. This behavior parallels that of a benzene solution of HOCl, which decomposes rapidly under photolysis (313 nm), and, just like in the photolysis of **3** and **6**, produces chlorobenzene and a solution that oxidizes PPh_3.

Further support for HOCl formation is provided by the trapping experiments with **2** and TME. Complex **2** reacts with HOCl to produce trichloro complex **9**. Any HOCl produced in the photolysis of **6** could react with photogenerated **2** to produce **9**. In fact, **9** is observed in a 35% yield in the absence of added TME. Adding **2** at the beginning of the reaction increases the yield of **9** such that 96% of the theoretical HOCl would have been consumed in the formation of **9** from **2**. With added TME, only traces of **9** form andthe expected TME HOCl reaction products, chlorohydrin **10** and chlorinated **11**, are observed. However, the yield is rather low, especially for **3**, and a number of other products (**12-14**) are also produced, but these could arise from HOCl decomposition products.

Alternatives to HOCl elimination to consider are ionic and radical processes. Bromide photodissociation is reported for $[PtBr_6]^{2-}$ in water and MeOH[42f, 42g, 47] and we have shown that net bromide photodissociation also occurs in CH_2Cl_2.[11] Chloride or hydroxide photodissociation from **3** or **6** would produce a Pt(IV) complex,[48] perhaps in an excited state and capable of alkene or even benzene oxidation. Alkene chlorination by Pd(IV) chloro complexes has been reported and Pt(IV) complexes are involved in hydrocarbon

oxidation in Shilov-type chemistry.[49] Arguing against an ionic pathway is the absence of any significant change in reactivity and products on going from CH_2Cl_2 to benzene (at least for **3**) where ion formation should be disfavored. The DFT modeling of chloride and hydroxide photodissociation suggests that chloride dissociation is possible in CH_2Cl_2, though probably not in benzene. Hydroxide dissociation is, however, unlikely.

Another ionic pathway to consider is excited-state, single-electron transfer (SET). This has been proposed for photoplatination of aromatic compounds with $[PtCl_6]^{2-}$, [50] and for $[PtBr_6]^{2-}$ photoreduction in the presence of high bromide ion concentrations[51] or in methanol solution.[52] However, it was recently concluded that SET follows Br^- photodissociation for $[PtBr_6]^{2-}$.[42g] The photoreduction of **3**, **6** and **7** proceeds equally well in the presence of electron-rich TME or simply in toluene, benzene, CH_2Cl_2, or $CDCl_3$ solvent. Oxidation by SET in these various solvents seems unlikely.

A radical reaction pathway would be consistent with the near solvent independence of the photochemistry of **3**, **6** and **7** and radical photoelimination from Pt(IV) is known. $[PtCl_6]^{2-}$ is thought to photoeliminate a chlorine atom[42g, 53] and Pt(IV) methyl complexes photoeliminate a methyl radical.[54] In addition, the DFT calculations on triplets **3'^{T1}**, **3'^{T2}** and **6'^{T2}** show large spin density on the OH and Cl axial ligands and elongation of the Pt-OH and Pt-Cl bonds, suggesting insipient formation of a geminate Pt(III)/OH radical pair from the triplet excited state. An OH or Cl radical would certainly be reactive enough to drive the photochemistry under a variety of conditions. According to the DFT calculations, OH radical formation is more favorable and the resulting Pt(III) complexes (modeled with **20'** and **21'**) have large spin densities on the axial Cl atoms, suggesting possible Cl atom abstraction from Pt by the OH radical (probably within the solvent cage)

with net HOCl elimination. (Teets and Nocera suggested something similar for molecular halogen photoelimination from Au(III) halide complexes.[10]) To account for the preferred *cis*-elimination indicated by the photochemistry of bromo-hydroxo complex **7**, we propose that geometric isomerization of the 5-coordinate Pt(II) complexes (**20'** and **21'**) interconverts the axial and equatorial chloro ligands bringing the former *cis*-chloro ligand into the axial position for abstraction by the OH radical. This pathway is summarized in Scheme 2.3. and assumes either direct excitation into the triplet manifold or rapid intersystem crossing following singlet excitation. TDDFT does indicate matching triplet transitions for the first two singlet transitions and small energy gaps, consistent with facile intersystem crossing.

Scheme 2.3.5. Possible photoelimination pathway with DFT gas-phase free energies in kcal/mol for model complexes. (Black for R = 9-phenanthryl, blue for R = 4-$CF_3C_6H_4$.)

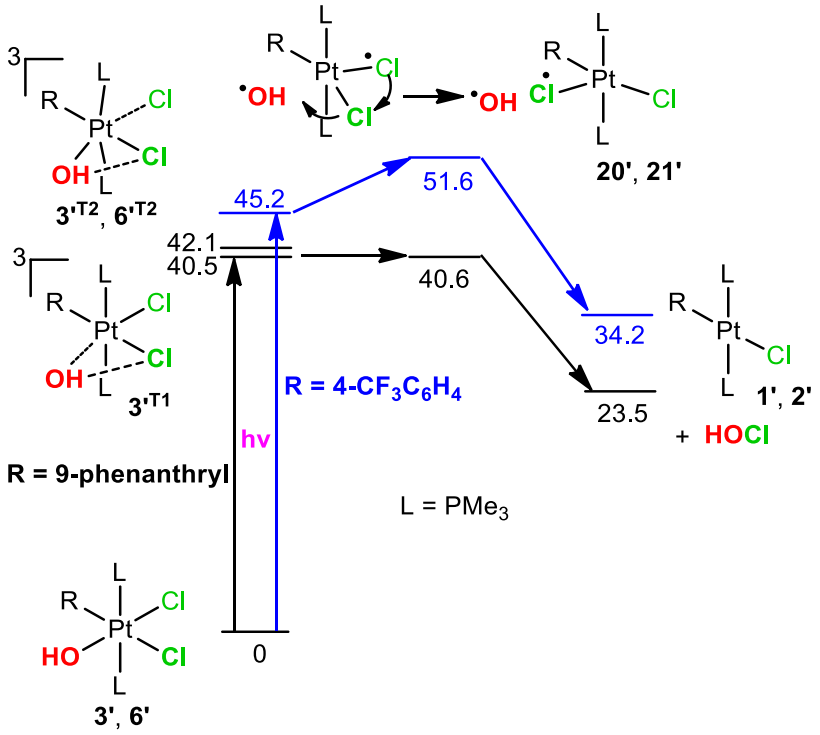

An alternative to HOX elimination that could also follows from OH radical formation is depicted in Scheme 2.3.. In this scheme, the OH radical either abstracts a hydrogen atom from solvent or TME or adds to solvent or TME. In either case, a carbon-based radical is then generated which can then abstract a halogen atom from the Pt(III) center. This scheme accounts for solvent oxidation, TME chlorination and formation of the chlorohydrin.

Scheme 2.3.6. Substrate-assisted *cis*-elimination pathway from hydroxo radical/Pt(III) geminate pair.

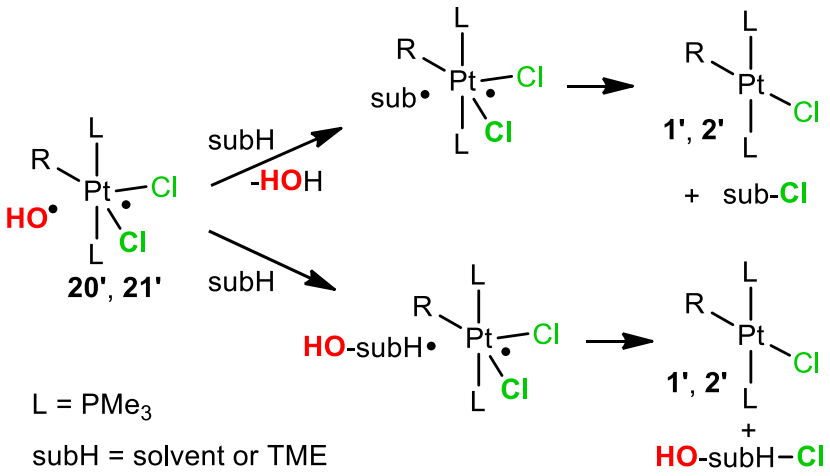

2.4 Conclusions.

The low kinetic reactivity of the Pt(II) phosphine complexes with H_2O_2 bodes well for H_2O_2 photoelimination from Pt(IV) dihydroxo complexes as this is the back reaction and H_2O_2 disproportionation may not be required to prevent it. When oxidation of the Pt(II) center by H_2O_2 does occur, the required high H_2O_2 concentrations result in trapping of the initial oxidation product with H_2O_2 and hydroperoxo-hydroxo complexes result

instead of the expected dihydroxo complexes. Selective replacement of the hydroperoxo ligand with a halide ligand can occur spontaneously in CH_2Cl_2 or by treatment with HX.

The photochemistry of the hydroxo-halo complexes is net HOX elimination. The photochemical pathway most consistent with the behavior of the system (trapping products and solvent insensitivity) and the DFT modeling is excitation into the lowest energy triplet excited state (either directly or via internal conversion and intersystem crossing) followed by geminate Pt(III)/hydroxo radical pair formation. The hydroxo radical can then either abstract a halide from the Pt(III) center forming HOX that decomposes and reacts with solvent and/or trap or the hydroxo radical can react directly with the alkene trap and/or solvent to produce a carbon-based radical that then abstracts a halogen from the Pt(III) center.. Both processes could be operating simultaneously.

2.5 Experimental section.

General considerations. $Pt(PEt_3)_4$[55] was prepared by a reported procedure. Reagents and solvents were purchased from commercial sources (Aldrich or Acros). Synthetic procedures were performed without exclusion of air with unpurified solvents unless otherwise noted. Platinum complex photolysis samples were prepared under a dinitrogen atmosphere in a Vacuum Atmospheres Corporation drybox or on a Schlenk line. Photolysis solvents were dried, degassed and stored under dinitrogen over 4 Å molecular sieves. NMR spectra were recorded on Bruker AMX-250, -300, or -500 spectrometers at ambient probe temperatures except as noted. NMR shifts are given in δ with positive values downfield of tetramethylsilane, $Si(CH_3)_4$ (^1H and ^{13}C), external H_3PO_4 (^{31}P),

external $CFCl_3$ (^{19}F), or external K_2PtCl_4 (aq) (^{195}Pt, δ -1630). ^{13}C, ^{19}F, ^{195}Pt and ^{31}P NMR spectra were recorded in proton-decoupled mode. Microanalyses were completed by ALS Environmental or Atlantic Microlab. UV-Visible absorption spectra were recorded on a Cary 50 or Hewlett-Packard 8452 diode array spectrophotometer in quartz cells. Photolyses were performed in quartz (UV) or borosilicate glass vessels using a Philips PL-S 9W/01, 9 W lamp (313 nm emission), or LED's (superbrightleds.com) of the indicated wavelength.

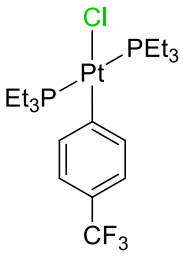

***trans*-Pt(PEt$_3$)$_2$Cl(4-trifluoromethylphenyl) (2).** A solution of 1-chloro(4-trifluoromethy)benzene (23 mg, 0.13 mmol) in THF (~2 mL) was added to a clear orange solution of $Pt(PEt_3)_4$ (70 mg, 0.10 mmol) in THF (~2 mL). The resulting clear orange solution was stirred for ~20 h at 140 ^oC in a sealed tube to yield a pale yellow solution. The mixture was cooled to ambient temperature and the volatiles were removed in *vacuo*. The solid residue was dissolved in ~2 mL CH_2Cl_2 and transferred to a 4 mL vial. The volume was reduced in *vacuo* to ~0.5 mL followed by the addition of ~1 ml of methanol. The vial was capped and stored in at -20 ^oC overnight to afford colorless crystals. The mother liquor was pipetted out and the crystals were dried *in vacuo* to yield 40 mg (63 %) of **2**.

^{31}P NMR (101 MHz, $CDCl_3$): 14.5 (s with satellite, J_{PtP} = 2733 Hz).

^{19}F NMR (235 MHz, $CDCl_3$,): -62.0 (s).

^{1}H NMR (250 MHz, $CDCl_3$): 7.47 (d with satellites, J_{HH} = 7.95 Hz, J_{PtH} = 65 Hz, 2H), 7.12 (m, 2H), 1.78-1.53 (m, 12H, CH_2), 1.14-1.01 (app quintet, J_{app} = 8.27 Hz, 18H, CH_3).

***trans*-Pt(PEt$_3$)$_2$(Cl)(9-phenanthryl) (1).** This complex was prepared from 9-chlorophenanthrene by a procedure similar to that for **2**.

^{31}P NMR (101 MHz, CD_2Cl_2): 14.10 (s with satellite, J_{PtP} = 2735 Hz). ^{31}P NMR (101 MHz, C_6D_6): 13.97 (s with satellite, J_{PtP} = 2736 Hz).

^{1}H NMR (250 MHz, CD_2Cl_2): 8.97-8.93(m, 1H), 8.62-8.57 (m, 2H), 7.82 (s with satellites, J_{PtH} =75 Hz, 1H), 7.69-7.65 (m, 1H), 7.57-7.46 (m, 4H), 1.70-1.40 (m, 12H, CH_2), 1.08-0.96 (app quintet, J = 8.2 Hz, 18H, CH_3).

^{1}H NMR (250 MHz, C_6D_6): 9.28 (d, J_{HH} = 7.50 Hz, 1H), 8.59 (t, J_{HH} = 7.50 Hz, 2H), 8.09 (s with satellites, J_{PtH} = 75.0 Hz, 1H), 7.75 (d, J_{HH} = 7.50 Hz, 1H), 7.58 (t, J_{HH} = 7.50 Hz, 1H), 7.49-7.37 (m, 3H), 1.62-1.28 (m, 12H, CH_2), 0.89-0.77 (app quintet, J = 8.2 Hz, 18H, CH_3).

Preparation of H_2O_2 in ether.[56] Approximately 7 mL of 30% H_2O_2 was placed in a 20 mL vial and then 7 mL of diethylether was added. The vial was capped tightly and the contents stirred vigorously for a minimum of 2 h. (*Caution*: while we never observed H_2O_2 decomposition and O_2 evolution, this is a possibility and a mechanism for pressure release should be provided.) The ether layer (upper layer) was then pipetted into another 20 mL vial. The solution was then concentrated *in vacuo* to 0.5-1 mL. The concentrated solution was not stored but used immediately in the following syntheses.

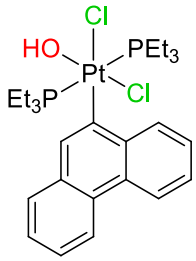

***trans,cis*-Pt(PEt$_3$)$_2$Cl$_2$(OH)(9-phenanthryl) (3).** *trans*-Pt(PEt$_3$)$_2$Cl(9-phenanthryl) (**1**) (10.1 mg, 0.0157 mmol) in 1.5 mL dichloromethane was mixed in a 20 mL vial with 1 mL of a freshly prepared H_2O_2 solution in diethylether. (The preparation of the H_2O_2 solution is described above.) The vial was capped with a rubber septum and a needle inserted to release the pressure generated during the reaction. The mixture was stirred and monitored by ^{31}P NMR spectroscopy. The colorless solution became yellowish orange and conversion of **1** (δ 14.1) to product **3** along with small amounts of OPEt$_3$ (δ 50-60) was observed. (^{31}P NMR shifts varied with the water content of the reaction mixture.) An intermediate (**5**) was detected at δ 6-7 and was gone by the end of the reaction. If the reaction was not complete after 10-12 h additional H_2O_2 solution was added. Once the reaction was complete, the dichloromethane layer was separated from the aqueous layer (from H_2O_2 decomposition) and washed with 3 x 5 mL of deionized water and then dried over $MgSO_4$. After filtering, the volatiles were removed *in vacuo*. The resulting solid was re-dissolved in about 0.5 mL of dichloromethane and 1 mL of hexane was added. A pale orange precipitate (not identified) formed and was removed by filtration. The yellow filtrate was checked by ^{31}P NMR spectroscopy and showed only product **3**. The filtrate was concentrate and then stored at -20 ^{o}C to obtain 7.4 mg (68%) of yellow **3**. Yellow crystals for the X-ray analysis were grown similarly but in an open vial in the freezer. Anal. Calc. (found) for $PtP_2Cl_2OC_{26}H_{40}\cdot 0.3MeOH\cdot 0.5H_2O$: C, 44.26 (44.03); H, 5.86

(5.90). (The water and MeOH content was confirmed by ^{1}H NMR spectroscopy.) MS (APCI) m/z: $[M-H]^+$ 695, $[(M-H)-HCl]^+$ 659, $[(M-H)-HOCl]^+$ 643, $[(M-H)-OCl_2]^+$ 608. The fragment isotope patterns matched those predicted.

^{31}P NMR (101 MHz, CD_2Cl_2): 3.22 (s with satellites, J_{PtP} = 1740 Hz). ^{31}P NMR (101 MHz, C_6D_6): 2.29 (s with satellites, J_{PtP} = 1757 Hz).

^{195}Pt NMR (64MHz, CD_2Cl_2): -1754 (t, J_{PtP} = 1751 Hz).

^{1}H NMR (250 MHz, CD_2Cl_2, $CDCl_3$): 9.14 (d, J_{HH} = 7.50 Hz, 1H), 8.54 (t, J_{HH} = 7.50 Hz, 2H), 8.18 (s with satellites, J_{PtH} = 50.02 Hz, 1H), 7.78 (d, J_{HH} = 7.50 Hz, 1H), 7.64-7.52 (m, 4H), 2.06-1.99 (m, 12H, CH_2), 1.02-0.89 (app quintet, J_{HH} = 8.0 Hz, 18H, CH_3), -0.13 (s, 1H, OH). The OH group signal was observed only after treating the sample with polymer bound diethylamine and could be eliminated by D_2O addition.

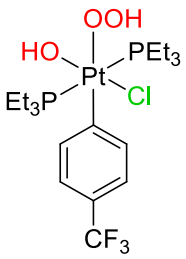

***trans*-Pt(PEt$_3$)$_2$Cl(OH)(OOH)(4-trifluoromethylphenyl) (4).** *trans*-Pt(PEt$_3$)$_2$Cl(4-trifluoromethylphenyl) (**2**) (13.5 mg, 0.022 mmol) in 1.5 mL of dichloromethane was mixed in a 20 mL vial with a freshly prepared H_2O_2 solution in diethylether (1 mL). The vial was capped with a rubber septum and a needle inserted to release the pressure generated during the reaction. The mixture was stirred for 3 h at room temperature during which time the solution turned pale yellow and conversion of **2** (δ 14.4) to *trans*-Pt(PEt$_3$)$_2$Cl(OH)(OOH)(4-trifluoromethylphenyl) (**4**) (δ 5-4) was observed by ^{31}P NMR spectroscopy (^{31}P NMR shifts varied slightly with the water content of the reaction mixture.). Once the reaction was complete, the dichloromethane layer was separated,

washed with 3 x 5 mL of deionized water and dried with $MgSO_4$. After filtering, the volatiles were removed *in vacuo*. The resulting solid was re-dissolved in about 0.5 mL of dichloromethane and 1 mL of hexane was added. Evaporation of the solution at -20 ^oC yielded 13 mg (89 %) of pale yellow crystals that were suitable for X-ray analysis.

^{31}P NMR (101 MHz, $CDCl_3$): 1.09 (s with satellite, J_{PtP} = 1770 Hz).

^{19}F NMR (235 MHz, $CDCl_3$): -62.27 (s).

^1H NMR (250 MHz, $CDCl_3$): 8.05 (d with satellites, J_{HH} = 7.50 Hz, J_{PtH} = 45 Hz, 1H), 7.88 (d with satellites, J_{HH} = 7.50 Hz, J_{PtH} = 45 Hz, 1H), 7.29 (m, 2H), 6.42 (s, 1H, OOH), 2.00-1.89 (m, 12H, CH_2), 1.11-1.00 (app quintet, J_{app} = 7.9 Hz, 18H, CH_3), 0.20 (s with satellites, J_{PtH} = 40 Hz, 1H, OH). The OH group signal is concentration dependent in $CDCl_3$ (and CD_2Cl_2). As concentration increases (above ~0.01 mol L^{-1}) the signal broadens and the ^{195}Pt satellites move in and eventually merge with the main peak. The OOH signal also broadens. D_2O addition causes complete loss of the OH and OOH signals.

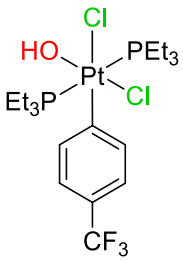

***trans,cis*-Pt(PEt$_3$)$_2$(Cl)$_2$(OH)(4-trifluoromethylphenyl) (6).** Compound **4** was dissolved in 1 mL of dichloromethane and approximately 2 mL of deionized water and 0.05 mL dilute HCl (50 µL of conc HCl in 1-2 mL water) was added and the mixture was stirred for 1 min. ^{31}P NMR spectroscopy showed complete conversion of **4** to **6** (δ 1.09). The

dichloromethane layer was washed with 10 mL of deionized water and dried with $MgSO_4$. After filtration, the volatiles were removed *in vacuo*. The resulting solid was washed with 1.0 mL of cold hexane and dried *in vacuo* to give 12.0 mg (88%) of **6**. Pale yellow crystals for the X-ray analysis were grown in ether/heptane (1:5) by slow evaporation in the freezer.

^{31}P NMR (101 MHz, $CDCl_3$ or CD_2Cl_2): 1.09 (s with satellites, J_{PtP} = 1708 Hz). ^{31}P ^{57} NMR (101 MHz, C_6D_6): 0.16 (s with satellites, J_{PtP} = 1708 Hz).

^{19}F NMR (235 MHz, $CDCl_3$ or CD_2Cl_2): -62.30.

^{195}Pt NMR (64 MHz, $CDCl_3$): -1944 (t, J_{PtP} =1720 Hz).

^{1}H NMR (250 MHz, $CDCl_3$): 8.16 (d with satellites, J_{HH} = 7.50 Hz, J_{PtH} = 42 Hz, 1H), 7.93 (d with satellites, J_{HH} = 7.50 Hz, J_{PtH} = 42 Hz, 1H), 7.33 (m, 2H), 2.00-1.85 (m, 12H, CH_2), 1.13-1.03 (app quintet, J_{app} = 8.0 Hz, 18H, CH_3), -0.48 (s with satellites, J_{PtH} = 40 Hz, 1H, OH). The OH group signal is concentration dependent in $CDCl_3$ (and CD_2Cl_2). As concentration increases (above ~0.01 mol L^{-1}) the signal broadens and the ^{195}Pt satellites move in and eventually merge with the main peak. D_2O addition causes complete loss of the OH signal.

^{1}H NMR (250 MHz, C_6D_6): 8.41 (d with satellites, J_{HH} = 8.25 Hz, J_{PtH} = 42 Hz ,1H), 8.25 (d with satellites, J_{HH} = 8.25 Hz, J_{PtH} = 38.5 Hz ,1H), 7.36 (d, J_{HH} = 8.25 Hz,1H), 7.31 (d, J_{HH} = 8.25 Hz, 1H), 1.78-1.63 (m, 12H, CH_2), 0.81-0.68 (app quintet J_{app} = 8.0 Hz, 18H, CH_3), -0.4 (br s, 1H, OH).

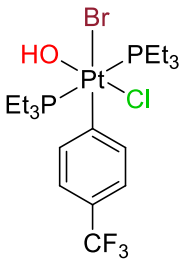

***trans*-Pt(PEt$_3$)$_2$(Br)(Cl)(OH)(4-trifluoromethylphenyl)** (**7**). Compound **4** was dissolved in 1 ml of dichloromethane and approximately 2 mL of deionized water and 0.05 mL 50% HBr was added and the mixture stirred for 1 min. ^{31}P NMR spectroscopy showed complete conversion of **4** to **7** (δ -2.09). The dichloromethane layer was washed with 10 mL of deionized water dried with $MgSO_4$. After filtering, the volatiles were removed *in vacuo*. The resulting solid was washed with 1.0 mL of cold hexane and dried *in vacuo* to give **7**. Pale yellow crystals for the X-ray analysis were grown in CH_2Cl_2/heptane (1:2) by slow evaporation in the refrigerator.

^{31}P ^{57} NMR (101 MHz, CD_2Cl_2): -2.09 (s with satellite, J_{PtP} = 1703 Hz).

^{1}H NMR (250 MHz, CD_2Cl_2): 8.15 (d with satellites, J_{HH} = 7.50 Hz, J_{PtH} = 44 Hz, 1H), 7.95 (d with satellites, J_{HH} = 9.50 Hz, J_{PtH} = 39 Hz, 1H), 7.38-7.34 (m, 2H), 2.00-1.86 (m, 12H, CH_2), 1.11-0.98 (app quintet, J_{app} = 7.75 Hz, 18H, CH_3), -0.6 (brs,1H, OH).

UV-Visible absorption spectra. *Trans,cis*-Pt(PEt$_3$)$_2$(OH)Cl$_2$(9-phenanthryl) (**3**) (3.2 mg, 0.0046 mmol) was dissolved in HPLC grade CH_2Cl_2 and diluted to the mark in a 5.00 mL volumetric flask. This solution (0.92 mM) was used as a stock solution for the analysis. A series of concentrations was prepared by diluting 40, 50, 60, 70 and 80 μL into 5.0 mL volumetric flasks. The solvent blank was obtained and spectra were recorded from 200 to 800 nm for each sample. *Trans*-Pt(PEt$_3$)$_2$(OH)Cl$_2$(4-trifluoromethylphenyl) (**6**) (20.1 mg,

0.0303 mmol) was dissolved in HPLC grade CH_2Cl_2 and diluted to the mark in a 10.00 mL volumetric flask. This stock solution (3.03 mM) was used to prepare a series of concentrations was prepared by diluting 20, 30, 40 and 50 μL into 5.0 mL volumetric flasks. All the experimental conditions were kept identical for **3** and **6** except for the concentrations. The absorbance data collected for the above samples were converted to molar extinction coefficient, averaged, and plotted (Figure 2.2.4).

Preparation of HOCl from $Ca(OCl)_2$. Solid $Ca(OCl)_2$ (100 mg, 0.70 mmol) was added to a 100 mL Schlenk flask. The stopcock plug was removed from the flask and replaced with a rubber septum. The flask was then connected to a vacuum line. Solvent (H_2O, C_6D_6, or $CDCl_3$; 0.50 mL) was added into a 5 mm NMR tube. The tube was connected to the vacuum line and immersed in LN_2. The frozen NMR tube and the Schlenk flask were connected and kept under vacuum for 10 min. After reaching a vacuum of 50 mtorr, the connection to the vacuum line was closed and concentrated H_2SO_4 or HCl (0.10 mL) was injected through the rubber septum onto the solid $Ca(ClO)_2$. (The Schlenk flask was isolated from the NMR tube prior to the addition of H_2SO_4 and reconnected 5 min post injection.) The gaseous products were condensed into the NMR tube. The tube was thawed and the solution was transferred into a 1 cm path length quartz cuvette for recording of the UV-Vis absorption spectrum (Fig S2). Solid NaOH (~20 mg, 0.50 mmol) was added to the cuvette with stirring. The spectrum was recorded and showed λ_{max} for the ClO^- at 292 nm, as reported in previous studies.[58]

Synthesis of HOCl from HgO and Cl_2.[36] Freshly prepared HgO (100 mg, 0.46 mmol) was added to 2 mL of double distilled water (DDW) in an 8 mL vial. Chlorine gas (1 mL, 0.045 mmol), dissolved in 1 mL of DDW, was immediately added and the mixture was

stirred for 30 min. Filtration through diatomaceous earth yielded a clear solution. The solution was transferred to a 1 cm path-length cuvette and the UV-Vis absorption spectrum was recorded (Fig S2).

Reaction of HOCl with TME. (A) HOCl was generated from $Ca(OCl)_2$ as described above but the gaseous products were condensed into a mixture of $CDCl_3$ (0.50 mL) and TME (2,3-dimethyl-2-butene) (~30 µL) instead of water. The mixture was thawed and ^1H NMR analysis indicated the formation of TME products. **(B)** A solution of HOCl from HgO and Cl_2 was generated as described above but with water saturated $CDCl_3$ as the solvent instead of DDW. After thawing the NMR tube, TME was added and the mixture was analyzed by ^1H NMR spectroscopy.

Photolysis of HOCl. Three identical samples of HOCl in C_6D_6 were prepared from $Ca(OCl)_2$ as described above. TME (~30 µL) was added to one and the products determined by ^1H NMR spectroscopy (Chart1). Another sample was photolyzed at 313 nm for 8 min and then TME was added. No TME products were observed except for **11** (TME and Cl_2 yields **11**). The third sample was photolyzed at 380 nm for 8 min and then TME was added. No TME oxidation was detected. In other experiments, C_6H_6 samples of HOCl were photolyzed at 313 nm and 380 nm without trap. Chlorobenzene was detected by ^1H NMR in both samples.

Reaction of HOCl with PPh_3 and 1. PPh_3 (3.5 mg, 0.015 mmol) was dissolved in 0.8 mL of C_6D_6. A dilute C_6D_6 solution of HOCl, prepared by diluting a 0.05 mL aliquot of a C_6D_6 HOCl solution (prepared from $Ca(OCl)_2$ as described above) to 0.4 mL, was added in portions until the ^{31}P NMR signal for PPh_3 (δ -4.9) disappeared. The only product detected by ^{31}P NMR spectroscopy was $OPPh_3$ (δ 28.0).

Reaction of HOCl with 1 or 2. A solution of **1** (0.02 M) in C_6D_6 was mixed with 0.05 mL aliquot of HOCl made in C_6D_6 (prepared from $Ca(OCl)_2$). The ^{31}P NMR signal for **8**

was observed. The only product detected by ^{31}P NMR spectroscopy was **8** and remaining **1**. Similar experiment was carried out with **2** and yielded **9.**

Reaction of photolyzed 3 with PPh_3. A sample of **3** (2.0 mg**,** 0.0029 mmol) was photolyzed at 313 nm in ~0.5 mL C_6D_6 until all **3** had been consumed. Excess PPh_3 (5 mg, 0.019 mmol) was added. A 22 % yield of $OPPh_3$ was observed by ^{31}P NMR spectroscopy.

Photolysis of *trans,cis*-$Pt(PEt_3)_2Cl_2$(OH)(9-phenanthryl) (3). Photolysis experiments were performed at 313 and 380 nm in C_6D_6 and CD_2Cl_2. A 0.011 M solution of **3** was added to a 5 mm J. Young NMR tube. Photolysis was then carried out with periodic ^{31}P NMR and ^{1}H NMR monitoring. Compound **3** was observed to convert to **1** (colorless) although the solution remained yellow orange and did not become colorless as expected for **1**.

Photolysis of *trans,cis*-$Pt(PEt_3)_2Cl_2$(OH)(4-trifluoromethylphenyl) (**6**)**.** The photolysis experiments were performed at 313 nm in $CDCl_3$, CD_2Cl_2 and C_6D_6. Solutions of **6** (0.018 M) were photolyzed in the presence of variable amounts of TME. Irradiation times were 14-17 min. Spectroscopic analysis (NMR) was carried out within 5 min of the photolysis and the results are given in Table 2.2.4.

Photolysis of 6 in the presence of 2. A 5 mm NMR tube was charged with 0.5 mL of a CH_2Cl_2 solution that was 0.018 M in of **6** and 0.016 M in **2**. A capillary tube containing a solution of PPh_3 was added to the tube to serve as an integration standard. The sample was then photolyzed at 313 nm. ^{31}P NMR analysis was carried out at 30 s intervals until all **6** was consumed (13 min total). At the end of the photolysis a 48% conversion of **2**

into trichloro complex **9** was indicated. A maximum conversion of 50% is expected from the available chlorine in **6**.

Photolysis of *trans*-Pt(PEt$_3$)$_2$(Br)(Cl)(OH)(4-trifluoromethylphenyl) (**7**)**.** The photolysis experiments were performed similarly to those for **6** in CD_2Cl_2 both with and without TME. The bromohydrin **16** was identified by comparison of the NMR properties (^{1}H NMR in $CDCl_3$: δ 1.84, 1.35) with an authentic sample prepared by HBr addition to the epoxide. NMR data for **17** have been reported.[59]

NMR data for *trans*-Pt(PEt$_3$)$_2$(Br)(4-trifluoromethylphenyl) (15).

^{31}P ^{57} NMR (101 MHz, CD_2Cl_2): 12.4 (s with satellite, J_{PtP} = 2709 Hz).

^{1}H NMR (250 MHz, CD_2Cl_2): 7.50 (d with satellites, J_{HH} = 10 Hz, J_{PtH} = 67.50 Hz, 2H), 7.17-7.11 (m, 2H), 1.74-1.59 (m, 12H, CH_2), 1.12-0.99 (app quintet, J_{app} = 8.10 Hz, 18H, CH_3).

Quantum Yield Determination. Irradiations were performed in the compartment of a Cary 50 UV-Vis spectrometer equipped with a magnet stirrer and temperature control. The sample was contained in a 1 cm quartz cuvette sealed at the top with a quartz microscope slide. The light source was positioned over the sample compartment allowing irradiations through the top of the cuvette.[60] The photon flux was measured (Fe oxalate actinometry[61]) before and after each sample irradiation and the average of the before and after measurements was used as the photon flux during the sample irradiation. Sample solution concentrations were sufficiently high to assure complete photon absorption (absorbance ≥ 2 at the irradiation wavelength) over the ~3 cm depth of the solution. Reaction progress was monitored by the UV-Vis absorbance of product *trans*-Pt(PEt$_3$)$_2$Cl$_3$(4-trifluoromethylphenyl) (**8**) over the region of 310-400 nm where *trans*-

$Pt(PEt_3)_2Cl$(4-trifluoromethylphenyl) (**2**) does not absorb and *trans*-$Pt(PEt_3)_2Cl_2(OH)$(4-trifluoromethylphenyl) (**6**) absorbance is relatively weak. The yield of **8** from the UV-Vis (0. 3 mM) data is 34% and matches the yield determined by ^{31}P NMR spectroscopy (1 mM). The absorbance increase at three wavelengths (365 nm, 375 nm, 390 nm) during the first 10% of the reaction was used to calculate the quantum yield. The average of three runs gave a final quantum yield for **6** of 51 ± 2% in dichloromethane.

Computational Details

Gaussian 09 (revision A.1 or C.1)[62]with the M06[63] or CAM-B3LYP[64] (TDDFT) functional were used for all calculations. The LANL2DZ[65,66,67,68] basis set was employed for Pt, Cl and P with an added d function (α = 0.05) for Pt, d (α = 0.648) and p (α = 0.0467) functions for Cl, and d (α = 0.434) and p (α = 0.0376) functions for P.[69] The 6-31G(d) basis set was used for all other atoms. Initial structures were derived from crystal coordinates and were modified with Gaussview.[70,71] All geometries were optimized with no symmetry constraints in the gas phase. Free energies, enthalpies, and entropies were calculated at 298.15 K and 1 atm. Analytical frequency calculations gave no imaginary frequencies for the complexes except for **3'**, which had a small imaginary frequency of -11 cm^{-1} associated with a methyl group rotation. TDDFT calculations included solvent (dichloromethane) with the polarized continuum model (pcm)[72] and employed the gas-phase optimized structures.

CHAPTER 3: DIHYDROGEN TRIOXIDE (HOOOH) PHOTOELIMINATION FROM A PLATINUM(IV) HYDROPEROXO-HYDROXO COMPLEX.

3.1 Introduction.

The synthesis of *trans*-Pt(PEt_3)$_2$(Cl)(OH)(OOH)(4-tft) **4** was already discussed in the previous chapter.[27] Here now is reported the thermal and photo chemistry of **4**, which includes reductive elimination of HOOOH (H_2O_3, dihydrogen trioxide or trioxidane), a rare example of O-O bond formation by photo reductive elimination. (Other examples feature hydrogen peroxide elimination.[73]). The chemistry discussed later in this chapter includes computational modeling studies on the thermodynamics and mechanisms for these unusual reactions.

3.2 Photochemistry.

Irradiation (380 nm) of t*rans*-Pt(PEt_3)$_2$(Cl)(OH)(OOH)(4-tft) **4** (4-tft = 4-trifluoromethylphenyl) at ambient temperature for ~8 min in C_6D_6 results in Pt-center reduction, yielding the Pt(II) complex *trans*-Pt(PEt_3)$_2$(Cl)(4-tft) **2**, water, and presumably O_2 (eq 6).

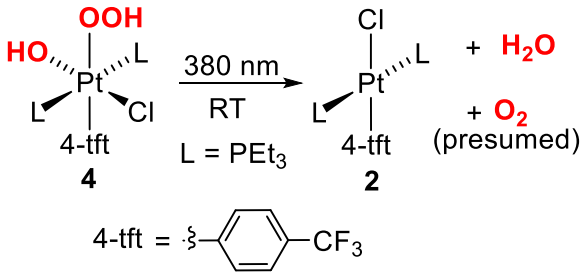

eq 6

This observation caught our attention as there are at least two possible pathways to water and O_2. One would be directly through photo-driven OH abstraction of a hydrogen atom from the OOH ligand. (We initially considered this to be the more likely pathway.) The other would be by decomposition of H_2O_3, the expected photo reductive- elimination product if the photochemistry of **4** follows that of the analogous hydroxo-halo complexes t*rans*-$Pt(PEt_3)_2(Cl)(OH)(X)(4\text{-tft})$ (X = Cl, Br)[27] and bromo complexes *trans*-$Pt(PEt_3)_2(Br)_3R$.[11] With these possibilities in mind, the photolysis of **4** was reexamined at -78 ^oC.

An acetone-d_6 sample of **4** in an NMR tube was cooled to -78 ^oC and irradiated at 380 nm. ^1H NMR analysis was then carried out at -60 C° and revealed a singlet at δ 13.4 that reached a maximum at 40-60% conversion of **4** into **2** and then declined and disappeared as the irradiation continued. The peak also disappeared when the sample was warmed to RT. The experiment was repeated in toluene-d_8 where H_2O_3 gives a singlet at δ 9.9.[26] A singlet at this chemical shift was observed at -60 C° confirming the formation of H_2O_3 from the photolysis of **4** (eq 7). ^1H NMR spectral integration indicated an H_2O_3 yield[74] of 16 ± 2% in toluene-d_8 and 6 ± 2% in acetone-d_6 at 40-60% conversion of **4**. However, it was noticed that the OOH signal of **4** was considerably diminished (by 70%) in acetone-d_6 and that a signal for HOD was present. We interpret this as deuterium exchange of the OH and OOH ligands with residual D_2O from the acetone-d_6 preparation.[75,76] Correcting for this exchange increases the H_2O_3 yield in acetone-d_6 to 20%, similar to that in toluene-d_8.

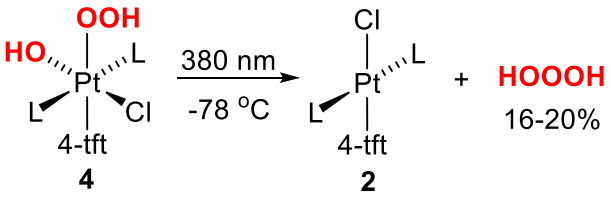

eq 7

Also detected in the low temperature acetone-d_6 sample were ^{1}H NMR peaks in the δ 9-12 region attributed to H_2O_2 (9%) and acetone adducts **19** (16%) and **20** (36%) giving a total product yield of 81%. (Yields[74] include adjustment for H/D-exchange.) Acetone adducts **19** and **20** are known to form in reactions of H_2O_2 with acetone.[77,78,79] (Adduct **20** could also form by net addition of OOH and OH from **4** across the acetone double bond. We have observed similar photo reactions of alkenes with halogen analogs of **4**.[12]) No high-shift peaks, other than H_2O_3, are observed in the toluene-d_8 samples but the H_2O_2 ^{1}H NMR signal is in the aromatic region and is broad, making it difficult to observe in toluene-d_8.

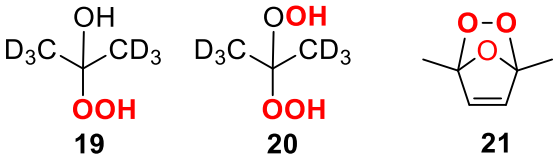

Room temperature photolysis of **4** was also conducted in the presence of singlet-oxygen traps 2,5-dimethylfuran (DF) and 2,3-dimethyl-2-butene (TME). The DF singlet oxygen trapping product, endoperoxide **21**[80] (see above), is not observed in the photolysis of **4** in the presence of DF (C_6D_6). Instead, its dimer **22** is formed in 25% yield[74] (Scheme 1). Dimerization of **5** has been reported to be slow at room temperature but rapid above 55-60 °C.[75] With TME (CD_2Cl_2) the expected singlet oxygen product, hydroperoxide **13**,[81] is observed in 8% yield[74] along with tetramethyl-1,2-dioxetane **23**[82] (9%) and acetone

(4%) (Scheme 3.2.1). Further photolysis converts **23** to acetone[82] indicating that acetone is likely a secondary product and the dioxetane is actually produced in 11% yield.[74] Dioxetane **23** is not an expected product from singlet oxygen and its formation appears to be from the direct reaction of H_2O_3 with TME. This reaction has not been reported but we find that addition of TME to a photogenerated solution of H_2O_3 at -60 °C does yield **23** (see SI).

Scheme 3.2.1. Photolytic trapping reaction.

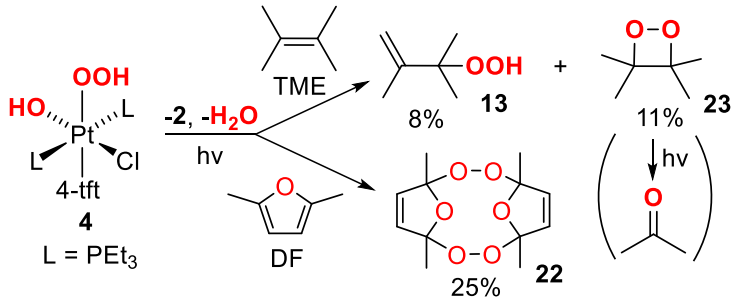

Complex **4** is also thermally active to elimination. Heating a toluene-d_8 solution shows no immediate change until about 80 °C, at which point gas evolution is observed. Like the photolytic reactions, ^{31}P and ^{1}H NMR spectroscopy show the formation of **2** and water indicating that the thermal reaction products are similar to the photolytic reaction (eq 6). We again tested for singlet oxygen by repeating the decomposition in the presence of TME and DF (Scheme 3.2.2). The decomposition rate is unaffected showing that there is no direct reaction between the traps and **4**. A 15% yield[74] of dioxetane **23** is produced in the TME reaction. Again, this is not the expected product from singlet oxygen but is one of the same products of the photolytic reaction and a product of the reaction of H_2O_3 with TME (see above). Photolytic conversion of **23** to acetone was confirmed with this sample. The DF thermal reaction gives a 10% yield[74] of endoperoxide dimer **22**, which is

the expected singlet oxygen product above 55-60 °C.[75] A kinetic study of the decomposition (no trap) revealed a first order reaction in **4** with activation parameters $\Delta H^{\ddagger}$ = 19(1) kcal/mol and $\Delta S^{\ddagger}$ = -18(4) cal/mol·K.

Scheme 3.2.2. Thermal trapping reaction.

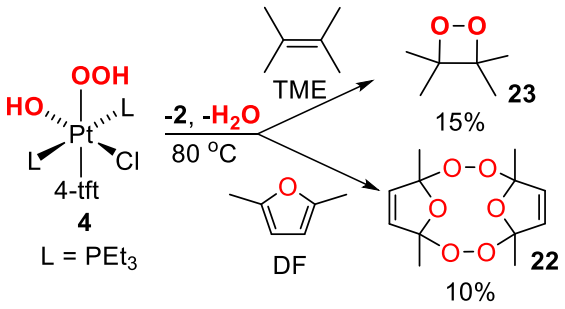

The chemistry of **4** was modeled using density functional theory (DFT) computations with PMe_3 in place of PEt_3 (indicated with a prime on the complex numbers). An issue that immediately arises is the hydrogen bonding in **4**. While the solid-state structure of **4** is a dimer with intermolecular OOH hydrogen bonding,[27] a DOSY diffusion NMR experiment (SI) in acetone-d_6 indicates negligible dimer formation in solution. However, there are still options for intramolecular OH and OOH ligand hydrogen bonding (Figure 3.2.1). In model complex **4a'** the OH ligand is the donor and the OOH ligand the acceptor. This is the intramolecular hydrogen-bonding pattern in the solid-state structure of **4**.[27] Complex **4b'** has the reverse pattern. Gas-phase optimization of **4a'** and **4b'** converged to minima with **4b'** at 3.6 kcal/mol higher free energy suggesting that, at least in non-polar, non-hydrogen-bonding solvents, the majority hydrogen-bonding structure for monomeric **4** is of type **4a'**, the same intramolecular hydrogen-bonding pattern observed in the solid-state dimer.[27]

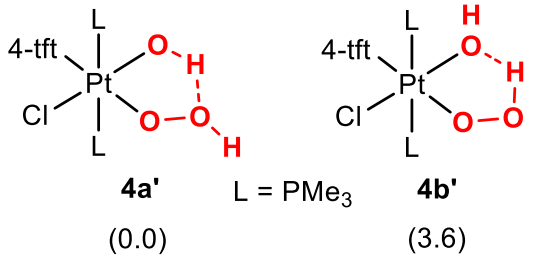

Figure 3.2.1. Intramolecular hydrogen-bonding models for 4 with calculated relative energies in kcal/mol in parentheses.

Reductive elimination thermodynamic values (gas phase) for **4a'** were calculated and are given in Table 3.2.1. H_2O_3 elimination is endergonic by 14.4 kcal/mol. Water and $^1O_2$ ($^1\Delta_g$) elimination is exergonic with ΔG = -11.4 kcal/mol. Expectedly, $^3O_2$ ($^3\sum_g^-$) and water elimination is more favorable with a calculated value of -28.2 kcal/mol. The energy difference between $^1O_2$ and $^3O_2$ elimination corresponds to the O_2 singlet-triplet energy gap. Thus, our calculated gap value is 16.8 kcal/mol, somewhat smaller than the experimental value of 22.5 kcal/mol.[83] The fault likely lies with the singlet oxygen as DFT methods are known to have difficulty with open-shell singlets.[84] Thus, the value (-11.4) for conversion of **4a'** to **2'**, H_2O, and $^1O_2$ is likely ~6 kcal/mol too low.

As Pt(IV) complex photochemistry usually involves the lowest-energy triplet excited state, arrived at either through direct excitation or through rapid (fs) internal conversion and intersystem crossing,[42f, 42g] structures **4a'** and **4b'** were optimized as triplets. No intact structure is found for the triplet from **4b'**. Instead, optimization rapidly yields a "plateau" structure with a 5-coordinate Pt η^1-O_2 complex and a hydrogen-bonded water molecule. Further optimization gives **2'**, $^3O_2$, and H_2O, although a stationary point was not achieved

Table 3.2.1. Energies (DFT) for reductive elimination from 4a' (gas phase, 25 oC, 1 atm).

Products[a]	ΔG *(kcal/mol)*[b]
2' + H_2O_3	14.4
2' + H_2O + $^1O_2$ ($^1\Delta_g$)	-11.4[c]
2' + H_2O + $^3O_2$ ($^3\sum_g^-$)	-28.2

a **2'** = *trans*-Pt$(PMe_3)_2$(Cl)(4-tft). b These values will be somewhat more positive in solution due to the entropy difference between solution and the gas phase.[85] c From the known O_2 singlet-triplet energy gap this value is likely ~6 kcal/mol too low (see text).

.

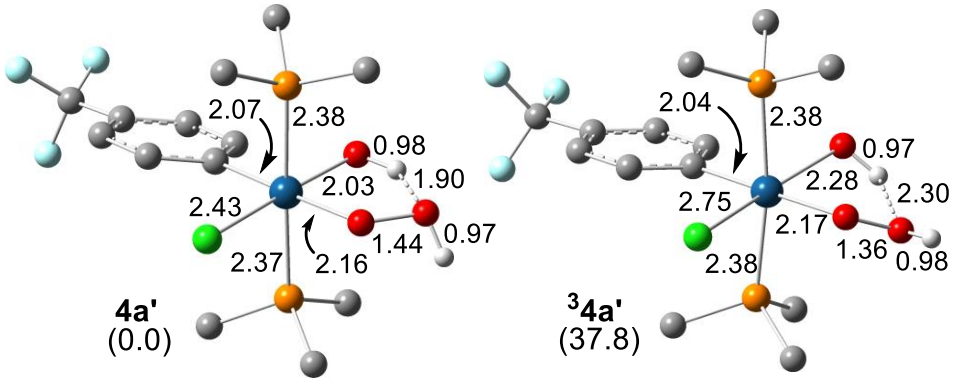

Figure 3.2.2. Optimized model structures 4a' and ^{3}4a' (bond distances in Å, blue = Pt, green = Cl, orange = P, red = O, grey = C, white = H, carbon-bonded H-atoms omitted). Calculated relative energies in kcal/mol in parentheses.

In contrast, the triplet from **4a'** optimizes to a stationary point (37.8 kcal/mol above **4a'**) with minimum structure **^{3}4a'** (Figure 3.2.2) containing intact OOH and OH ligands. A comparison of the metrical parameters of **^{3}4a'** with **4a'** shows that the bonds along the Cl-Pt-OH axis have lengthened and that the O-O bond has shortened. The shorter O-O distance in **^{3}4a'** is similar to that in the OOH radical[86] suggesting OOH radical character in **^{3}4a'**. This is supported by the Mulliken atom spin densities (Figure 3.2.3) which show nearly a full electron spin on the OOH ligand. Substantial spin density is also located on the OH ligand. Thus, **^{3}4a'** is a likely model precursor to H_2O_3 by coupling of the radical-like OH and OOH ligands. (H_2O_3 formation from OH and OOH radical coupling in photolyzed argon-matrix mixtures of H_2O_2 and O_3 has been proposed.[87]) Triplet **^{3}4a'** should also be a good OOH radical donor.

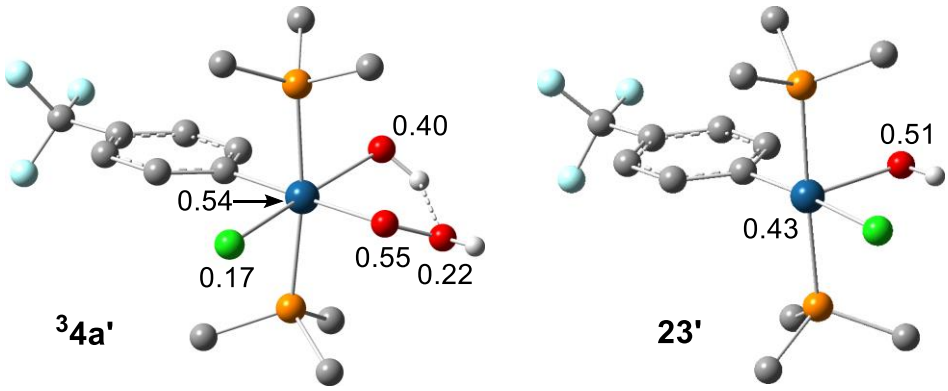

Figure 3.2.3. Mulliken atomic spin densities in ^{3}4a' and 23' (blue = Pt, green = Cl, orange = P, red = O, grey = C, white = H, carbon-bonded H-atoms omitted).

The thermal reductive elimination from **4** was also examined with DFT computations. Three pathways to dioxygen, water, and **2** were considered: 1) concerted H_2O_3 reductive elimination from **4a'** or **4b'** followed by rapid H_2O_3 decomposition to singlet oxygen and water, 2) intramolecular OOH ligand proton transfer to the OH ligand of **4b'** to give

dioxygen and water, and 3) OOH radical dissociation from **4a'** followed by abstraction of the OH ligand to form H_2O_3.

A concerted H_2O_3 reductive-elimination pathway was found but can be eliminated as the transition state is prohibitively high (68.3 kcal/mol) (SI). Relax potential energy scans (unrestricted) to promote proton transfer in **4b'** were conducted to probe the second pathway but failed to directly yield singlet oxygen. Instead, a scan along the O-H-OO coordinate gave η^2-O_2-complex **9'** (optimized to a stationary point) and water (Scheme 3.2.3). We have not been able to locate a transition state but the scan suggests a ~25 kcal/mol barrier, consistent with the experimental free energy of activation (24 kcal/mol at 298 K). The negative entropy of activation would also be consistent with the required H-bonding interaction. Separate water and **9'** lie 15.5 kcal/mol above **4b'**. (Note that **9'** is isoelectronic with known Ir(III) dioxygen complexes.[88]) A transition state (**TS9'**, SI) for dioxygen loss from **9'** was located at 7.6 kcal/mol above **9'** showing that formation of **9'** and water would be rate-limiting.

Scheme 3.2.3. Hydrogen bonding favorable toward direct elimination of H_2O and O_2.

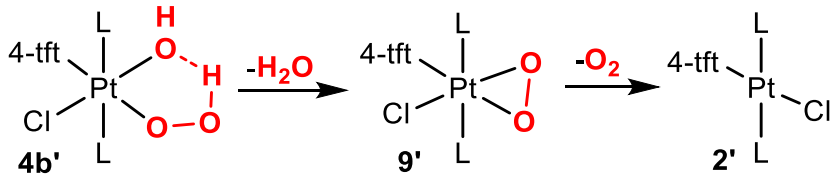

Thermolysis of the Pt-OOH bond of **4a'** was evaluated by calculating the energy difference between **4a'** and OOH radical plus doublet $Pt(PMe_3)_2(Cl)(OH)(4\text{-tft})$ **23'**. (Cl or OH radical loss is higher energy.) Geometry optimization of **23'** yielded three square-

pyramidal isomers with an axial OH ligand (**23'**), an axial Cl ligand (**23a'**) and an axial 4-tft ligand (**23b'**). The lowest-energy isomer is **23'** (4.1 kcal/mol to **23a'** and 11.7 kcal/mol to **10c'**) and with an OOH radical lies only 22.8 kcal/mol above **4a'** making Pt-OOH bond homolysis a viable first step in the thermal decomposition (Scheme 3.2.4). Coupled isomerization with Pt-OOH bond breaking could account for the experimental negative activation entropy. Additionally, spin density in **23'** is strongly localized on the OH ligand (Scheme 3.2.4) suggesting facile OH abstraction by the OOH radical and formation of H_2O_3.Crossing of the singlet thermal pathway and photochemical triplet pathway to H_2O_3 may occur at this point.

Finally, it should be noted that thermal access to the triplet is possible although triplet ^{3}**4a'** is calculated to be nearly 40 kcal/mol above singlet **4a'**. If the analogous triplet for **4** is situated at a similar energy relative to **4** then thermal access to the triplet would not be consistent with the activation parameters for the thermal elimination.

Scheme 3.2.4. Hydrogen bonding favorable toward elimination of H_2O_3.

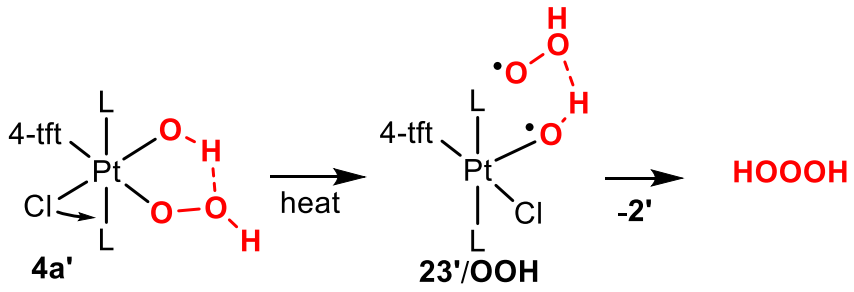

3.3 Conclusion.

In conclusion, hydroperoxo-hydroxo complex **4** has been found to photoreductively eliminate H_2O_3 in ~ 20% yield at -60 ^oC. DFT results suggest the photoreaction occurs through a triplet excited state (modeled with ^{3}**4a'**) with high OOH and OH radical character that leads to OH and OOH coupling. The hydrogen peroxide and acetone peroxides **19** and **20**, also formed in acetone-d_6, may be produced by "leakage" of OOH radicals from the excited state or, in the case of **19** and **20**, by direct reaction of acetone with the excited state. DFT results also suggest that the photolysis products may depend on the intramolecular hydrogen-bonding state of **4** with the lowest-energy state yielding the H_2O_3 products and a slightly higher state giving water and dioxygen. Thermolysis and room temperature photolysis of **4,** both give water and dioxygen. In both cases, trapping experiments with TME and DF give results generally inconsistent with trapping of singlet oxygen but consistent with trapping of H_2O_3. The small yield of singlet oxygen trapping product (**13**), observed with TME in the room temperature photolysis may result from partial decomposition of H_2O_3 to singlet oxygen and water prior to reaction with TME. Singlet oxygen emission experiments would provide information on the presence or absence of singlet oxygen in these reactions.[83b] Given the above results and our previous results[12,11] with analogous complexes, the *trans*-Pt(IV)L_2(R)X_3 system is proving to be a versatile platform for elimination chemistry. Other complexes that should eliminate unusual molecules are currently under investigation.

3.4 Experimental.

General procedures. *Trans,cis*-Pt(PEt_3)$_2$(Cl)(OH)(OOH)(4-tft) **4** and *trans*-Pt(PEt_3)$_2$Cl(4-tft) **2** synthesis have reported in Chapter 2 . Authentic samples of C(CH_3)$_2$(OOH)(OH) **19**[89] and C(CH_3)$_2$(OOH)$_2$ **20**[79] for NMR identification were prepared by literature methods. Reagents and solvents were purchased from commercial sources (Aldrich or Acros). Platinum complex photolysis samples were prepared under a dinitrogen atmosphere in a Vacuum Atmospheres Corporation drybox or on a Schlenk line. Photolysis solvents were purged with an N_2-stream and stored under an N_2 atmosphere in a drybox. NMR spectra were recorded on Bruker AMX-250, -300 and -500 spectrometers at ambient probe temperature or as noted. NMR shifts are given in δ with positive values downfield of TMS (^{1}H) or external H_3PO_4 (^{31}P). ^{31}P NMR spectra were recorded in proton-decoupled mode. Photolysis were performed at -78 ˚C in quartz (UV) or borosilicate glass NMR tubes using a home-built tube photoreactor, which consisted of a short section of 4.2 cm PVC pipe lined with 32 LED's (380 nm, superbrightleds.com, RL5-UV031) connected in series.

NMR data for trans-Pt(PEt3)2(Cl)(OH)(OOH)(4-tft) (4). ^{31}P NMR (101 MHz, toluene-d_8): 2.9 (s with satellite, J_{PtP} = 1800 Hz). ^{31}P NMR (101 MHz, acetone-d_6): 3.4 (s with satellite, J_{PtP} = 1800 Hz)**.** ^{1}H NMR (300 MHz, toluene-d8): 8.36-8.28 (m, 2H), 7.38-7.29 (m, 2H), 1.90-1.60 (m, 12H, CH_2), 0.98-0.75 (m, 18H, CH_3), OOH was observed as a broad singlet at 8.5-7.5 region. ^{1}H NMR (300 MHz, acetone-d_6): 8.7 (s, OOH), 8.30-8.05 (m, 2H), 7.43- 7.30 (m, 2H), 2.05-1.85 (m, 12H, CH_2), 1.15-0.95 (m, 18H, CH_3).

NMR data for trans-Pt(PEt$_3$)$_2$(Cl)(4-tft) (2). ^{31}P NMR (101 MHz, toluene-d$_8$): 14.4 (s with satellite, J_{PtP} = 2770 Hz). ^{31}P NMR (101 MHz, acetone-d$_6$): 15.7 (s with satellite, J_{PtP} = 2770 Hz).

Photolysis of *trans*-Pt(PEt$_3$)$_2$(Cl)(OH)(OOH)(4-tft) (4).

Ambient Temperature. Complex **4** (8.0 mg, 0.012 mmol, 0.024 M) in 0.5 mL C_6D_6 was photolyzed at 380 nm for 8 min. ^{1}H and ^{31}P NMR spectroscopy showed the formation of **2** and water.

With 2,5-dimethylfuran (DF). Complex **4** (5.7 mg, 0.0087 mmol, 0.017 M) and 2,5-dimethylfuran (0.65 M) in C_6D_6 (0.50 mL) were photolyzed at 380 nm for 10 min. ^{31}P NMR spectroscopy showed the formation of **2** and ^{1}H NMR spectroscopy showed 2,5-dimethylfuran endoperoxide dimer (25%). ^{1}H NMR (250 MHz, C_6D_6): 5.48 (s, 2H),1.77 (s, 6H). The dimer was converted to diketone 3-ene-2,5-hexadione by PPh_3 addition[90] and then the solvent was changed to CCl_4 for comparison to the literature NMR data.[91] The ^{1}H NMR spectrum matched that reported. ^{1}H NMR (250 MHz, CCl_4): 6.61 (s, 2H), 2.25 (s, 6H).

With 2,3-dimethyl-2-butene (TME). Complex **4** (9.0 mg, 0.014 mmol, 0.027 M) and 2,5-dimethylfuran (0.35 M) in CD_2Cl_2 (0.50 mL) were photolyzed for 30 min (slow conversion) at 380 nm. Subsequent ^{31}P NMR spectroscopy showed the formation of **2** and ^{1}H NMR spectroscopy showed acetone (4.0 %), tetramethyl-1,2- dioxetane (9.0 %) , 3-2,3-dimethyl-3-hydroperoxy-1-butene (8.0%).[57] The identity of the dioxetane was confirmed by comparison to a sample in CD_3CN[82] and by further photolysis to acetone.

Low Temperature. Complex **4** (8.5 mg, 0.013 mmol, 0.026 M) was dissolved in 0.5 mL acetone-d_6 or toluene-d_8 and then transferred into an NMR tube. The tube was placed into a dry ice/acetone filled Dewar with an unsilvered finger (Figure 1). The cold sample was then photolyzed at 380 nm for ~13-16 min (approximately 50% conversion of **4** into **2**). After photolysis the NMR tube was quickly (<30 s) transferred to the precooled (-60 ˚C) NMR spectrometer probe for recording the NMR spectra (Figs S13-S18). The ^{1}H NMR spectrum in acetone-d_6 showed peaks for H_2O_3,[25,26] H_2O_2,[25] $C(CD_3)_2(OOH)_2$,[79] $C(CD_3)_2(OOH)(OH)$ (Figure 3.4.1), and *trans*-Pt$(PEt_3)_2$Cl(4-tft) **2**. The spectrum in toluene-d_8 showed only H_2O_3,[26] and **2**.

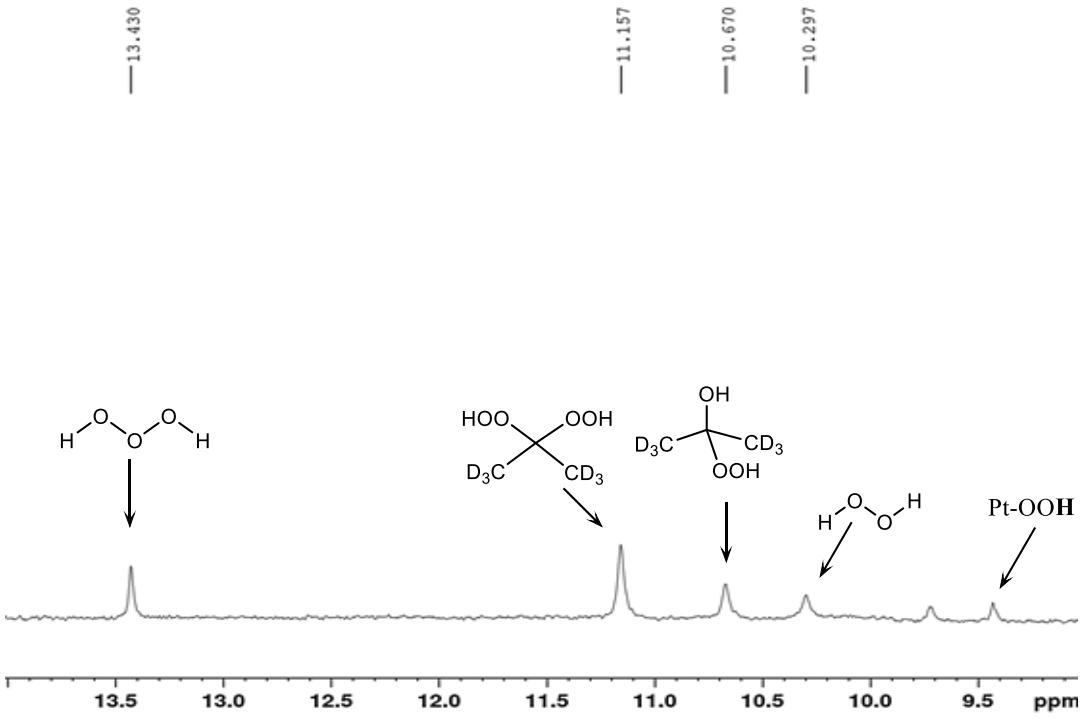

Figure 3.4.1. The down field region (δ 14-9) of the 1H NMR spectrum obtained from photolyized 4 in acetone-d6 at -78℃ (The Pt-OOH signal shifts downfield upon sample cooling to -60˚C) The small signal at δ 9.7 is unidentified. The Pt-OOH peak is from remaining 4.

H_2O_3 reaction with TME

Complex **4** (11.0 mg, 0.017 mmol, 0.0 33M) was dissolved in 0.5 mL toluene-d_8 and photolyzed at 380 nm for 15 min at -78 ˚C. The sample was transferred to the precooled (-65˚C) ^{1}H NMR probe and H_2O_3 (14 % yield) was observed. The sample was then transferred to a -78˚C bath and TME (~ 20 μL) dissolved in toluene-d_8 (0.15 mL) was added. The sample was immediately transferred back into the ^{1}H NMR probe at -65˚C and the spectrum showed no H_2O_3. The TME product, tetramethyl-1,2- dioxetane (36 % yield based H_2O_3 present), was observed at δ 1.11 and converted to acetone (δ 1.57) by photolysis after warming to room temperature.

DF reaction with $^1O_2$ generated by *meso*-tetraohenylporphyrin (TPP).

TPP (1.50 mg) was dissolved in 0.70 mL of a DF (~20 μL) solution in C_6D_6. The mixture was saturated with O_2 and then photolysed at 470 nm for 3 min. The ^{1}H NMR spectrum (250 MHz, C_6D_6) showed the endoperoxide **21** at δ 5.81 (s, 2H), 1.42 (s, 6H). Heating the sample at 75˚C for 5 min converted **21** to dimer **22**: δ 5.48 (s, 2H), 1.77 (s, 6H).

Thermal decomposition of 4

With 2,5-dimethylfuran (DF). Complex **4** (5.7 mg, 0.0087 mmol, 0.017 M) was dissolved in 0.5 mL of a 0.65 M 2,5-dimethylfuran solution in C_6D_6. The mixture was heated at 78 ˚C for 15 min. ^{31}P and ^{1}H NMR spectroscopy showed the formation of **2** and 2,5-dimethylfuran endoperoxide dimmer (14%). ^{1}H NMR (250 MHz, C_6D_6): 5.48 (s, 2H), 1.77 (s, 6H).

With 2,3-dimethyl-2-butene (TME). Complex **4** (5 mg, 0.0076 mmol, 0.015 M) was dissolved in 0.5 mL of a 0.40 M TME solution in C_6D_6. The mixture was heated at ~70 ˚C for 10 min. ^{31}P and ^{1}H NMR spectroscopy showed formation of **2** and tetramethyl-1,2- dioxetane (15 %). ^{1}H NMR (250 MHz, C_6D_6): 1.12, s, 12H. The dioxetane was converted to acetone by irradiating the sample at 313 nm for 20 min. The identity of the dioxetane was confirmed by comparison to a sample in CD_3CN.[82]

The rate constants for the thermal decomposition of **4** (6.0 mg, 0.0091 mmol) in 0.50 mL of toluene were determined at four temperatures (65, 70, 75 and 80℃) by ^{31}P NMR spectroscopy at probe temperature. Multiple spectra were collected at constant time intervals. Percentage conversion of **4** at each time interval was determined by integration. The thermally stable complex *trans,cis*-Pt(IV)$(PEt_3)_2Cl_2$(OH)(4-trifluoromethylphenyl) was used as an integration internal standard for the reaction at 80 ºC and confirmed a 100% conversion of **4** to **2**.

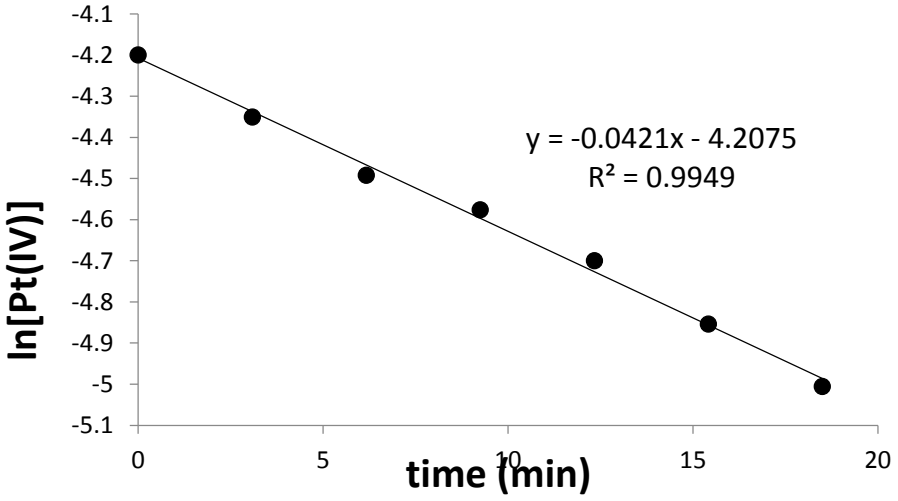

Figure 3.4.2. Plot of ln[4] vs time for the first-order decomposition of 4 in toluene at 65℃.

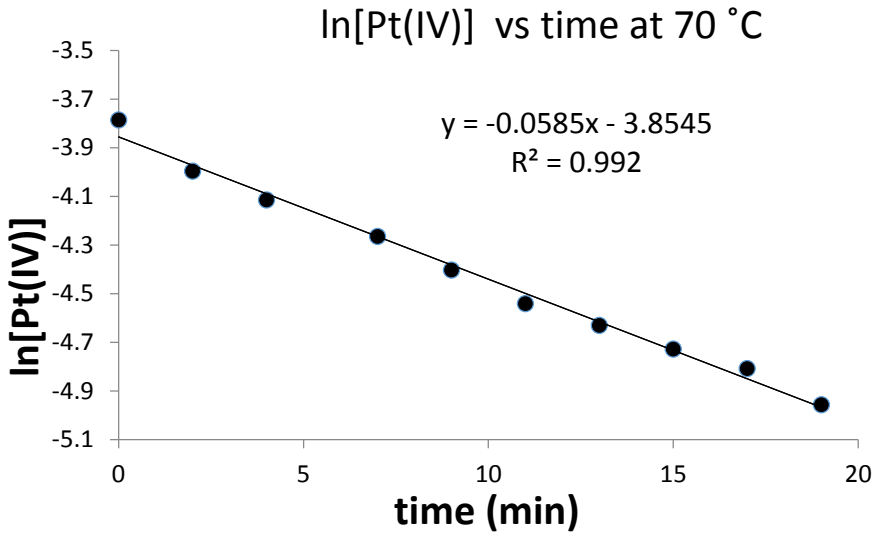

Figure 3.4.3. Plot of ln[**4**] vs time for the first-order decomposition of **4** in toluene at 70℃.

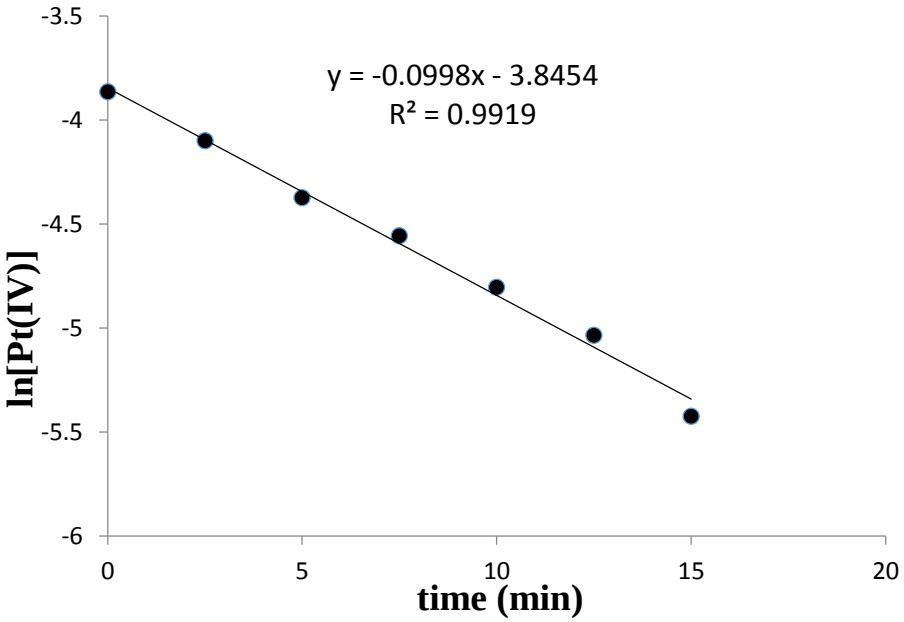

Figure 3.4.4. Plot of ln[**4**] vs time for the first-order decomposition of **4** in toluene at 75℃.

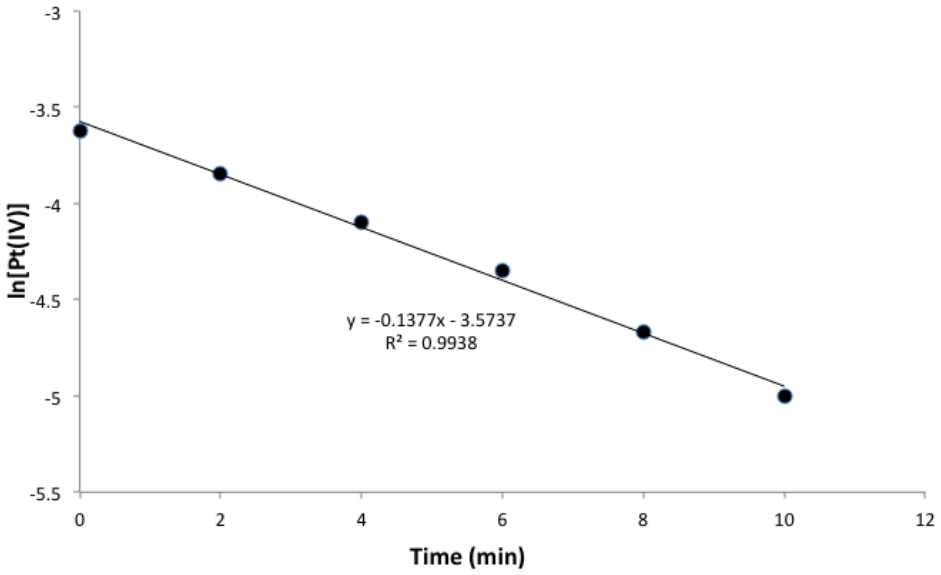

Figure 3.4.5. Plot of ln[**4**] vs time for the first-order decomposition of **4** in toluene at 80℃.

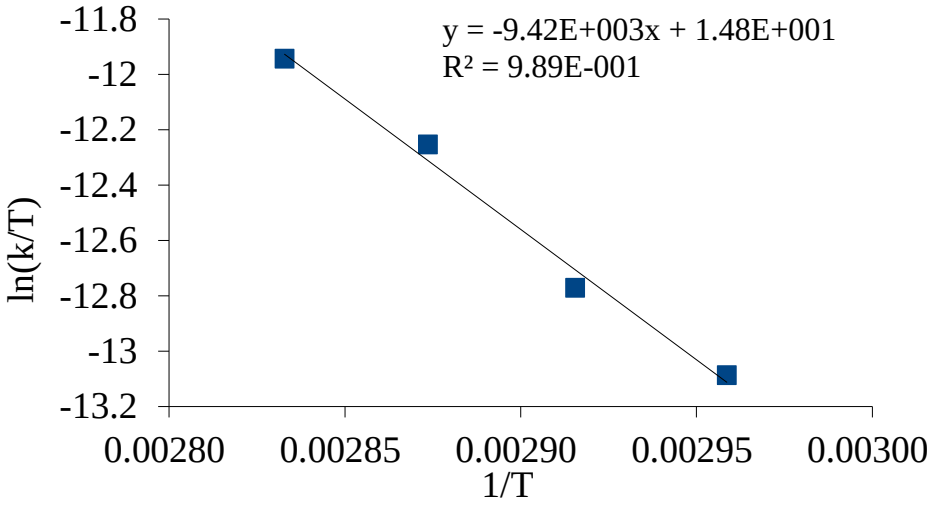

Figure 3.4.6. Rate constant/T vs 1/T plot for the thermal decomposition of 4 in toluene at 65, 70, 75 and 80℃.

Application of the Eyring equation yielded the activation parameters given below. Data were analyzed using the LINEST function in the Microsoft EXCEL program.

Temp (°C)	**Temp (K)**	**1/T(K)**	**Rate constant (s^{-1})**	**ln(k/T)**
65	338	0.00296	7.00E-004	-13.09
70	343	0.00292	9.75E-004	-12.77
75	348	0.00287	1.66E-003	-12.25
80	353	0.00283	2.30E-003	-11.94

slope =	-9.42E+003	enthalpy (kJ/mol)=	78.32	in kcal/mol	18.72
Intercept=	1.48E+001	entropy (J/Kmol)=	-74.50	in cal/Kmol	-17.81
R (J/Kmol)=	8.3145				
kb (J/K)=	1.38E-023	free energy (298K)=	100.5	in kcal/mol	24.03
h =	6.63E-034				
		Enthalpy std=	5.77	in kcal/mol=	1.34
		Entropy std=	16.7	in cal/Kmol=	3.99

CHAPTER 4: HYDROXO RADICALS, C-H ACTIVATION AND PT-C BOND FORMATION

4.1 Introduction.

Transition metal hydroxo complexes are attracting considerable interest as key species in hydrocarbon oxidation,[92] C-H activation,[93] water oxidation,[94] solar energy conversion and storage,[8, 73c, 73e, 95] and in other catalytic schemes.[73d, 96] Room-temperature photolysis of *trans,cis*-$Pt(PEt_3)_2Cl_2(OH)(4\text{-tft})$ leading to HOCl elimination have thoroughly discussed in chapter 2. Here we discuss chemistry derived mainly from the hydroxo radical, unlike reductive elimination of simple molecules. This discussion is laid out mainly as initial observations of this chemistry (section 1) and its advancement (section 2). Firstly, we report an unusual result obtained from 77 K photochemistry of *trans,cis*-$Pt(PEt_3)_2Cl_2(OH)(4\text{-tft})$, which leads to a sequence of hydroxo radical formation, C-H activation, Pt-C bond formation, and C-Cl reductive elimination. Secondly, the advancement of this chemistry with necessary modification to the metal complex, mainly via intramolecular hydrogen bonding. The initial result of C-H activation and Pt-C bond formation was first obtained by photolysis of *trans,cis*-$Pt(PEt_3)_2Cl_2(OH)(4\text{-tft})$ in frozen matrix and it is quite different from room temperature photolysis. The potential importance of intramolecular hydrogen bonding in the photochemistry of Pt(IV) hydroxo complexes was highlighted for *trans,cis*-$Pt(PEt_3)_2(Cl)(OH)(OOH)(4\text{-tft})$ **4** in previous chapter where DFT calculations suggested that the hydrogen-bonding pattern of the hydroxido and the hydroperoxido ligands could affect the outcome of the photochemistry. Changing the OOH in complex **4** into a carboxylate ligand is expected to have stronger

hydrogen bonding to the OH hydrogen. Remarkably, this simple modification gave results similar to that of the 77 K photolysis, but in solution phase at room temperature as well as -78℃. Even though intramolecular hydrogen bonding is observed for complex **4**, irradiation of **4** under similar condition (in CD_2CL_2) does not yield any of the above results. This remarkable change inspired us to study this chemistry further seeking more information as regards the behavior of the hydroxo radical.

4.2 Section 1: Results and discussion for *trans,cis*-$Pt(PEt_3)_2(Cl)_2(OH)$(4-tft) photolysis at 77 K.

Irradiation (380 nm) of *trans,cis*-$Pt(PEt_3)_2(Cl)_2(OH)$(4-tft) **6** for several hours in glassy 2-methyltetrahydrofuran (MeTHF) or toluene at 77 K followed by warming to room temperature gives a mixture of a new complex **24** and *trans*-$Pt(PEt_3)_2(Cl)$(4-tft) **2** (Scheme 4.2.1). (Yields in Scheme 4.2.1 were determined by ^1H NMR integration against an internal standard.) Complex **2** is the sole Pt-containing product at room temperature and it is produced in minutes instead of hours (discussed in Chapter 2).

Scheme 4.2.1. Photolysis of **6** at 77 K in glassy solvents and formation of phospha-platinacycle at 298 K.

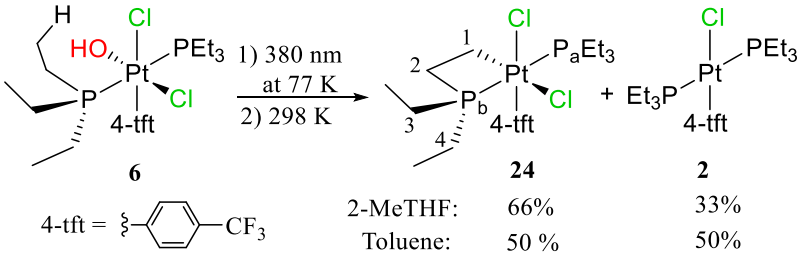

New **24** is unstable at room temperature (~ 4 h to decay) and was not isolated but is readily characterized by NMR spectroscopy as the phospha-platinacycle pictured in

Scheme 4.2.1. Most diagnostic for the formation of **24** is the ^{31}P NMR shift for the P atom in the 4-membered ring. Four-membered ring ^{31}P NMR signals are strongly upfield shifted from those not in a ring[97] and this is observed in **24** where the ring-P_b signal is at δ -65, while that for the unaltered PEt_3 ligand (P_a) is at δ -7.7, near that of **6** (The P centers are coupled to each other (doublet, J_{PP} = 513 Hz) and to ^{195}Pt with J_{PtP} = 1853 Hz (PEt_3) and 1410 Hz (P_b) (see Figure 4.2.1). ^1H-^1H COSY and ^1H-^{13}C HMQC NMR spectroscopy and comparisons to data for Pt(II) phospha-platinacycle complexes[98] allowed identification and assignment of all ^1H NMR shifts for **24**. The ring-system methylene protons appear as diastereotopic pairs. The Pt-bonded methylene group protons, H_{1a} and H_{1b}, are found at δ 2.71 and 1.73, and are bonded to the same carbon, C1, found at δ -0.2 in the ^{13}C NMR spectrum. The P-bonded methylene group protons are located at δ 2.98 and 2.37, and are bonded to C2, found at δ29.7 in the ^{13}C NMR spectrum. The diastereotopic nature of the methylene protons establishes a *cis* configuration for the chloro ligands and the stereochemistry for **24** given in Scheme 4.2.1.

After several hours at room temperature in toluene-d_8 or MeTHF, or more rapidly in chloroform, platinacycle **24** completely converts to Pt(PEt_3)($Et_2PCH_2CH_2Cl$)(Cl)(4-trifluoromethylphenyl) **25** by reductive elimination (Scheme 4.2.2). The ^{31}P NMR spectrum of **25** shows two closely-spaced signals at δ 13.7 and 13.0 with ^{195}Pt satellites (J_{PtP} = 2770 and 2722 Hz, respectively). The shifts and coupling constants are very similar to those of **2**,[99] consistent with the formation of an analogous Pt(II) complex. The ^1H NMR spectrum shows a distinctive set of multiplets at δ 3.87 and 2.25 assigned to the chloroethyl group. A crystal grown from the mixture of **2** and **25**was subjected to an X-ray crystal structure analysis, which showed that **2** and **25** co-crystallized in an 11:14

ratio (Figure 4.2.2). Complex **24** is also photo-decomposed (380 nm) to **25** at room temperature or at 77 K. (A Au(III) complex was recently reported to undergo photolytic reductive elimination of aryl chloride.[100]

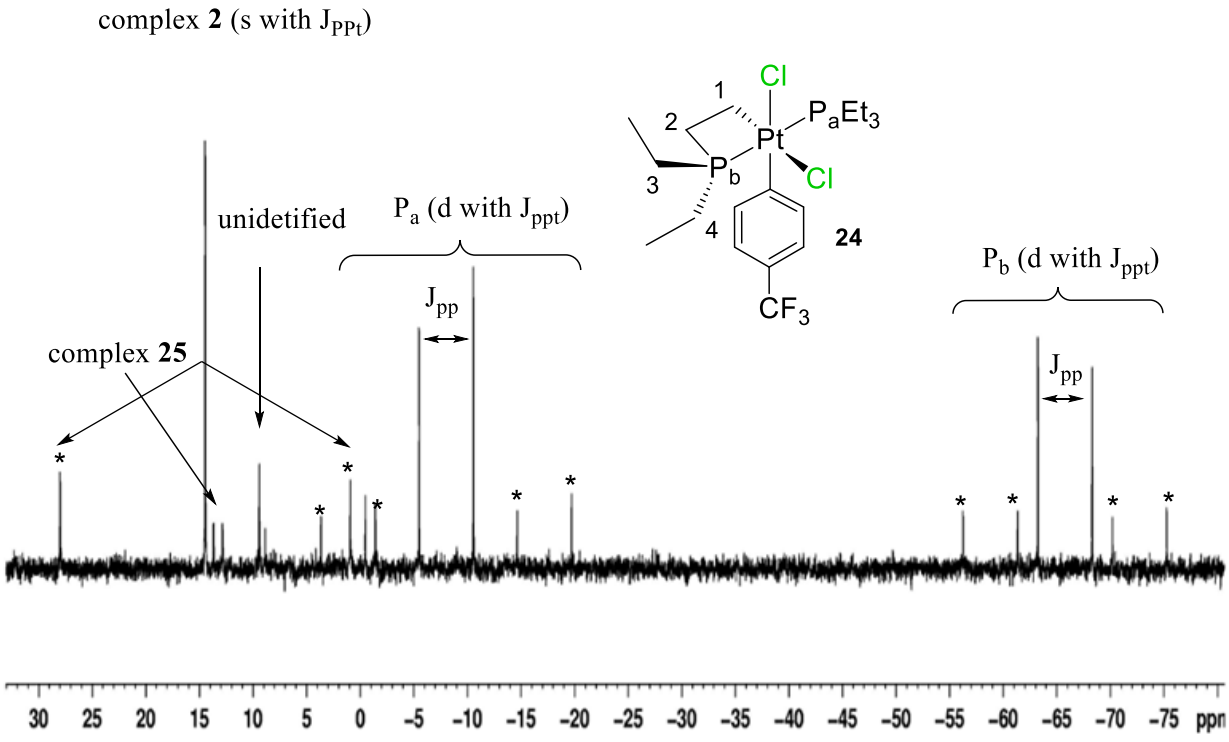

Figure 4.2.1. 31P NMR spectrum observed for 24 and 2 in MeTHF (* represent satellite and signal at δ 9.40 is an unidentified compound with 5 % yield).

Scheme 4.2.2. Reductive elimination of alkyl chloride from phospha-platinacycle.

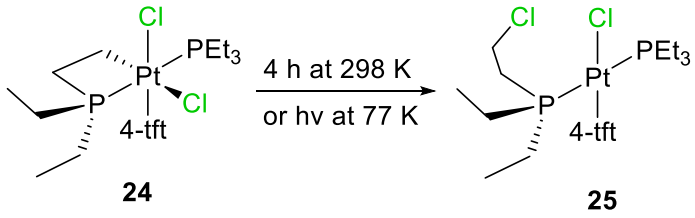

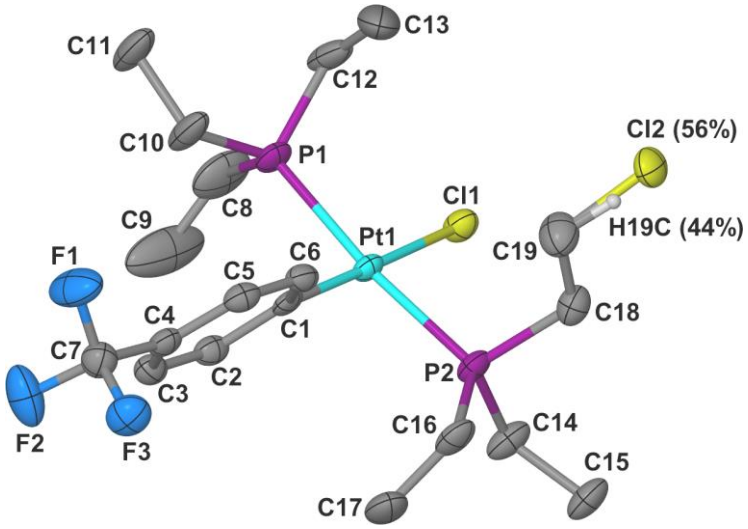

Figure 4.2.2. Drawing of the solid-state structure of co-crystallized 2 (44%) and 25 (56%).

In addition to its photochemical reactivity, **6** is photoluminescent in MeTHF glass at 77 K. Irradiation at 380 nm gives visible salmon-pink emission (λ_{max} = 620 nm). The emission lifetime (38 μs) and the intensity decrease as the photolysis progresses indicate that emission is from a triplet excited state of a species that is photo-decaying, in other words, the emission is from a triplet of **6**. Remarkably, our previously reported DFT calculations (in Chapter 2) of the lowest-energy triplet and singlet of the PMe_3 analog of **6** gave a ground-state singlet to lowest-energy triplet gap corresponding to 630 nm.[99] The calculations also indicate high spin density on a loosely bonded OH ligand in the triplet excited state. Switching solvent from MeTHF to toluene-d_8 changes the emission to blue, which, in contrast to the salmon-pink emission, brightens as the photolysis progresses. The blue emission spectrum (Figure 4.2.3) is characteristic of the benzyl radical.[101]

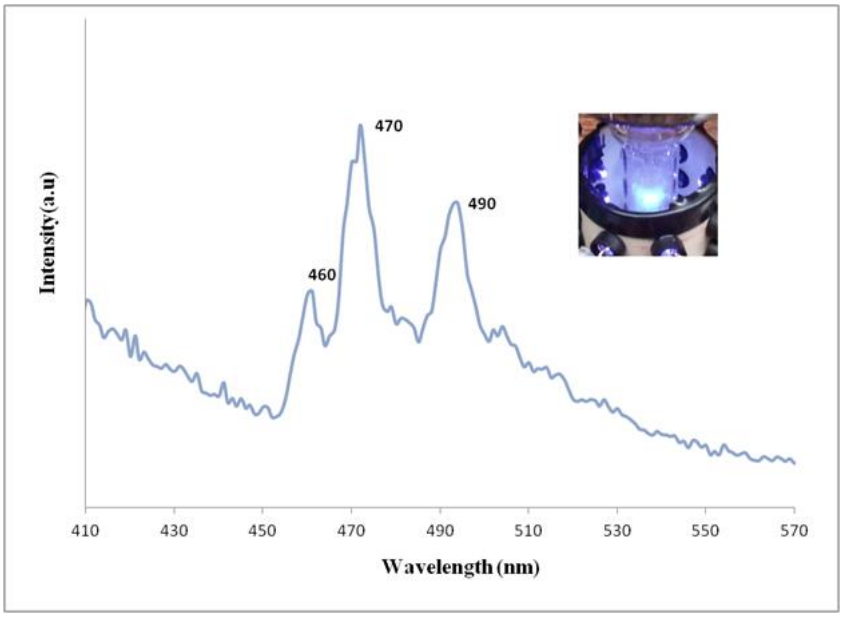

Figure 4.2.3. Benzyl radical emission spectrum from toluene photolyzed sample of 6 at 77 K. Insert shows visible blue emission during photolysis (λ = 380 nm).

The picture (Scheme 4.2.3) that thus emerges is that photolysis of **6** generates a triplet excited state (**6**^{T}) that decays to the ground state by emission or progresses to a geminate Pt(III)/OH radical pair (**A**). The highly reactive OH radical then abstracts H-atoms from solvent or the PEt_3 ligand with the ratio depending on the solvent. Greater solvent reaction occurs with the weak C-H bonds of the toluene methyl group and less with the stronger MeTHF bonds (Scheme 4.2.1). Warming the frozen matrix results in carbon/Pt(III) radical pair (**B**) coupling to form platinacycle **24**. Platinacycle **24** formation must occur as the frozen matrix is warmed as it is photosensitive to reductive elimination, even at 77 K. The possibility that coupling of the solvent radical and the Pt(III) radical occurs on warming to give a Pt-solvent complex that then reductively eliminates to give chlorinated solvent can be eliminated since Pt-solvent complexes are not observed by

low-temperature NMR of a photolyzed sample warmed from 77 K to -60 °C; only **2** and **25** are detected.

Scheme 4.2.3. Proposed mechanism for the overall observation.

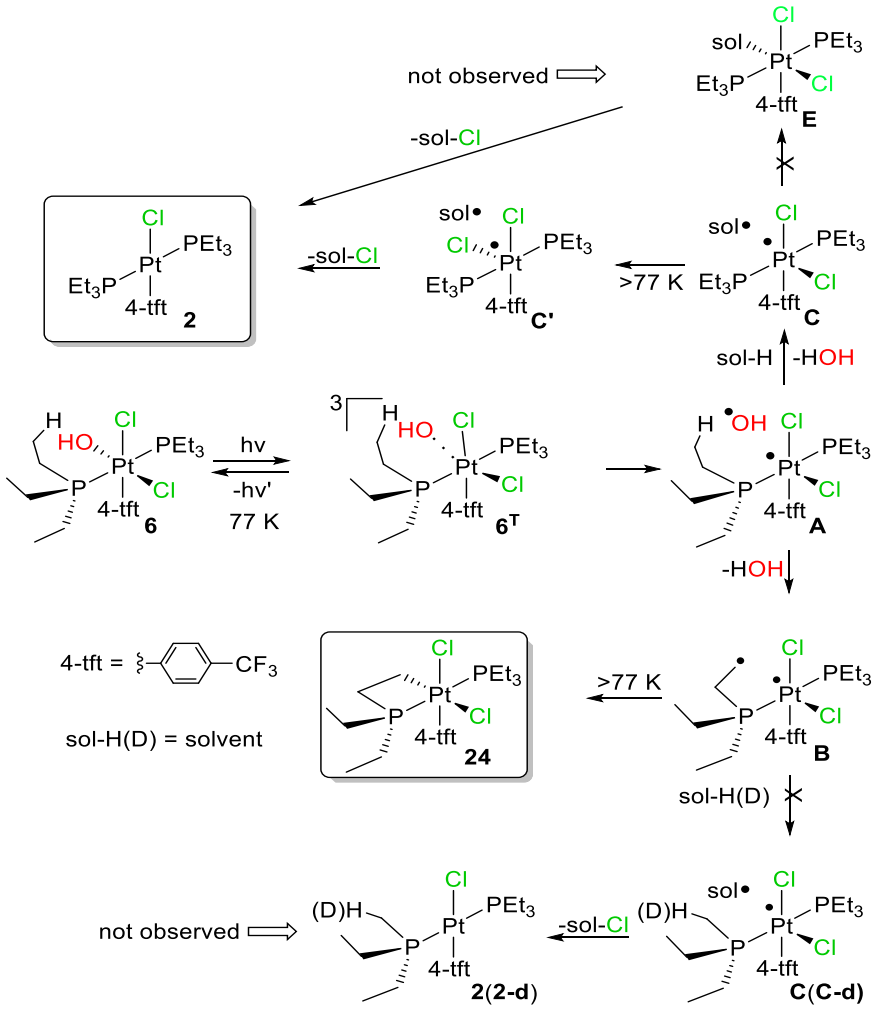

A question that arises is why is the 77 K frozen matrix photochemistry of **6** different from the room temperature solution photochemistry (net HOCl elimination[99])? A likely explanation is that in the frozen matrix the PEt_3 ligand may be locked into a position

favorable for abstraction and the Cl ligand may be inhibited from attaining a position favorable for abstraction.

4.3 Section 2: Results and discussion for the advancement of the hydroxo radical chemistry discussed in previous section.

The synthesis of new Pt(IV)(OH) complexes with carboxylate ligands (**26**, **27**, and **28**) in place of the hydroperoxo ligand were accomplished by simple protonation of the OOH ligand in **4** with acids (Scheme 4.3.1).

Scheme 4.3.1. Protonation of the OOH ligand in 4 with acids.

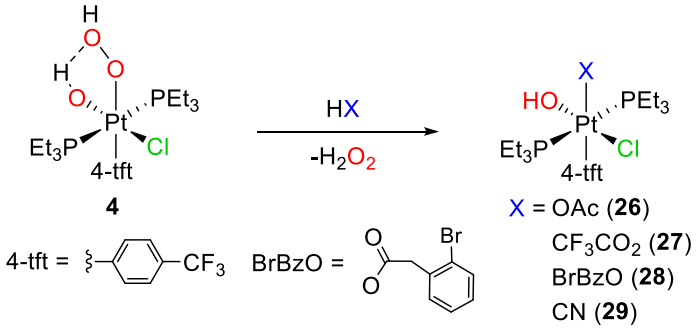

As shown by the solid-state structures for **26** (Figure 4.3.1) and **27** (Figure 4.3.2), there is strong intramolecular hydrogen bonding between the carboxylate and the hydroxo ligands. The hydroxo ligand ^{1}H NMR resonances in **26**, **27**, and **28** also indicate hydrogen bonding and are downfield shifted compared to the OH signal in non-hydrogen bonded **6**. Complex **27** shows a slightly longer hydrogen bond to the carbonyl group than in **26** (O1--O3 = 2.840(6) Å for **27**, 2.815(3) Å for **26**) consistent with the expected weaker hydrogen bond acceptor properties of the trifluoroacetate ligand.

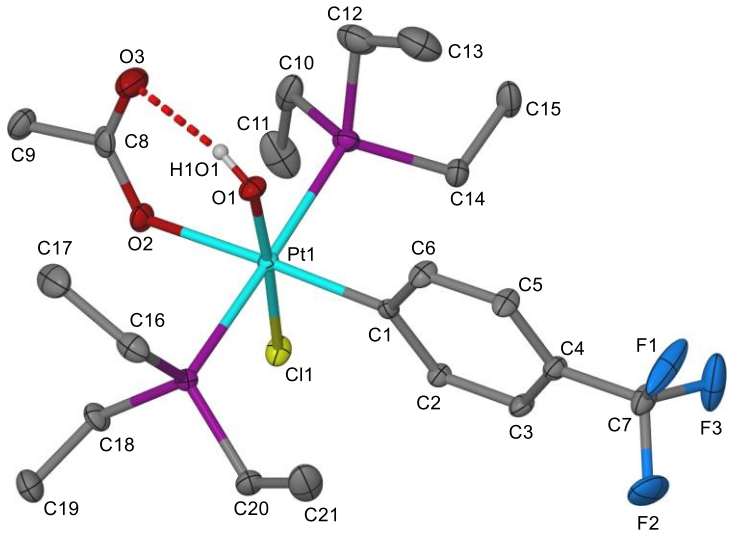

Figure 4.3.1. Drawing of the solid-state structure of trans-Pt(PEt_3)$_2$(4-tft)(Cl)(OH)(OAc) **26** (50% probability ellipsoids, hydrogen atoms omitted). Rotational disorder in the CF3 group is not shown. Distances (Å): O3-O1 = 2.815(4), O1-H1O1 = 0.75(3), O3--H1O1 = 2.11(3)

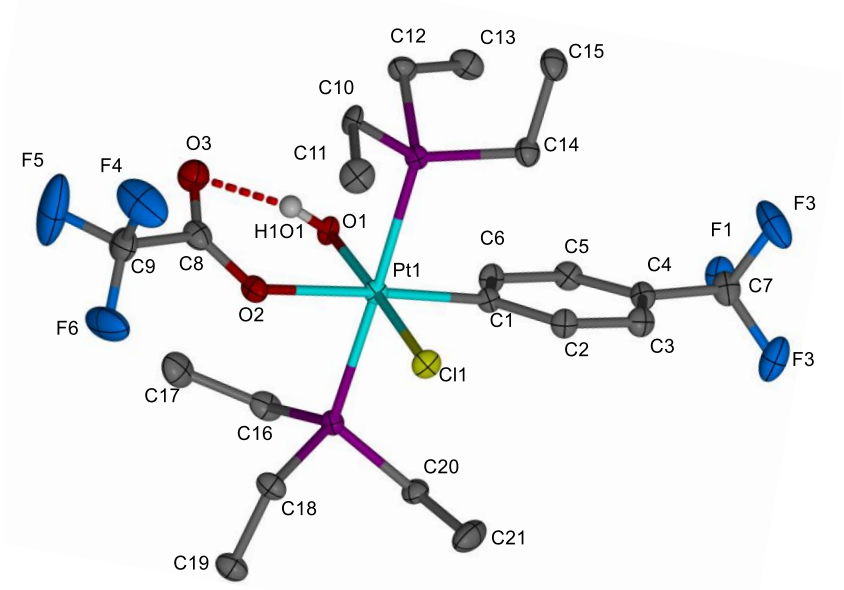

Figure 4.3.2. Drawing of the solid-state structure of trans-Pt(PEt_3)$_2$(4-tft)(Cl)(OH)(CF_3CO_2) 27 (50% probability ellipsoids, hydrogen atoms omitted).

Scheme 4.3.2. Photolysis of Pt(IV)(OH)(carboxylate) at -78 or 25 ^{o}C.

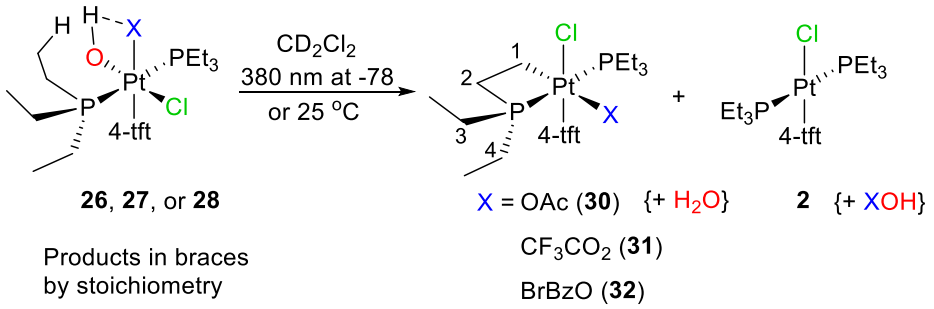

Remarkably, photolysis (380 nm) of **26**-**28** at room temperature in CD_2Cl_2 gives C-H activation products phospha-platinacycles **30**-**32** in yields as high as 50% (Scheme 4.3.2, Table 4.3.1). At -78 °C the yields of the phospha-platinacycles increase to as high as 90%. The choice of solvent for the photolysis is critical and in toluene the yield of **30** from **26** is 0 at 25 °C and 50% at -78 °C. Since our original studies of **6** were in MeTHF and toluene we repeated the photolysis of **6** in CD_2Cl_2. As before, at 25 °C phospha-platinacycle **24** is not detected and **2** is the only product. At -78 °C, the yield of **2** drops to 45% and some **24** is formed (15%) but the major secondary product is $OPEt_3$ (24%).

^{31}P spectra of phospha-platinacycles **30**-**32** are similar to that of previously reported **24** (Figure 4.2.1). Signals for the platinum-bonded phospha-platinacycle carbon atoms (C1) are also evident in the ^{13}C-DEPT NMR (Figure 4.3.3) and HMQC NMR (Figure 4.3.4) spectra and show platinum coupling and two bonded diastereotopic protons. Except complex **30**, the other phospha-platinacycles were not attempted to fully characterize. What has changed with the new complexe **30** is the ^{1}H NMR signals for the 4-tft ligand ortho-protons. In **24**, only one signal is observed whereas in **30** have two signals due to slow 4-tft rotation on the NMR time scale. As this change is most likely due to a change in the ligand *cis* to the 4-tft ligand we assign the structures of **30**-**32** as shown in Scheme 4.3.2.

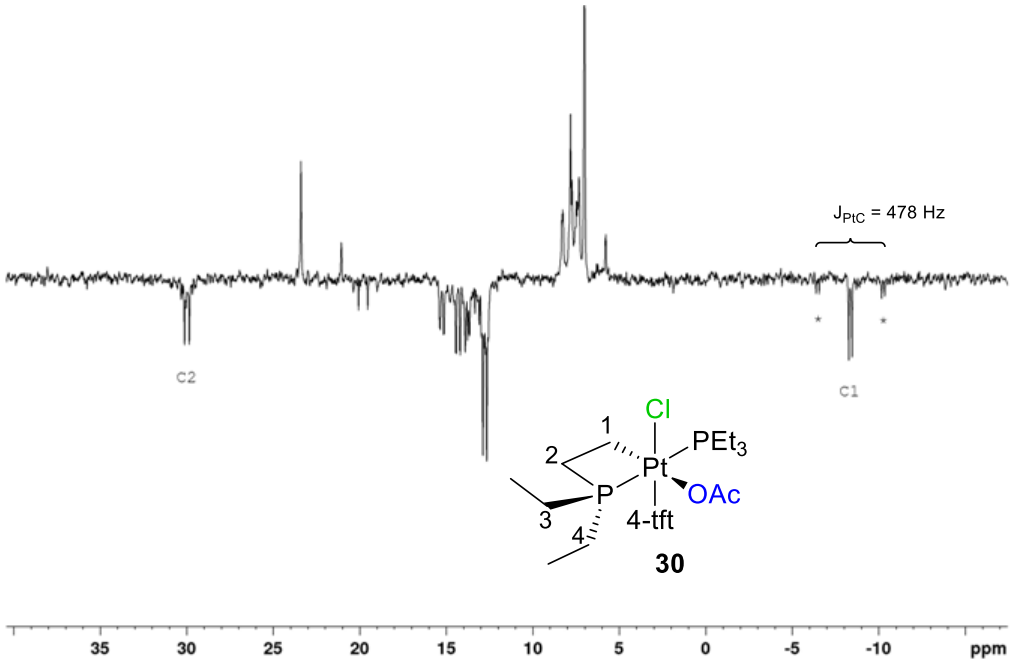

Figure 4.3.3. The ^{13}C-DEPT NMR spectrum of **30** showing ^{195}Pt satellites on C_1.

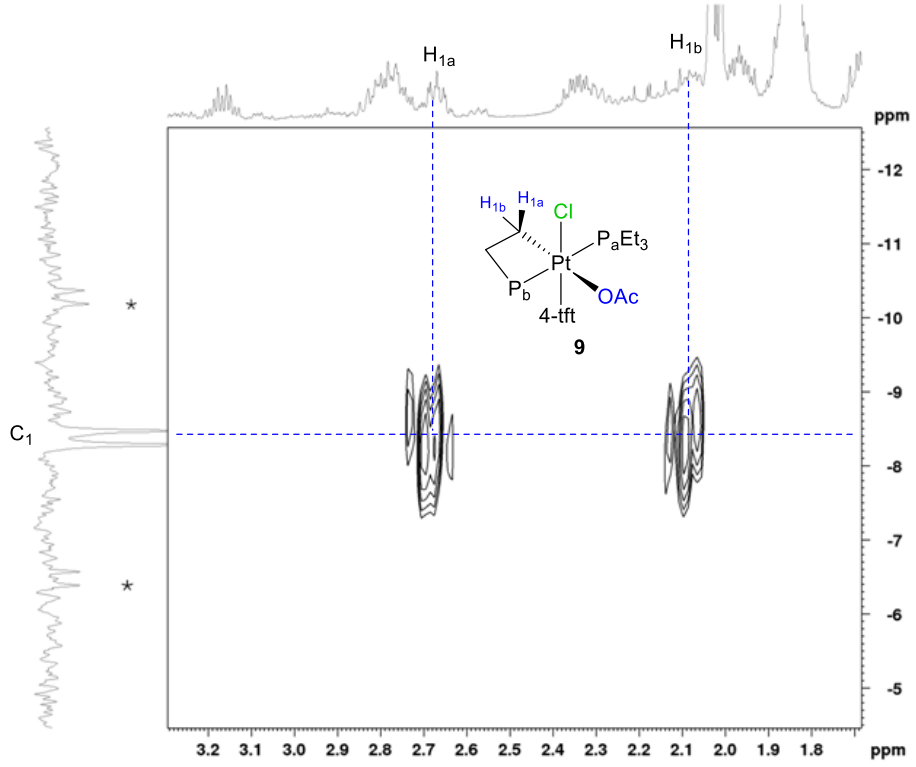

Figure 4.3.4. The ^{13}C-^{1}H HMQC NMR spectrum of **30** showing C_1 correlation with H_{1a} and H_{1b}. Asterisks mark ^{195}Pt satellites.

Table 4.3.1. Photolysis products (%)a from trans-Pt(PEt_3)$_2$(Cl)(X)(OH)(4-tft) in CD_2Cl_2.

X	-78 ℃		25 ℃	
	platinacycle	Pt(II)[b]	platinacycle	Pt(II)[b]
OAc (**26**)	90	10	50	50
O_2CCF_3 (**27**)	90	10	15	85
 (**28**)	81	19	50	50
CN (**29**)	30	70	0	95[e]
Cl (**6**)	15[c]	45[c]	0	100
OAc (**26**) (in toluene)	50[d]	50[d]	0	100

[a] Yields determined by ^{31}P NMR spectral integration. [b] Pt(II) = *trans*-Pt(PEt_3)$_2$(4-tft)X or *trans*-Pt(PEt_3)$_2$(4-tft)Cl. [c] $OPEt_3$ (24%) and other unidentified products also observed. [d] Same at 77 K (LN_2). [e] Remaining unidentified product observed at δ17 (s) in ^{31}P NMR spectrum.

Scheme 4.3.3. Photo isomerization of phospha-platinacycle.

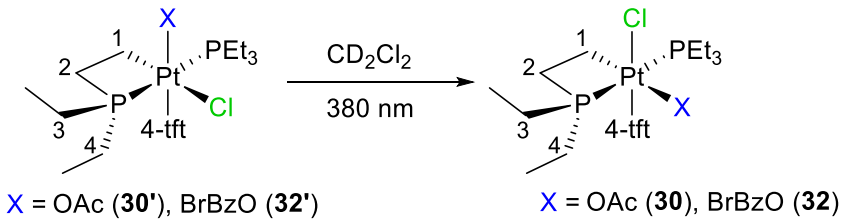

Monitoring the photolysis of **26** shows the formation of a second phospha-platinacycle **30'.** Both **30** and **30'** initially grow in together in a 1:1 ratio but as the photolysis continues **30'** converts to **30** (Scheme 4.3.3). We assign the structure of **30'** to the isomer of **30** where the chloro ligand, instead of the OAc ligand, is *cis* to the 4-tft ligand (Scheme 4.3.3). Consistent with this assignment the ^{1}H NMR spectrum of **30'** shows only

one *ortho*-tft proton signal, the same as **24** which also has a chloro ligand *cis* to the 4-tft ligand. Careful examination of the ^{31}P NMR spectra of **32** also reveals low concentrations of a second phospha-platinacycle which we assign as the isomer (**32'**) with same structure as **30'**. No other isomer was detected from **31**.

The above results suggest that intramolecular hydrogen bonding to the hydroxo group is an important factor in the formation of the phospha-platinacycles. However, the *cis* ligand, subject to abstraction, has also been changed and this may have suppressed the competitive formal reductive elimination to give **2**. We investigated this possibility by DFT (gas phase) and by the synthesis and photolysis of two other complexes. The free energy of AcOOH reductive elimination for **26** was calculated and compared to the previously calculated value for HOCl reductive elimination from **6**. The values are essentially identical at 32.8 (**26**) and 32.3 kcal/mol (**6**) indicating that the net thermodynamics of the elimination are unchanged. The removal of a Cl radical from Pt(III) doublet *trans*-$Pt(PEt_3)_2(Cl)_2$(4-tft) and an OAc radical from doublet *trans*-$Pt(PEt_3)_2(Cl)(OAc)$(4-tft) were also compared to evaluate changes in the abstraction step. Acetate radical removal takes only 17.3 kcal/mol while Cl radical loss requires 33.3 kcal/mol. Clearly, replacement of the chloro ligand in **6** with an acetate ligand does not appear likely to inhibit reductive elimination and explain the enhanced yield of phospha-platinacycles for carboxylate complexes **26**-**28**.

To experimentally test the importance of strong *cis*-ligand bonding, **29** was prepared with a cyano ligand (Scheme 4.3.4). Despite the strongly bonded cyano ligand *cis* to the OH ligand photolysis of **29** at 25 ^{o}C yields only reductive elimination product *trans*-$Pt(PEt_3)_2(CN)$(4-tft) (Scheme 4.3.4) indicating that if *cis* elimination is supressed a *trans*

elimination can occur. However, at -78 °C a 30% yield of phospha-platinacycle **33**, is obtained. While not as high a phospha-platinacycle yield as the hydrogen-bonded carboxylate systems it is double the yield from **6** suggesting that strong bonding of the ligand adjacent to the OH group can slow reductive elimination and allow greater C-H activation.

Scheme 4.3.4. Photolysis of Pt(IV)(OH)(CN) complex in CD_2Cl_2.

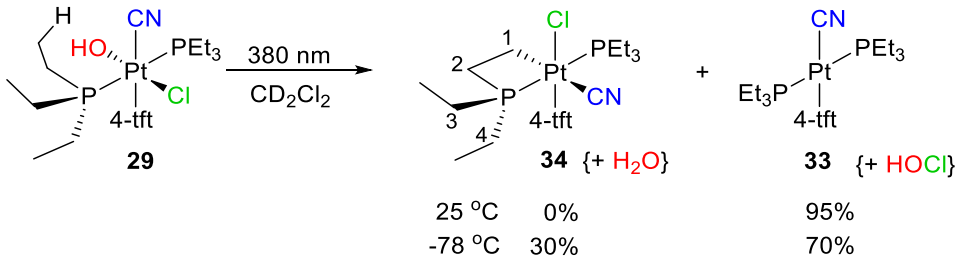

The above results can be interpreted with the three pathways presented in Scheme 4.3.5. All three pathways start from the lowest-energy triplet excited state, which has been previously modelled with DFT for **6** and now for **26** and **27** (see below). The model complexes show elongation of the Pt-OH bond and high spin density on the OH group indicating a weakly interacting Pt(III)-OH geminate radical pair. Path B is phosphine H-atom abstraction by the hydroxyl radical to give water and, after ring closing, the phosha-platinacycle. Competitive with this pathway are the nest reductive elimination pathways A and C. In Path A the hydroxyl radical abstracts a ligand from the Pt(III) center while in Path C a solvent H-atom is first abstracted by the hydroxyl radical and then the resulting solvent radical abstracts a ligand from the Pt(III) center. Path C is favoured with toluene and other solvents which contain relative weakly bonded hydrogen atoms and may also be favoured when the hydroxyl radical escapes the first coordination sphere of the Pt center. Path A generally results in abstraction of a *cis* ligand but in the case of **29** where

the CN ligand is not easily given up the OH radical can evidently migrate and abstract the trans Cl ligand. Path B then is favoured by OH radical tethering to the complex preventing escape, migration, and ligand abstraction. Consistent with entropically unfavourable tethering, Path B is more sensitive to temperature than Path A and C and the amount of Path B product (phospha-platinacycle) decreases from -78 to RT. Indeed, the strength of the H-bond tethering is reflected in the yields. At -78 all three carboxylate complexes give comparable yields which drop as the temperature is raised and the other pathways began to operate. However, the strongest H-bonding is expected to be present in **26** and **28** and these give 50% at RT, whereas the weaker H-bonding in **27** limits the yield to 15% at RT as OH escape, migration, and ligand abstraction dominate.

Scheme 4.3.5. Plausible reaction pathways for the observed overall results.

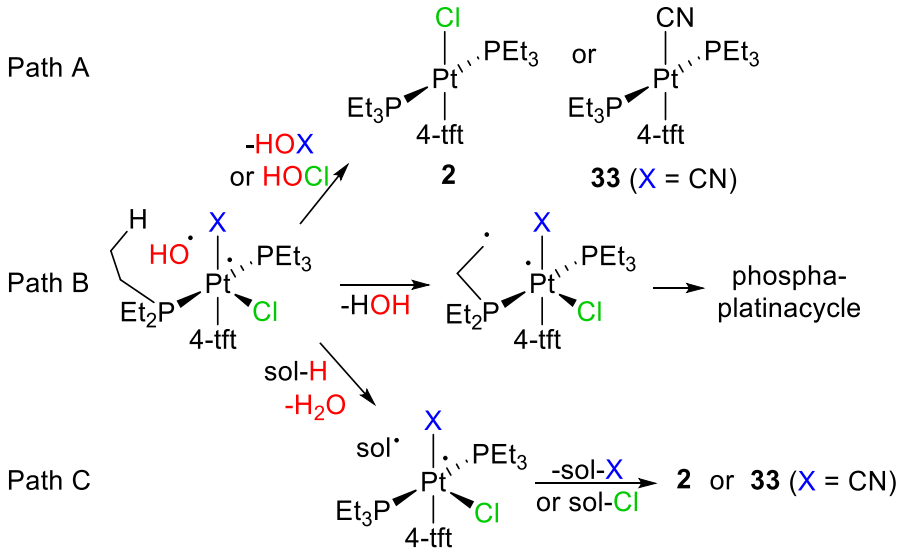

The lowest-energy triplet states (^{T}**26** for **26** and ^{T}**27** for **27**) were by DFT to examine the H-bonding and the spin density distribution. Both complexes show H-bonding between the carboxylate and OH groups. The OAc complex ^{T}**26** appears to have a particularly strong interaction with a remarkably short H--O distance of 1.65 Å consistent with strong

tethering of the OH radical and positioning it for efficient abstraction of the PEt_3 hydrogen atom. The expected weaker H-bond acceptor property of the CF_3OAc ligand is evident in the longer O--H distance of 1.73 Å indicating a weaker tethering and more facile migration of the OH radical away from the PEt_3 ligand. Spin density values show the expected high spin density on the OH group indicating high radical character.

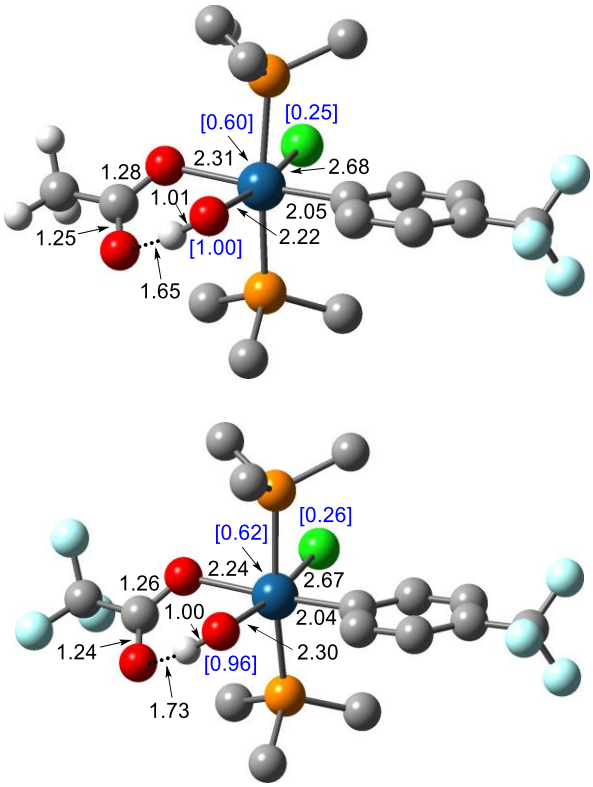

Figure 4.3.5. Drawings of the DFT triplets trans-$Pt(PEt_3)_2$(4-tft)(Cl)(OH)(OAc) ^{T}**26** (top) and trans-$Pt(PEt_3)_2$(4-tft)(Cl)(OH)(O_2CCF_3) ^{T}**27** (bottom) (hydrogen atoms omitted except for OH and OAc). Black numbers are distances (Å) and blue numbers in brackets are Mulliken electron spin densities on Cl, Pt, and the OH. Pt = blue, P = orange, Cl = green, F = light blue, O = red, C = grey.

Finally, we sought to incorporate alternative hydroxo hydrogen bonding to enhance path B to the phospha-platinacycle and replaced the 4-tft ligand with a 2-methoxyphenyl group to give **36** (Figure 4.3.6).

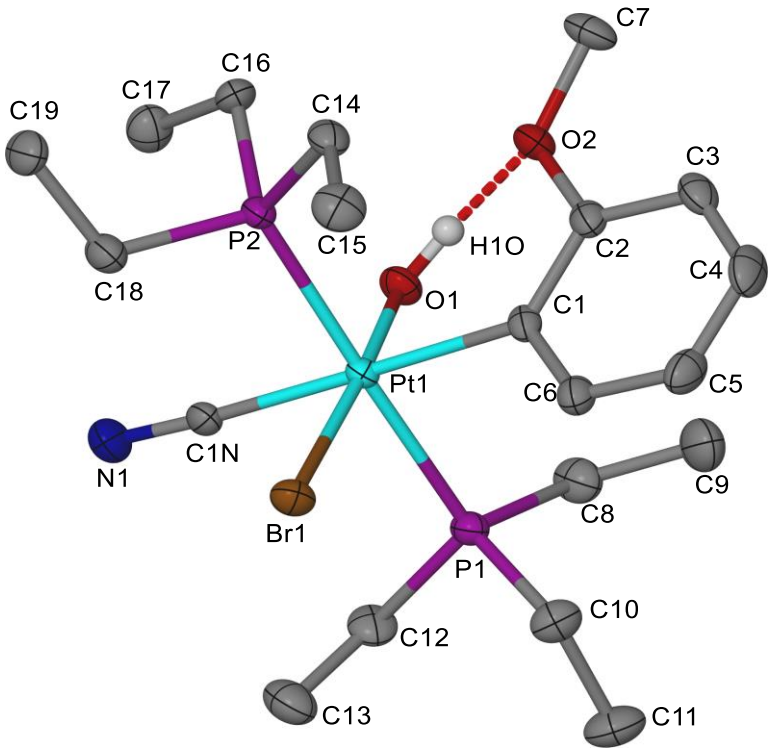

Figure 4.3.6. Drawing of the solid-state structure of trans-Pt(PEt3)2(2-MeOPh)(Br)(OH)(CN) **36** co-crystallized with ~15% trans-Pt(PEt3)2(2-MeOPh)(Br)2(OH) (50% probability ellipsoids, hydrogen atoms omitted). Approximately 15% Br atom occupancy at the CN ligand position not shown.

Photolysis of **36** at -78 ºC gives a 40% yield of phospha-platinacycle **37**, improved from the 30% yield for analogous 4-tft complex **29**. This is not to the 90% level observed for **26** but the hydrogen bonding of the methoxyphenyl ligand with the OH ligand should be relatively weak compared to that in the carboxylic acid complexes and the effect of changing the aryl group on the other pathways is unknown and could be significant.

Scheme 4.3.6. Photolysis of Pt(IV)(OH)(CN)(2-methoxyphenyl) complex at -78℃.

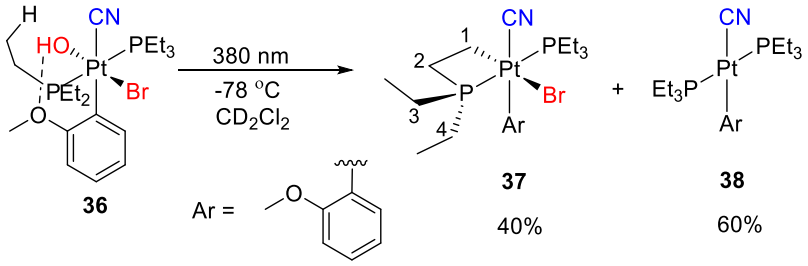

The new platinacycles obtained from the carboxylate and the cyano complexes are unstable to thermal reductive elimination. In the case of the carboxylate complexes **30-32** reductive elimination involving the chloro ligand and the carboxylate ligand occurs forming a mixture of the chloro-substituted PEt_3 ligand complex **39** and the carboxylate-substituted PEt_3 ligand complex **40** (Scheme 4.3.7).

Scheme 4.3.7. Thermal reductive elimination of new the phospha-platinacycles

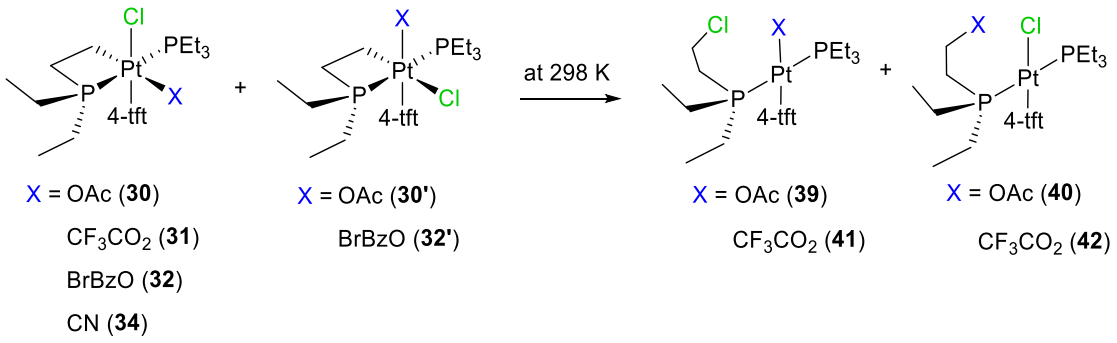

Kinetics for reductive coupling.

Monitoring the elimination reaction of the two isomers of **30** at 29 °C reveals first-order kinetics for both isomers but with slightly different rate constants (Figure 4.3.7). The initial ratio of **30'/30** (0.20) varied during the thermal decomposition and it is 0.30 after ~85% decomposition. This observation indicates the absence of a thermal equilibrium

between these isomers. Formation of the corresponding Pt(II) complexes **39** and **40** was also examined and the result indicates first-order kinetics for both **39** and **40** (Figure 4.3.8). However, ^{1}H NMR integration (against an internal standard) indicated a ~25% loss of Pt by the end of decomposition. This disappearance of Pt makes it difficult to explain the exact mechanism for the thermal reductive elimination.

Based on literature data for such reductive eliminations,[102,103] here we propose a nonassociative S_N2 type mechanism indicating an initial loss of a ligand (*trans* to alkyl carbon) leading to a unsaturated five-coordinate intermediate. The above five-coordinate Pt intermediate preserves the required configuration for the S_N2 type nucleophilic attach on alkyl carbon leading to square planar Pt(II) (Scheme 4.3.8).

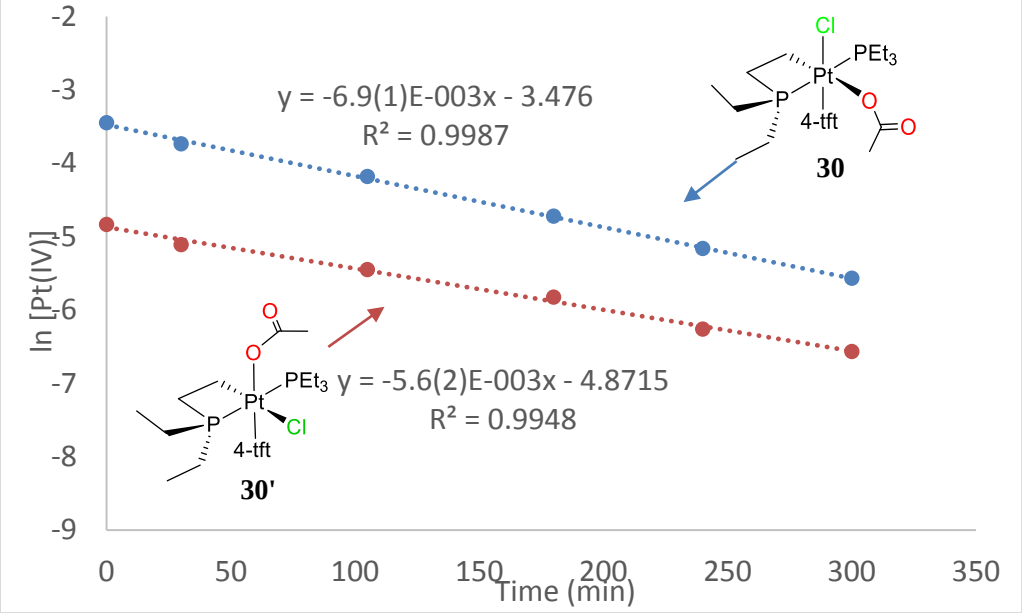

Figure 4.3.7. Kinetic plots for first-order decomposition of isomers of 30 at 29℃.

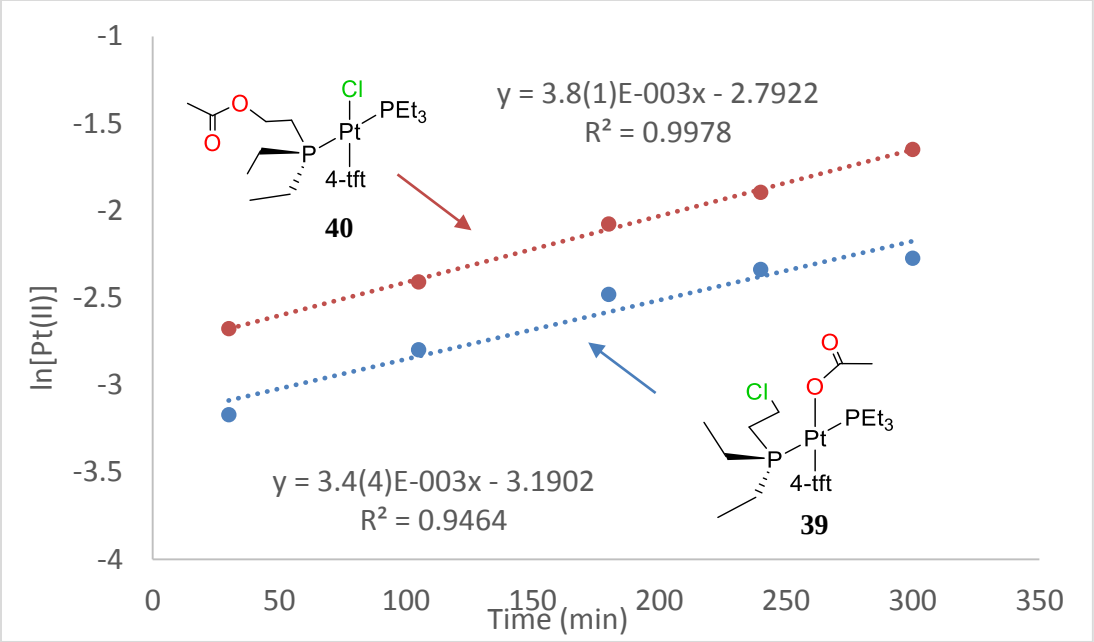

Figure 4.3.8. Kinetic plots for first-order formation of each Pt(II) compound at 29℃.

Scheme 4.3.8. Proposed mechanism for the thermal reductive elimination.

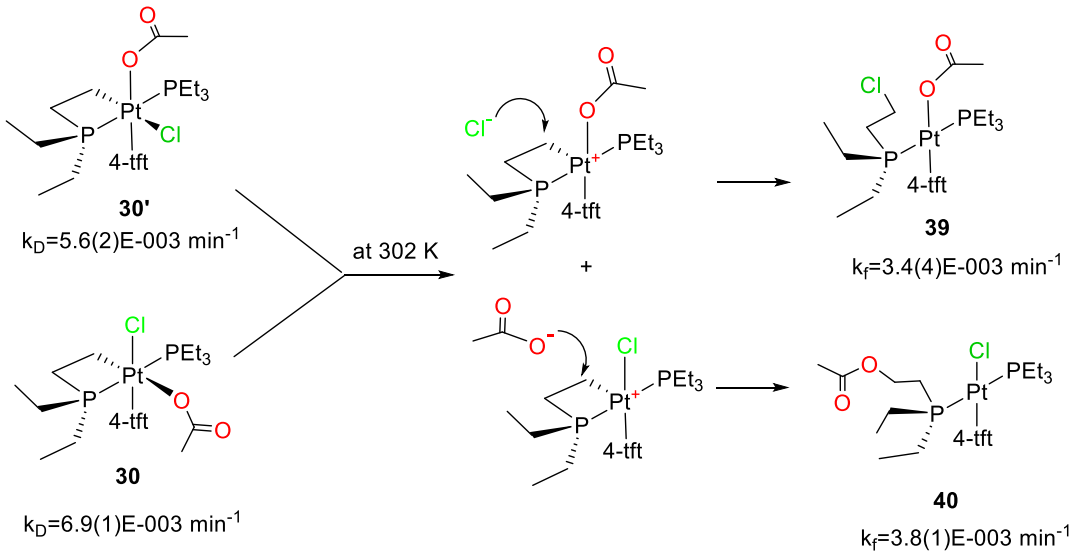

Scheme 4.3.9. Proposed kinetics for allyl-carboxylate elimination.

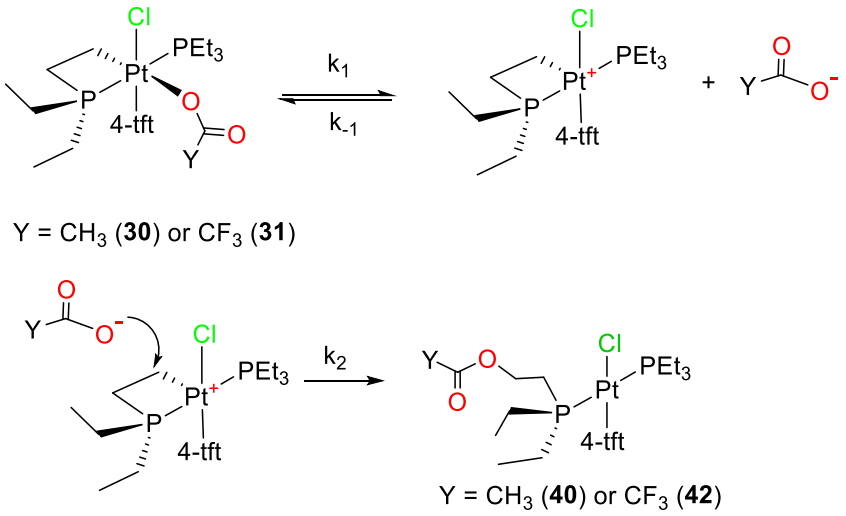

Rate equation derived for overall decomposition of Pt(IV) platinacycle.

$$\frac{d[Pt(IV)]}{dt} = \frac{k_1 k_2 [Pt(IV)]}{k_{-1}+k_2} \qquad \text{eq 8}$$

If $k_{-1} << K_2$, $k_{-1} + k_2 \approx k_2$

$$\frac{d[Pt(IV)]}{dt} = k_1[Pt(IV)] \qquad \text{eq 9}$$

The observed product ratio (**40:39)** of 2.0 from **30** is slightly lower than that of **31** (**42:41**) which is 2.4. We have attempted to explain this result with more elaborated kinetic equations derived for alkyl-carboxylate reductive elimination (Scheme 4.3.9). If the rate constant for the backward reaction (k_{-1}) is significantly smaller than k_2 the overall rate will simplify to eq 9 and it should only be influenced by initial ligand dissociation (k_1). If the ligand dissociation is the rate determine step in this reaction, more labile trifluoroacetate would give a slightly higher yield of **42**. However this thermal reductive elimination mechanism requires further studies. In order to further study the reaction,

monitoring the kinetics in the presence of acetate can be done. Doing kinetics in a polar protic solvent may change the rate constant of k_2 due to stabilization of the anionic ligand. Since the phospha-plainacycles were not isolated the reaction kinetics may have been influenced by impurities and purified samples would be needed.

Reaction of complex 4 with di and tri protic acids.

A sulfate-bridged dimer, [trans-Pt$(PEt_3)_2$Cl(4-tft)(OH)]$_2SO_4$ (**43**), and a boric acid product that incorporates the OOH ligand, *trans*-Pt$(PEt_3)_2$Cl(4-tft)[κ-O,O-OB(OH)OO] (**44**), were also prepared by the method shown in

Scheme **4.3.1** and characterized by X-ray crystallography (Figure 4.3.9 and Figure 4.3.10) and NMR spectroscopy. Complexes **43** and **44** are photoactive. Photolysis at 380 nm under ambient conditions yield **2,** and further characterization of the photolysis products was not attempted.

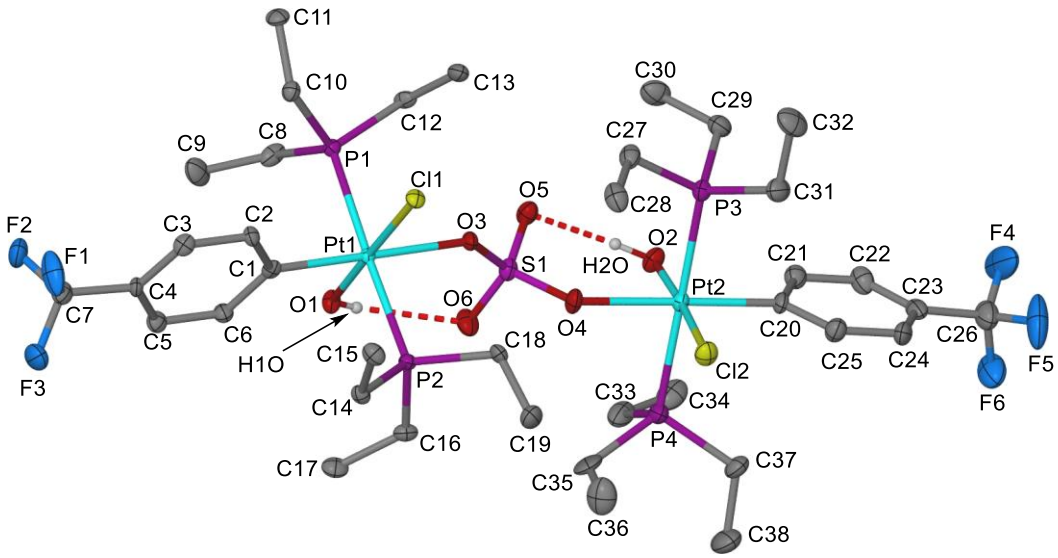

Figure 4.3.9. Drawing of the solid-state structure of [trans-Pt$(PEt_3)_2$(4-tft)(Cl)(OH)]$_2SO_4$ (50% probability ellipsoids, hydrogen atoms omitted).

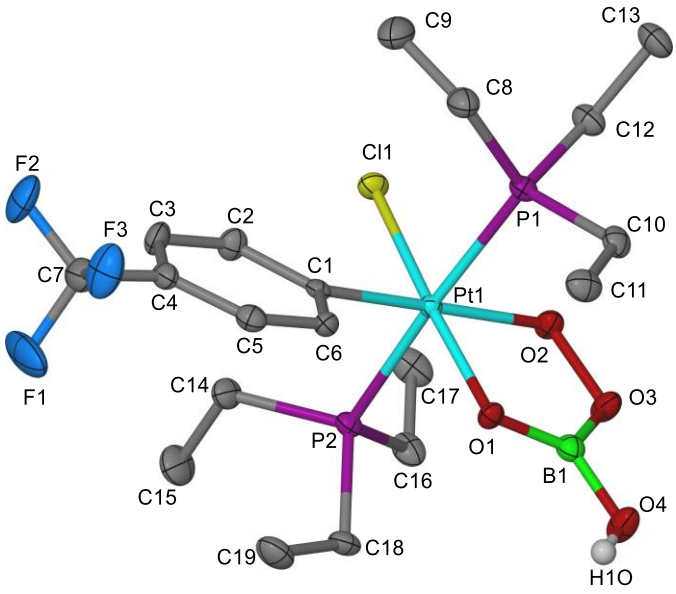

Figure 4.3.10. Drawing of the solid-state structure of *trans*-Pt(PEt_3)$_2$Cl(4-tft)[κ-O,O-OB(OH)OO] (**44**) (50% probability ellipsoids, hydrogen atoms omitted).

4.4 Conclusion.

Irradiation of **6** at 77 K shows salmon pink emission and the life-time measurement indicates generation of a triplet excited state. Formation of a phospha-platinacycle has been confirmed mainly by ^{31}P NMR and other spectroscopy techniques. Platinum satellites observed in ^{1}H-^{13}C HMQC has strengthen the observation of a new metal carbon bond formation. Reductive elimination of the C-Cl is confirmed by x-ray crystallography and NMR spectroscopy. Characteristic emission spectrum observed for photolyzed sample of **6** in toluene at 77 K indicated formation of a benzyl radical. The benzyl radical formation and phospha-platinacycle yields in MeTHF and toluene suggest a competition reaction for OH radical.

Incorporating hydrogen bonding into hydroxo complexes using carboxylate ligands eliminates the difficulty of 77 K photolysis. Spectroscopic data indicate intramolecular

hydrogen abstraction and formation of phospha-platinacycle analogous to the 77 K photolysis, but in solution phase. Reductive elimination of C-Cl and C-carboxylate has also been observed. Strong hydrogen bonding and the ligand field strength in Pt(IV)-carboxylate complex photolysis contrast with the Pt(IV)(OH)(OOH/Cl) system. The overall result of C-H activation and metal-carbon bond formation via hydrogen bonding gives better control of one of competitive reactions shown in Scheme 4.3.5.

4.5 Experimental.

Reagents and solvents were purchased from commercial sources (Aldrich or Acros). MeTHF (anhydrous, Inhibitor-free) and toluene-d_8 (Cambridge Isotope Laboratories, Inc.) used as received. MeTHF was stored under a dinitrogen atmosphere in a drybox. NMR spectra were recorded on Bruker AMX-250, -500 and 800 spectrometers at ambient probe temperatures except as noted. NMR shifts use the δ scale with positive values downfield of TMS (^{1}H and ^{13}C), external H_3PO_4 (^{31}P), external $CFCl_3$ (^{19}F). Emission spectra and lifetime were obtained on a Cary Eclipse Fluorescence spectrophotometer with samples in borosilicate glass tubes at 77 K. Photolyses were performed at 380 nm in borosilicate glass tubes using a home-built photo-reactor consisting of a short section of 4.2 cm PVC pipe lined with 24 LED's (superbrightleds.com, RL5-UV031 5mm UV LED) connected in series. Photolysis and emission experiments at 77 K utilized a liquid nitrogen filled Dewar with an unsilvered glass finger.

Apparatus.

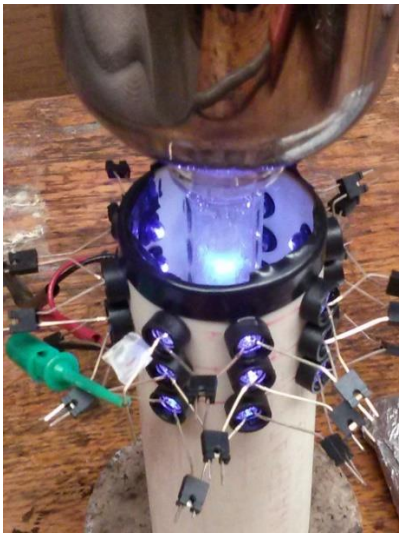

Figure 4.5.1. Apparatus (380 nm LED tube photo-reactor and LN_2 Dewar with unsilvered finger) for the photolysis of Pt compounds at 77 K.

***Trans,cis*-Pt(PEt$_3$)(Et$_2$PCH$_2$CH$_2$)Cl$_2$(4-tft) (24).** *trans,cis*-Pt(PEt$_3$)$_2$(Cl)$_2$(OH)(4-trifluoromethylphenyl) **6** (7 mg, 0.01 mmol) was dissolved in 0.50 mL of 2-Methyltetrahydrofuran (MeTHF) or toluene-d_8 and transfer into an NMR tube. The MeTHF sample was prepared in air and was degassed by three freeze-pump-thaw cycles. The MeTHF sample was prepared under N_2. The sample was then immersed in LN_2 and irradiated at 380 nm for 4 h. After warming to room temperature the NMR spectra were quickly collected and showed complete conversion of **6** into **24** and **2** (yields are given in Scheme 4.2.1). Another sample was warmed only to -60 ^oC in the NMR spectrometer probe. The ^{31}P NMR spectrum showed **24** and **2** as the only significant products.

NMR peaks assignments were assisted by ^1H-^1H COSY and ^1H-^{13}C HMQC experiments and by comparison to data for Pt(II) phospha-platinacycle complexes.[98] The higher-field

^{1}H NMR signals for the ring methylene proton pairs (a and b) and the PEt_2 methylene groups have been assigned to those proximate to the 4-tft ring where they experience shielding from the ring current.

$^{31}P\{^{1}H\}$ NMR (101 MHz, MeTHF or toluene-d_8): -7.7 (d with satellites, J_{PtP} = 1853 Hz, J_{PtP} = 513Hz, PEt_3), -65.86 (d with satellites, J_{PtP} = 1410 Hz, J_{PtP} = 513 Hz, $PEt_2CH_2CH_2$).

^{1}H NMR (800 MHz, toluene-d_8): 8.95 (d with satellites, J_{HH} = 8.0 Hz, J_{PtH} = 48.8 Hz, 2H, 4-tft), 7.28 (d, J_{HH} = 8.0 Hz, 2H, 4-tft), 2.98 (m with satellites, J_{PtH} ~ 60 Hz, 1H, H_{2a}), 2.71 (m with satellites, J_{PtH} ~ 100 Hz, 1H, H_{1a}), 2.63 (m, 1H, H_{4a} or H_{4b}) 2.37 (m with satellites, J_{PtH} ~ 60 Hz, 1H, H_{2b}), 1.77 (overlapping, 1H, H_{4a} or H_{4b}),1.73 (overlapping, 1H & 9H, H_{1b} & $P(C\underline{H}_2CH_3)_3$), 1.08-1.03 (m, 6H, $P(CH_2C\underline{H}_3)_2$), 0.74-0.68 (m, 9H, $P(CH_2C\underline{H}_3)_3$), 0.57 (m, 1H, H_{3a} or H_{3b}), 0.25 (m, 1H, H_{3a} or H_{3b}). Overlapping peaks were located by a ^{1}H-^{1}H COSY spectrum. ^{195}Pt satellites confirmed in 500 MHz spectra and in ^{1}H-^{13}C HMQC spectra (see SI for all spectra).

^{13}C(DEPH) NMR (201 MHz, toluene-d_8, ring carbon signals): -0.2 (d with satellites, J_{PC} = 26.5 Hz, J_{PtC} = 450 Hz, Pt-C1), 29.7 (d, J_{PC} = 36.4 Hz, C2).

***Trans*-Pt(PEt_3)($Et_2PCH_2CH_2Cl$)Cl(4-tft) (25).** A photolyzed sample of **6** in MeTHF (or toluene-d_8) containing a mixture of **24** and **2** was left over-night at ambient temperature in the dark to convert all **24** into **25.** ^{31}P NMR analysis indicated a **2**:**25** ratio of 1:2 (MeTHF). The volatiles were then removed in *vacuo* and the solid residue was dissolved in ~1 mL CH_2Cl_2. Methanol (~1 mL) was added and slow evaporation in a refrigerator at

~5 °C yielded colourless crystals for the X-ray analysis. Complexes **2** and **25** could not be separated by crystallization and the X-ray structural data indicate co-crystallization in an 11:14 ratio.

$^{31}P\{^{1}H\}$ NMR (101 MHz, $CDCl_3$, toluene-d_8, MeTHF): 13.7 (s with satellite, J_{PtP} = 2770 Hz), 13.0 (s with satellite, J_{PtP} = 2722 Hz).

^{1}H NMR (250 MHz, $CDCl_3$): 7.47 (d with satellites, J_{HH} = 7.5 Hz, J_{PtH} = 65 Hz, 2H), 7.15 (d, 2H), 3.90 (q of d, J_{HH} = 7.5 Hz, J_{PH} = 2.5 Hz, 2H, $PCH_2C\underline{H}_2Cl$), 2.28 (m, 2H, $PC\underline{H}_2CH_2Cl$), 1.75-1.50 (m overlapping with **2**, 10H, $PC\underline{H}_2CH_3$), 1.17-1.00 (m overlapping with **2**, 15H, $PCH_2C\underline{H}_3$).

^{1}H NMR (500 MHz, toluene-d_8): 7.45 (d with satellites, J_{HH} = 8.0 Hz, J_{PtH} = 63 Hz, 2H, 4-tft), 7.20 (d, 2H, 4-tft), 3.79-3.74 (q, J_{HH} = 8.0 Hz, 2H, $PCH_2C\underline{H}_2Cl$), 2.02 (q, J_{HH} = 8.0 Hz, 2H, CH_2), 1.47-1.20 (m overlapping with **2**, 10H, $P(C\underline{H}_2CH_3)$), 0.87-0.78 (m overlapping with **2**, 9H, $P(CH_2C\underline{H}_3)_3$), 0.75-0.67 (m, 6H, $P(CH_2C\underline{H}_3)_2$).

***Trans*-Pt(PEt$_3$)$_2$Cl(OH)(OAc)(4-tft) (26).** *trans*-Pt(PEt3)2(Cl)(OH)(OOH)(4-tft) **4** (10 mg, 0.015 mmol) was dissolved in 1.0 mL of dichloromethane and approximately 1 mL of deionized water, 0.05 mL of glacial acetic acid was added and the mixture was stirred for 1 min. 31P NMR spectroscopy showed complete conversion of **4** to **26**. The dichloromethane layer was washed with 4 × 5 mL deionized water and dried with $MgSO_4$. After filtration, volatiles were removed in vacuo. The resulting solid was washed with 1 mL cold hexane and dried in vacuo. Yield: 9.60 mg (92 %). Yellow crystals for the X-ray analysis were grown in hexane/ CH_2Cl_2 (1:1) by slow evaporation in a freezer.

$^{31}P\{ 1H\}$ NMR (101 MHz, CD_2Cl_2): 4.78 (s with satellite, J_{PtP} = 1760 Hz), ^{1}H NMR (250 MHz, CD_2Cl_2): 8.10 (d with satellites, JHH = 8.50 Hz, J_{PtH} = 42 Hz, 1H), 8.00 (d with satellites, J_{HH} = 8.75 Hz, JPtH = 37 Hz, 1H), 7.30 (d, J_{HH} = 8.50, 1H), 7.23 (d, JHH = 8.50, 1H), 4.68 (J_{PtH} = 44 Hz, 1H, OH), 2.018 (s, 3H, $OCOCH_3$),1.96−1.76 (m, 12H, CH_2), 1.09−0.97 (app quintet, J = 7.75 Hz, 18H, CH_3).

^{1}H NMR (250 MHz, toluene-d8): 8.34 (d with satellites, J_{HH} = 8.25 Hz, J_{PtH} = 39.5 Hz, 2H), 7.32 (d, J_{HH} = 7.25, 1H), 7.215 (d, J_{HH} = 7.25, 1H), 5.05 (J_{PtH} = 43 Hz, 1H, OH), 2.113 (s, 3H, $OCOCH_3$),1.74−1.60 (m, 12H, CH_2), 0.84−0.71 (app quintet, J = 7.75 Hz, 18H, CH_3).

***trans*-Pt(PEt$_3$)$_2$Cl(OH)(OCOCF$_3$)(4-tft) (27).** *trans*-Pt(PEt$_3$)$_2$(Cl)(OH)(OOH)(4-tft) **4** (15 mg, 0.023 mmol) was dissolved in 1.0 mL of dichloromethane and 0.05 mL of trifluoroacetic acid was added and the mixture was stirred for 1 min. ^{31}P NMR spectroscopy showed complete conversion of **4** to **27**.The dichloromethane layer was washed with 4 × 5 mL deionized water and dried with $MgSO_4$. After filtration, volatiles were removed in vacuo. The resulting solid was washed with 1 mL cold hexane and dried in vacuo. Yield: 15.60 mg (93 %). Yellow crystals for the X-ray analysis were grown in hexane/ CH_2Cl_2 (1:1) by slow evaporation in a freezer. $^{31}P\{ ^{1}H\}$ NMR (101 MHz, CD_2Cl_2): 6.48 (s with satellite, J_{PtP} = 1725 Hz), ^{1}H NMR (250 MHz, CD_2Cl_2): 8.12 (d with satellites, J_{HH} = 8.50 Hz, J_{PtH} = 30 Hz, 1H), 8.03 (d with satellites, J_{HH} = 9.00 Hz, J_{PtH} = 39 Hz, 1H), 7.35 (d, J_{HH} = 8.25, 1H), 7.27 (d, J_{HH} = 8.25, 1H), 3.3-3.0 (broad S, 1H, OH), 2.01−1.74 (m, 12H, CH_2), 1.12−0.99 (app quintet, J = 7.75 Hz, 18H, CH_3).

***Trans*-Pt(PEt$_3$)$_2$Cl(OH)(2-bromophenylacetato)(4-tft) (28)**. *trans*-Pt(PEt$_3$)$_2$(Cl)(OH)(OOH)(4-tft) **4** (20.0 mg, 0.030 mmol) was dissolved in 1.0 mL of dichloromethane and 40 mg (0.188 mmol) 2-bromophenylacetic acid was added and the mixture was stirred for 10 min. ^{31}P NMR spectroscopy showed complete conversion of **4** to **28**. The dichloromethane layer was stirred with 2 × 5 mL (1.8 M) KOH for 1 min. The dichloromethane layer was washed with 2 × 5 mL deionized water and dried with $MgSO_4$. After filtration, volatiles were removed in *vacuo*. The resulting solid was washed with 0.50 mL cold pentane and dried in *vacuo*. Yield: 23.0 mg (91%). Yellow crystals for the X-ray analysis were grown in hexane/acetone (1:1) by slow evaporation in a freezer. ^{31}P{ ^{1}H} NMR (101 MHz, CD_2Cl_2): 4.84 (s with satellite, J_{PtP} = 1754.7 Hz), ^{1}H NMR (250 MHz, CD_2Cl_2): 8.10 (d with satellites, J_{HH} = 8.25 Hz, J_{PtH} = 40.0 Hz, 1H), 8.03 (d with satellites, J_{HH} = 8.75 Hz, J_{PtH} = 38.5 Hz, 1H), 7.57 (d, J_{HH} = 7.50, 1H), 7.36-7.29 (m, 2H), 7.28-7.20 (m, 2H), 7.20-7.07 (m, 1H), 4.32 (s, J_{PtH} = 43.8 Hz, 1H, OH), 3.81 (s, 2H, CH_2), 2.00−1.73 (m, 12H, CH_2), 1.09−0.96 (app quintet, J = 7.75 Hz, 18H, CH_3).

***trans*-Pt(PEt$_3$)$_2$Cl(OH)(CN)(4-tft) (29)**. *trans*-Pt(PEt$_3$)$_2$(Cl)(OH)(OOH)(4-tft) **4** (10 mg, 0.015 mmol) was dissolved in 1.0 mL of dichloromethane and approximately 1 mL of aqueous KCN (32 mg dissolved in 1.0 mL), 0.05 mL of conc $HClO_4$ acid was added and the mixture was stirred for 1 min. ^{31}P NMR spectroscopy showed complete conversion of **4** to **29**. The dichloromethane layer was washed with 4 × 5 mL deionized water and dried with $MgSO_4$. After filtration, volatiles were removed in vacuo. The resulting solid was washed with 1 mL cold hexane and dried in *vacuo*. Yield: 9.5 mg (97 %). ^{31}P{ ^{1}H} NMR (101 MHz, CD_2Cl_2): -1.75 (s with satellite, J_{PtP} = 1608 Hz), ^{1}H NMR (250 MHz, CD_2Cl_2): 8.17 (d with satellites, J_{HH} = 8.25 Hz, J_{PtH} = 28 Hz, 1H), 7.97 (d with satellites,

J_{HH} = 8.25 Hz, J_{PtH} = 25 Hz, 1H), 7.46-7.38 (m (overlapped dd)), J_{HH} = 6.75, 2H), 2.10−1.85 (m, 12H, CH_2), 1.13−1.00 (app quintet, J = 7.75 Hz, 18H, CH_3).

***trans*-Pt(PEt$_3$)$_2$(Br)(2-methoxyphenyl) (35).** A solution of 1-bromo-2-methoxybenzene (~100 mg, 0.53 mmol) in THF (~2 mL) was added to a clear orange solution of Pt(PEt$_3$)$_4$ (200 mg, 0.30 mmol) in THF (~2 mL). The resulting clear orange solution was stirred for ~20 h at 140 ^oC in a sealed tube to yield a pale yellow solution. The mixture was cooled to ambient temperature and the volatiles were removed in *vacuo*. The solid residue was dissolved in ~2 mL CH_2Cl_2 and transferred to a 4 mL vial. The volume was reduced in *vacuo* to ~0.5 mL followed by the addition of ~1 ml of methanol. The vial was capped and stored in at -20 ^oC overnight to afford colorless crystals. The mother liquor was pipetted out and the crystals were dried *in vacuo* to yield 150 mg (80 %) of *trans*-Pt(PEt$_3$)$_2$(Br)(2-methoxyphenyl). $^{31}P\{^1H\}$ NMR (101 MHz, CD_2Cl_2): 12.68 (s with satellite, J_{PtP} = 2753 Hz), ^1H NMR (500 MHz, CD_2Cl_2): 7.30 (d with satellites, J_{HH} = 7.42 Hz, J_{PtH} = 78 Hz, 1H), 6.92 (overlapped dd, J_{HH} = 7.63 Hz,1H), 6.60 (overlapped dd, J_{HH} = 7.21 Hz,1H), 6.51 (d, J_{HH} = 8.10, 1H), 3.70 (s, 3H, OCH_3), 1.70−1.58 (m, 12H, CH_2), 1.10−1.0 (app quintet, Japp = 7.83 Hz, 18H, CH_3).

***trans*-Pt(PEt$_3$)$_2$Br(OH)(CN)(2-methoxyphenyl) (36)**. *trans*-Pt(PEt$_3$)$_2$Br(2-methoxyphenyl) (13.5 mg, 0.020 mmol) in 1.5 mL of dichloromethane was mixed in a 20 mL vial with a freshly prepared H_2O_2 solution in diethylether (1mL). The vial was loosely capped. The mixture was stirred for 20 min at room temperature during which time the solution turned pale yellow and conversion of *trans*-Pt(PEt$_3$)$_2$Br(2-methoxyphenyl) (δ 12.5) to presumed *trans*-Pt(PEt$_3$)$_2$Br(OH)(OOH)(2-methoxyphenyl) (δ 2−0) was observed by ^{31}P NMR spectroscopy (^{31}P NMR shifts varied slightly with the

water content of the reaction mixture). Once the reaction was complete, the dichloromethane layer was separated, washed with 3 × 5 mL of deionized water to remove H_2O_2. Approximately 1 mL of aqueous KCN (32 mg dissolved in 1.0 mL), 0.05 mL of conc $HClO_4$ acid was added and the mixture was stirred for 1 min. ^{31}P NMR spectroscopy showed complete conversion to **36**. The dichloromethane layer was washed with 4 × 5 mL deionized water and dried with $MgSO_4$. After filtration, volatiles were removed in vacuo. The resulting solid was washed with 1 mL cold hexane and dried in *vacuo*. Yield: 12.0 mg (91 %). Yellow crystals for the X-ray analysis were grown in hexane/CH_2Cl_2 (1:1) by slow evaporation in a freezer. $^{31}P\{^1H\}$ NMR (101 MHz, $CDCl_3$): -1.29 (s with satellite, J_{PtP} = 1626 Hz), ^1H NMR (250 MHz, $CDCl_3$): 8.09 (d with satellites, J_{HH} = 8.00 Hz, J_{PtH} = 36 Hz, 1H), 7.13 (t, J_{HH} = 7.25 Hz,1H), 6.80 (t, J_{HH} = 7.75, 1H), 6.61 (d, J_{HH} = 7.75, 1H), 3.79 (s, 3H, OCH_3), 2.30−2.09 (m, 12H, CH_2), 1.20−1.0 (app quintet, J = 8.00 Hz, 18H, CH_3).

Photolysis of *trans*-Pt(PEt$_3$)$_2$Cl(OH)(OAc)(4-tft) (26). A sample of **26** (10 mg, 0.014 mmol) dissolved in 0.50 mL of CD_2Cl_2 or toluene-d_8 was photolyzed for 120 min or 40 min (toluene-d_8) at -78℃ giving complete conversion of **26** into **30** and **2**. Other samples of **26** in CD_2Cl_2 and toluene- d_8 with identical concentrations were photolyzed to completion (15 min) at 25℃. Yields of **30** and **2** are given in Table 4.3.1.

Data for **30**. $^{31}P\{^1H\}$ NMR (101 MHz, CD_2Cl_2): -2.9 (d with satellites, J_{PtP} = 1800 Hz, J_{PtP} = 529Hz), -60.7(d with satellites, J_{PtP} = 1566 Hz, J_{PtP} = 529 Hz).

^1H NMR (500 MHz, CD_2Cl_2): 7.77 (d with satellites, J_{HH} = 8.0 Hz, J_{PtH} = 45 Hz, 1H, 4-tft), 7.52(d with satellites, J_{HH} = 8.0 Hz, J_{PtH} = 52 Hz, 1H, 4-tft), 7.38 (d, J_{HH} = 8.0 Hz,

1H, 4-tft), 7.31 (d, J_{HH} = 8.0 Hz, 1H, 4-tft), 3.11-3.20 (m 1H, H_{2a}), 2.85-2.70 (m 2H, H_{2b} and H_{4a}), 2.75-2.55 (m with satellites, J_{PtH} ~ 100 Hz, 1H, H_{1a}), 2.40-2.25(m, 1H, H_{4b}) 2.15-2.05 (m, 1H, H_{1b}), 1.98 (s,3H, $OCOCH_3$), 1.90-1.78 (m, 6H, $P_a(C\underline{H}_2CH_3)_3$), 1.73-1.66 (m 1H, H_{3a}), 1.35-1.28 (m, 1H, H_{3a}), 1.20-1.10 (m, 3H, $P_b(C(4)H_2C\underline{H}_3)$, 1.00-0.94 (app quintet, *J*app = 7.75 Hz, 9H, $P_a(CH_2C\underline{H}_3)_3$), 1.81-0.72 (m, 3H, $P_b(C(3)H_2C\underline{H}_3)$. Overlapping peaks were located by a ^1H-^1H COSY spectrum.

^{13}C(DEPH) NMR (201 MHz, CD_2Cl_2, ring carbon signals): -8.40 (d with satellites, J_{PC} = 38.2 Hz, J_{PtC} = 478 Hz, Pt-C1), 29.95 (d, J_{PC} = 48.2 Hz, C2).

Partial photolysis of **26** at 2 min intervals at -78℃ showed the formation of another phospha-platinacycle (**30'**) assigned as the isomer of **30** shown in Scheme 4.3.3. At the completion of the photolysis almost all **30'** had converted to **30**.

Data for **30'**. $^{31}P\{^1H\}$ NMR (101 MHz, CD_2Cl_2): -6.0 (d with satellites, J_{PtP} = 1848 Hz, J_{PtP} = 501Hz), -64.5 (d with satellites, J_{PtP} = 1392 Hz, J_{PtP} = 501 Hz).

^1H NMR (500 MHz, CD_2Cl_2): 8.67(d with satellites, J_{HH} = 8.2 Hz, J_{PtH} = 50 Hz, 2H, 4-tft *o*-H), 7.32 (4-tft *m*-H, observed by COSY to overlap with a peak for **30**). Remaining peaks were too weak and/or obscured.

^{13}C(DEPH) NMR (201 MHz, CD_2Cl_2): 139.5 (s, 4-tft *o*-C), 134.9 (4-tft *m*-C overlapped with another signal). Peaks assigned by ^1H-^{13}C HMQC. Other peaks could not be assigned without matching ^1H NMR signal assignments.

Photolysis of *trans*-$Pt(PEt_3)_2Cl(OH)(OCOCF_3)$(4-tft) (27). A sample of **27** (8 mg, 0.011 mmol) dissolved in 0.50 mL of CD_2Cl_2 was photolyzed for 40 min at -78℃ giving

complete conversion of **27** into **31** and **2**. Another sample of **27** with the same concentration was photolyzed to completion (15 min) at 25℃. Yields are given in Table 4.3.1.

Data for **10**. $^{31}P\{^{1}H\}$ NMR (101 MHz, CD_2Cl_2): -0.3 (d with satellites, J_{PtP} = 1813 Hz, J_{PtP} = 504 Hz), -59.4(d with satellites, J_{PtP} = 1474 Hz, J_{PtP} = 504 Hz).

Photolysis of *trans*-Pt(PEt$_3$)$_2$Cl(OH)(2-bromophenylacetato)(4-tft) (28). A sample of **28** (9 mg, 0.014 mmol) dissolved in 0.50 mL of CD_2Cl_2 was photolyzed for 40 min at -78℃ giving complete conversion of **28** into **32** and **2**. Another sample of **28** with the same concentration was photolyzed to completion (15 min) at 25℃. Yields are given in Table 4.3.1.

Data for **32**. $^{31}P\{^{1}H\}$ NMR (101 MHz, CD_2Cl_2): -2.6 (d with satellites, J_{PtP} = 1803 Hz, J_{PtP} = 524 Hz), -59.4(d with satellites, J_{PtP} = 1543 Hz, J_{PtP} = 524 Hz).

A small amount of another phospha-platinacycle (**32'**) was observed in the NMR spectra and is assigned as the isomer of **32** shown in Scheme 4.3.2.

Data for **32'**. $^{31}P\{^{1}H\}$ NMR (101 MHz, CD_2Cl_2): -5.9 (d with satellites, J_{PtP} = 1849 Hz, J_{PtP} = 501 Hz), -64.2(d with satellites, J_{PtP} = 1501 Hz, J_{PtP} = 501 Hz).

Photolysis of *trans*-Pt(PEt$_3$)$_2$Cl(OH)(CN)(4-tft) (29).

A sample of **5** (9 mg, 0.014 mmol) dissolved in 0.50 mL of CD_2Cl_2 was photolyzed for 40 min at -78℃ giving complete conversion of **29** into of **33** and **34**. Another sample of **29** with the same concentration was photolyzed to completion (10 min) at 25℃. Yields are given in Table 4.3.1.

Data for **33**. $^{31}P\{^{1}H\}$(NMR (101 MHz, CD_2Cl_2): 11.10 (s with satellites, J_{PtP} =2527 Hz).

Data for **34**. $^{31}P\{^{1}H\}$ NMR (101 MHz, CD_2Cl_2): -2.6 (d with satellites, J_{PtP} = 1803 Hz, J_{PtP} = 524 Hz), -59.4(d with satellites, J_{PtP} = 1543 Hz, J_{PtP} = 524 Hz).

Photolysis of *trans*-Pt(PEt$_3$)$_2$Br(OH)(CN)(2-methoxyphenyl) (36). A sample of **36** (8 mg, 0.012 mmol) dissolved in 0.50 mL of CD_2Cl_2 was photolyzed for 50 min at -78℃ giving complete conversion of **36** into **37** (40%) and *trans*-Pt(PEt$_3$)$_2$(CN)(2-methoxyphenyl) **38** (60%) was observed.

Data for **37**. $^{31}P\{^{1}H\}$ NMR (101 MHz, CD_2Cl_2): -3.0 (d with satellites, J_{PtP} = 1820 Hz, J_{PtP} = 471 Hz), -73.0 (d with satellites, J_{PtP} = 1331 Hz, J_{PtP} = 471 Hz).

Data for **38**. ***trans*-Pt(PEt$_3$)$_2$(CN)(2-methoxyphenyl).**

$^{31}P\{^{1}H\}$ NMR (101 MHz, CD_2Cl_2): 11.33 (s with satellites, J_{PtP} =2570 Hz).

[*trans*-Pt(PEt$_3$)$_2$Cl(4-tft)(OH)]$_2$(μ-SO$_4$) (43). trans-Pt(PEt$_3$)$_2$(Cl)(OH)(OOH)(4-tft) **4** (10 mg, 0.015 mmol) was dissolved in 1.0 mL of dichloromethane and approximately 1 mL of deionized water, approximately 0.05 mL of conc. H_2SO_4 acid was added and the mixture was stirred for 1 min. ^{31}P NMR spectroscopy showed complete conversion to the title product. The dichloromethane layer was washed with 4 × 5 mL deionized water and dried with $MgSO_4$. After filtration, volatiles were removed in vacuo. The resulting solid was washed with 1 mL cold hexane and dried in *vacuo*. Yield: 9.90 mg (97.0 %). Yellow crystals for the X-ray analysis were grown in hexane/CH_2Cl_2 (1:1) by slow evaporation in a freezer. $^{31}P\{^{1}H\}$ NMR (101 MHz, CD_2Cl_2): 8.30 (s with satellite, J_{PtP} = 1735 Hz), ^{1}H

NMR (250 MHz, CD_2Cl_2): 8.10 (d with satellites, J_{HH} = 8.50 Hz, J_{PtH} = 44 Hz, 2H), 7.32-7.23 (m, 2H), 3.16 (J_{PtH} = 40 Hz, 1H, OH), 2.20−1.94 (m, 12H, CH_2), 1.16−1.04 (app quintet, J = 7.75 Hz, 18H, CH_3).

***trans*-Pt(PEt$_3$)$_2$Cl(4-tft)[κ-O,O-OB(OH)OO] (44).** *trans*-Pt(PEt_3)$_2$(Cl)(OH)(OOH)(4-tft) **4** (10 mg, 0.015 mmol) was dissolved in 1.0 mL of dichloromethane and 40 mg of $B(OH)_3$ (boric acid), dissolved in approximately 1 mL of warm deionized water, was added and the mixture was stirred for 10 min. ^{31}P NMR spectroscopy showed complete conversion to the title product. The dichloromethane layer was washed with 4 × 5 mL deionized water and dried with $MgSO_4$. After filtration, volatiles were removed in vacuo. The resulting solid was washed with 1 mL cold hexane and dried in *vacuo*. Yield: 9.9 mg (96.0 %). Yellow crystals for the X-ray analysis were grown in hexane/CH_2Cl_2 (1:1) by slow evaporation in freezer. $^{31}P\{^1H\}$ NMR (101 MHz, CD_2Cl_2): 5.05 (s with satellite, J_{PtP} = 1707 Hz), ^1H NMR (250 MHz, CD_2Cl_2): 8.04 (d ,J_{HH} = 8.50 Hz, 1H), 7.94 (d, J_{HH} = 8.50, 1H), 7.40-7.25 (m, 2H), 3.35 (s, 1H, OH), 2.10−1.82 (m, 12H, CH_2), 1.15−1.01 (app quintet, J = 7.75 Hz, 18H, CH_3).

Kinetic experiment

Thermal decomposition of a mixture of 30 and 30'.

A sample of **26** (10 mg, 0.014 mmol) dissolved in 0.50 mL of CD_2Cl_2 was photolyzed for 50 min at -78℃. At the end of the photolysis complete conversion of **26** into 90 % of **30 and 30'** (two isomers presented) and 10 % of **2** was observed. This sample was kept at 29℃ in a water bath and ^1H NMR spectra (NMR probe at 298 K) were collected at

various time intervals. Kinetic data (integration with respect to an internal standard) for two isomers presented were plotted separately. Data were analyzed using the LINEST function in the Microsoft EXCEL program. The decomposition is found to be first order. The decomposed products are *trans*-Pt(PEt_3)($Et_2PCH_2CH_2$(acetate))Cl(4-tft) and *trans*-Pt(PEt_3)($Et_2PCH_2CH_2Cl$)(acetate)(4-tft).

Table 4.5.1. Data for kinetic plots shown in Figure 4.3.7 and Figure 4.3.8.

time/min	ln[PtCP]		ln[Pt(II)]	
	30	**30'**	**39**	**40**
0	-3.44859	-4.83489		
30	-3.73627	-5.10932	-3.17009	-2.67655
105	-4.18256	-5.45107	-2.79688	-2.40795
180	-4.72156	-5.82375	-2.47932	-2.07545
240	-5.16339	-6.262	-2.33718	-1.89446
300	-5.56885	-6.56649	-2.27303	-1.64922

REFERENCES

1. (a) Harriman, A.; Kalyanasundaram, K., Energy Sources through Photochemistry and Catalysis. *Academic Press, Inc. 24/28 Oval Road, London* **1983**; (b) Bignozzi, C.; Schoonover, J. R.; Scandola, F., *Prog. Inorg. Chem.* **1997,** *44*, 1.
2. Hou, Y.; Vidu, R.; Stroeve, P., Solar Energy Storage Methods. *Industrial & Engineering Chemistry Research* **2011,** *50* (15), 8954-8964.
3. Durgun, E.; Grossman, J. C., Photoswitchable Molecular Rings for Solar-Thermal Energy Storage. *J. Phys. Chem. Lett.* **2013,** *4* (6), 854-860.
4. Frischmann, P. D.; Mahata, K.; Wuerthner, F., Powering the future of molecular artificial photosynthesis with light-harvesting metallosupramolecular dye assemblies. *Chem. Soc. Rev* **2013,** *42* (4).
5. Devabhaktuni, V.; Alam, M.; Shekara Sreenadh Reddy Depuru, S.; Green Ii, R. C.; Nims, D.; Near, C., *Renew. Sust. Energ. Rev* **2013,** *19 (0)*, 555.
6. Marinescu, S. C. B., P. J.; Winkler, J. R.; Gray, H. B., Solar fuels. AIP Conf. Proc. 2013, 1519 (Nobel Symposium 153: Nanoscale Energy Converters, 2012), 64-67. .
7. Eisenberg, R.; Gray, H. B., Preface on Making Oxygen. *Inorg. Chem.* **2008,** *47* (6), 1697-1699.
8. Chen, Y.; Han, J.; Fang, W.-H., Mechanism of Water Oxidation to Molecular Oxygen with Osmocene as Photocatalyst: A Theoretical Study. *Inorg. Chem.* **2012,** *51* (9), 4938-4946.
9. Cook, T. R.; McCarthy, B. D.; Lutterman, D. A.; Nocera, D. G., Halogen Oxidation and Halogen Photoelimination Chemistry of a Platinum–Rhodium Heterobimetallic Core. *Inorg. Chem.* **2012,** *51* (9), 5152-5163.
10. Teets, T. S.; Nocera, D. G., Halogen Photoreductive Elimination from Gold(III) Centers. *J. Am. Chem. Soc.* **2009,** *131* (21), 7411-7420.
11. Raphael Karikachery, A.; Lee, H. B.; Masjedi, M.; Ross, A.; Moody, M. A.; Cai, X.; Chui, M.; Hoff, C. D.; Sharp, P. R., High Quantum Yield Molecular Bromine Photoelimination from Mononuclear Platinum(IV) Complexes. *Inorg. Chem.* **2013,** *52* (7), 4113-4119.
12. Perera, T. A.; Masjedi, M.; Sharp, P. R., Photoreduction of Pt(IV) Chloro Complexes: Substrate Chlorination by a Triplet Excited State. *Inorg. Chem.* **2014,** *53* (14), 7608-7621.
13. Kohl, S. W.; Weiner, L.; Schwartsburd, L.; Konstantinovski, L.; Shimon, L. J.; Ben-David, Y.; Iron, M. A.; Milstein, D., Consecutive thermal H2 and light-induced O2 evolution from water promoted by a metal complex. *Science.* **2009,** *324* (5923), 74-7.
14. Ross, A.; Sharp, P. R., Triphos Iridium(III) Halide Complex Photochemistry: Triphos Arm Dissociation. *Inorg. Chem.* **2013,** *52* (21), 12645-12654.
15. Ozerov, O. V., Oxidative addition of water to transition metal complexes. *Chem Soc Rev* **2009,** *38* (1), 83-8.
16. Chung, T. S.; Na, Y. M.; Kang, S. W.; Jung, O.-S.; Lee, Y.-A., Facile generation of platinum(IV) compounds with mixed labile moieties. Hydrogen peroxide oxidation of platinum(II) to platinum(IV) compounds. *Transition Metal Chemistry* **2005,** *30* (5), 541-545.
17. Kim, K. M.; Sohn, Y. S., Reaction of Tetrahydroxo(2,2-dimethylpropanediamine)platinum(IV) with Trimethylsilylchoride. Pentacoordinative Si,,,OH Interaction Labilizing the PtIV-OH Bond. *Inorg. Chem.* **1998,** *37*, 6109-6112.
18. Pellarin, K. R.; McCready, M. S.; Sutherland, T. I.; Puddephatt, R. J., Oxidative Addition of Phthaloyl Peroxide to Dimethylplatinum(II) Complexes. *Organometallics* **2012,** *31* (23), 8291-8300.
19. Taylor, R. A.; Law, D. J.; Sunley, G. J.; White, A. J.; Britovsek, G. J., Hydrogen bonding directs the H2O2 oxidation of platinum(II) to a cis-dihydroxo platinum(IV) complex. *Chem Commun (Camb)* **2008,** (24), 2800-2.
20. Vedernikov, A. N., Direct Functionalization of M–C (M = PtII, PdII) Bonds Using Environmentally Benign Oxidants, O2 and H2O2. *Acc. Chem. Res* **2012,** *45* (6), 803-813.
21. Rostovtsev, V. V.; Henling, L. M.; Labinger, J. A.; Bercaw, J. E., Structural and Mechanistic Investigations of the Oxidation of Dimethylplatinum(II) Complexes by Dioxygen. In *Inorg. Chem.*, American Chemical Society: 2002; Vol. 41, pp 3608-3619.
22. Cerkovnik, J.; Plesnicar, B., *J. Am. Chem. Soc.* **1993,** *115*, 12169-12170.

23. Levanov, A. V.; Sakharov, D. V.; Dashkova, A. V.; Antipenko, E. E.; Lunin, V. V., Synthesis of Hydrogen Polyoxides H2O4 and H2O3 and Their Characterization by Raman Spectroscopy. *Eur. J. Inorg. Chem.* **2011,** *2011* (33), 5144-5150.
24. Wentworth, P., Jr.; Jones, L. H.; Wentworth, A. D.; Zhu, X.; Larsen, N. A.; Wilson, I. A.; Xu, X.; Goddard, W. A., 3rd; Janda, K. D.; Eschenmoser, A.; Lerner, R. A., Antibody catalysis of the oxidation of water. *Science.* **2001,** *293* (5536), 1806-11.
25. Nyffeler, P. T.; Boyle, N. A.; Eltepu, L.; Wong, C.-H.; Eschenmoser, A.; Lerner, R. A.; Wentworth, P., Dihydrogen Trioxide (HOOOH) Is Generated during the Thermal Reaction between Hydrogen Peroxide and Ozone. *Angew. Chem.* **2004,** *116* (35), 4756-4759.
26. Cerkovnik, J.; Plesnicar, B., Recent advances in the chemistry of hydrogen trioxide (HOOOH). *Chem Rev* **2013,** *113* (10), 7930-51.
27. Wickramasinghe, L. A.; Sharp, P. R., Photoreduction of Pt(IV) halo-hydroxo complexes: possible hypohalous acid elimination. *Inorg Chem* **2014,** *53* (3), 1430-42.
28. Wick, D. D.; Goldberg, K. I., *J. Am. Chem. Soc* **1999,** *121*, 11900.
29. Rostovtsev, V. V. H., L. M.; Labinger, J. A.; Bercaw, J. E. Inorg. Chem. 2002, 41, 3608−3619. .
30. Allen, F. H., The Cambridge Structural Database: a quarter of a million crystal structures and rising. *Acta Cryst.* **2002,** *B58*, 380-388.
31. Smythe, N. A.; Grice, K. A.; Williams, B. S.; Goldberg, K. I., Reductive Elimination and Dissociative Œ≤-Hydride Abstraction from Pt(IV) Hydroxide and Methoxide Complexes. *Organometallics* **2008,** *28* (1), 277-288.
32. Poverenov, E.; Efremenko, I.; Frenkel, A. I.; Ben-David, Y.; Shimon, L. J. W.; Leitus, G.; Konstantinovski, L.; Martin, J. M. L.; Milstein, D., Evidence for a terminal Pt(iv)-oxo complex exhibiting diverse reactivity. *Nature* **2008,** *455* (7216), 1093-1096.
33. Martin, R. L., Natural transition orbitals. *J. Chem. Phys.* **2003,** *118* (11), 4775-4777.
34. Unangst, P. C., Hypochlorous Acid. In *e-EROS Encyclopedia of Reagents for Organic Synthesis*, John Wiley & Sons, Ltd: 2001.
35. Wojtowicz, J. A., Dichlorine Monoxide, Hypochlorous Acid, and Hypochlorites. In *Kirk-Othmer Encyclopedia of Chemical Technology*, John Wiley & Sons, Inc.: 2000.
36. Cady, G. H.; Naughton, J. M.; Dexter, T. H., Chlorine(I) Compounds. In *Inorg. Synth.*, John Wiley & Sons, Inc.: 2007; pp 156-165.
37. Vogt, R.; Schindler, R. N., Product channels in the photolysis of HOCl. *Journal of Photochemistry and Photobiology A: Chemistry* **1992,** *66* (2), 133-140.
38. Oxley, J. C.; Smith, J. L.; Chen, H., Decomposition of a Multi-Peroxidic Compound: Triacetone Triperoxide (TATP). *Propellants, Explosives, Pyrotechnics* **2002,** *27* (4), 209-216.
39. Foote, C. S.; Wexler, S.; Ando, W.; Higgins, R., Chemistry of singlet oxygen. IV. Oxygenations with hypochlorite-hydrogen peroxide. *J. Am. Chem. Soc.* **1968,** *90* (4), 975-981.
40. DeRosa, M. C.; Crutchley, R. J., Photosensitized singlet oxygen and its applications. *Coord. Chem. Rev.* **2002,** *233,Âì234* (0), 351-371.
41. Luo, Y.-R., *Comprehensive Handbook of Chemical Bond Energies*. CRC Press: Boca Raton, FL, USA, 2007.
42. (a) Ford, P. C., The ligand field photosubstitution reactions of d6 hexacoordinate metal complexes. *Coord. Chem. Rev.* **1982,** *44* (1), 61-82; (b) Ford, P. C.; Wink, D.; Dibenedetto, J., Mechanistic Aspects of the Photosubstitution and Photoisomerization Reactions of d6 Metal Complexes. In *Prog. Inorg. Chem.*, John Wiley & Sons, Inc.: 1983; pp 213-271; (c) Langford, C. H.; Malkhasian, A. Y. S., Wavelength dependence in the ligand field photochemistry of cobalt(III) amines. *J. Am. Chem. Soc.* **1987,** *109* (9), 2682-2685; (d) Goursot, A.; Kirk, A. D.; Waltz, W. L.; Porter, G. B.; Sharma, D. K., Experimental and theoretical study of the nascent photoredox behavior of the aqueous hexachloroplatinate(IV) ion. *Inorg. Chem.* **2002,** *26* (1), 14-18; (e) Salassa, L.; Garino, C.; Salassa, G.; Gobetto, R.; Nervi, C., Mechanism of Ligand Photodissociation in Photoactivable [Ru(bpy)2L2]2+ Complexes: A Density Functional Theory Study. *J. Am. Chem. Soc.* **2008,** *130* (29), 9590-9597; (f) Zheldakov, I. L.; N. Ryazantsev, M.; Tarnovsky, A. N., Wavepacket Motion via a Conical Intersection in the Photochemistry of Aqueous Transition-Metal Dianions. *J. Phys. Chem. Lett.* **2011,** *2* (13), 1540-1545; (g) Glebov, E. M.; Kolomeets, A. V.; Pozdnyakov, I. P.; Plyusnin, V. F.; Grivin, V. P.; Tkachenko, N. V.; Lemmetyinen, H., Redox processes in photochemistry of Pt(iv) hexahaloid complexes. *RSC Advances* **2012,** *2* (13), 5768-5778.
43. (a) Babaeva, A. V., *Dokl. Akad. Nauk SSSR* **1939,** *23*, 653; (b) Kuroda, R.; Neidle, S.; Ismail, I. M.; Sadler, P. J., Crystal and molecular structure of three isomers of

dichlorodiamminedihydroxoplatinum(IV): cis-trans isomerization on recrystallization from water. *Inorg. Chem.* **1983,** *22* (24), 3620-3624; (c) Brandon, R. J.; Dabrowiak, J. C., Synthesis, characterization, and properties, of a group of platinum(IV) complexes. *J. Med. Chem.* **1984,** *27* (7), 861-865; (d) Vollano, J. F.; Blatter, E. E.; Dabrowiak, J. C., DNA breakage by a perhydrate complex of cis-dichloro-cis-diammine-trans-dihydroxyplatinum(IV) (cis,cis,trans-Pt(IV)Cl2(NH3)2(OH)2). *J. Am. Chem. Soc.* **1984,** *106* (9), 2732-2733; (e) Al-Baker, S.; Dabrowiak, J. C., Oxidation of a dinuclear platinum(II) complex with hydrogen peroxide. *Inorg. Chem.* **1987,** *26* (4), 613-617; (f) Thorshaug, K.; Fjeldahl, I.; Romming, C.; Tilset, M., Synthesis, characterization, and acid-base properties of (N-N)PtIV(CH3)2(OH)2 - (OCH3) (x = 0, 1) complexes. *Dalton Trans.* **2003,** *0* (21), 4051-4056; (g) Murray, P.; Koch, K. R., A 195Pt NMR study of the oxidation of [PtCl4]2- with chlorate, bromate, and hydrogen peroxide in acidic aqueous solution. *J. Coord. Chem.* **2010,** *63* (14-16), 2561-2577.

44. Rashidi, M.; Nabavizadeh, M.; Hakimelahi, R.; Jamali, S., Kinetics and mechanism of cleavage of the oxygen-oxygen bond in hydrogen peroxide and dibenzoyl peroxide by arylplatinum(ii) complexes. *J. Chem. Soc., Dalton Trans.* **2001,** (23), 3430-3434.

45. Rostovtsev, V. V.; Henling, L. M.; Labinger, J. A.; Bercaw, J. E., Structural and Mechanistic Investigations of the Oxidation of Dimethylplatinum(II) Complexes by Dioxygen. *Inorg. Chem.* **2002,** *41* (14), 3608-3619.

46. Nakabayashi, Y.; Erxleben, A.; Létinois, U.; Pratviel, G.; Meunier, B.; Holland, L.; Lippert, B., Spontaneous Reduction of Mixed 2,2′-Bipyridine/Methylamine/Chloro Complexes of PtIV in Water in the Presence of Light Is Accompanied by Complex Isomerization, Loss of Methylamine, and Formation of a Strong Oxidant, Presumably HOCl. *Chem. Eur. J.* **2007,** *13* (14), 3980-3988.

47. (a) Glebov, E. M.; Plyusnin, V. F.; Grivin, V. P.; Venediktov, A. B.; Korenev, S. V., Photochemistry of PtBr62- in aqueous solution. *Russ. Chem. Bull.* **2007,** *56* (12), 2357-2363; (b) Balzani, V.; Manfrin, M. F.; Moggi, L., Photochemistry of coordination compounds. XVI. Hexabromoplatinate(IV) and hexaiodoplatinate(IV) ions. *Inorg. Chem.* **1967,** *6* (2), 354-358; (c) Penkett, S. A.; Adamson, A. W., Flash Photolysis of Cobalt(III) Acidopentaammine and of PtBr6-2 and PtI6-2 Complexes. *J. Am. Chem. Soc.* **1965,** *87* (11), 2514 - 2515.

48. Grice, K. A.; Scheuermann, M. L.; Goldberg, K. I., Five-Coordinate Platinum(IV) Complexes. *Top. Organomet. Chem.* **2011,** *35*, 1-27.

49. (a) Labinger, J. A.; Herring, A. M.; Lyon, D. K.; Luinstra, G. A.; Bercaw, J. E.; Horvath, I. T.; Eller, K., Oxidation of hydrocarbons by aqueous platinum salts: mechanism and selectivity. *Organometallics* **1993,** *12* (3), 895-905; (b) Labinger, J. A.; Herring, A. M.; Bercaw, J. E., Selective hydroxylation of methyl groups by platinum salts in aqueous medium. Direct conversion of ethanol to ethylene glycol. *J. Am. Chem. Soc.* **1990,** *112* (14), 5628-5629; (c) DeVries, N.; Roe, D. C.; Thorn, D. L., Catalytic hydroxylation using chloroplatinum compounds. *J. Mol. Catal. A: Chem.* **2002,** *189* (1), 17-22; (d) Oblad, P. F.; Bercaw, J. E.; Hazari, N.; Labinger, J. A., Oxidation of Organometallic Platinum and Palladium Complexes Obtained from C,àíH Activation. *Organometallics* **2010,** *29* (4), 789-794.

50. Shibaeva, R. P.; Rozenberg, L. P.; Lobkovskaya, R. M.; Shilov, A. E.; Shul'pin, G. B., Formation of anionic [sigma]-aryl complexes of platinum (IV) in the reaction of H2PtCl6 with aromatic compounds. The crystal and molecular structures of platinum (IV) complexes of naphthalene and ortho-nitrotoluene. *J. Organomet. Chem.* **1981,** *220* (2), 271-276.

51. Glebov, E. M.; Grivin, V. P.; Plyusnin, V. F.; Venediktov, A. B.; Korenev, S. V., Photochemistry of [PtBr6]2- complex in aqueous solutions. Formation and decay of [Br2]- radical anions. *J. Photochem. Photobiol., A* **2010,** *214* (2-3), 181-187.

52. Glebov, E. M.; Plyusnin, V. F.; Venediktov, A. B.; Korenev, S. V., Photolysis of [PtBr6]2- complex in frozen methanol matrix. *Russ. Chem. Bull.* **2003,** *52* (6), 1305-1311.

53. (a) Fadnis, A. G.; Kemp, T. J., Photo-oxidation of alcohols by hexachlorometalate(IV) ions (M = Pt, Pd, or Ir): spin trapping and matrix isolation electron spin resonance studies. *J. Chem. Soc., Dalton Trans.* **1989**, 1237 - 1240; (b) Waltz, W. L.; Lilie, J.; Goursot, A.; Chermette, H., Photolytic and radiolytic study of platinum(III) complex ions containing aquo and chloro ligands. *Inorg. Chem.* **1989,** *28* (12), 2247-2256; (c) Rehorek, D.; Dubose, C. M.; Janzen, E. G., Spin trapping of chlorine atoms produced by photolysis of hexachloroplatinate(IV) in solution. *Inorg. Chim. Acta* **1984,** *83* (1), L7-L8; (d) Wright, R. C.; Laurence, G. S., Production of platinum(III) by flash photolysis of PtCl62–. *J. Chem. Soc., Chem. Commun.* **1972**, 132 - 133.

54. van Slageren, J.; Klein, A.; Z√°li≈°, S., Ligand-to-ligand charge transfer states and photochemical bond homolysis in metalÓó∏carbon bonded platinum complexes. *Coord. Chem. Rev.* **2002,** *230* (1,Äì2), 193-211.
55. Yoshida, T.; Matsuda, T.; Otsuka, S., Three-coordinate phosphine complexes of platinum(0). *Inorg. Synth.* **1990,** *28* (Reagents Transition Met. Complex Organomet. Synth.), 119-21.
56. Saito, I.; Nagata, R.; Yuba, K.; Matsuura, T., Synthesis of Œ±-silyloxyhydroperoxides from the reaction of silyl enol ethers and hydrogen peroxide. *Tetrahedron Lett.* **1983,** *24* (16), 1737-1740.
57. Murray, R. W.; Kong, W.; Rajadhyaksha, S. N., The ozonolysis of tetramethylethylene. Concentration and temperature effects. *The Journal of Organic Chemistry* **1993,** *58* (2), 315-321.
58. Feng, Y.; Smith, D. W.; Bolton, J. R., Photolysis of aqueous free chlorine species (HOCl and OCl¬ñ) with 254 nm ultraviolet light. *Journal of Environmental Engineering and Science* **2007,** *6* (3), 277-284.
59. Clennan, E. L.; Chen, X., Reactions of an allylic sulfide, sulfoxide, and sulfone with singlet oxygen. The observation of a remarkable diastereoselective oxidation. *J. Am. Chem. Soc.* **1989,** *111* (15), 5787-5792.
60. Comerford, J. J., The investigation of the photo-kinetics of a platinum organoamine complex using the Cary 50. *Varian Instruments At Work* **2003,** *87*, 1-8.
61. (a) Hatchard, C. G.; Parker, C. A., A New Sensitive Chemical Actinometer. II. Potassium Ferrioxalate as a Standard Chemical Actinometer. *Proc. R. Soc. London, Ser. A* **1956,** *235* (1203), 518-536; (b) Kurien, K. C., A modification to the ferrioxalate actinometer. *J. Chem. Soc. B* **1971**, 2081 - 2082.
62. Frisch, M. J. T., G. W.; Schlegel, H. B.; Scuseria, G. E.;; Robb, M. A. C., J. R.; Scalmani, G.; Barone, V.; Mennucci,; B.; Petersson, G. A. N., H.; Caricato, M.; Li, X.; Hratchian, H.; P.; Izmaylov, A. F. B., J.; Zheng, G.; Sonnenberg, J. L.; Hada, M.;; Ehara, M. T., K.; Fukuda, R.; Hasegawa, J.; Ishida, M.; Nakajima,; T.; Honda, Y. K., O.; Nakai, H.; Vreven, T.; Montgomery, J. A., Jr.;; Peralta, J. E. O., F.; Bearpark, M.; Heyd, J. J.; Brothers, E.; Kudin,; K. N.; Staroverov, V. N. K., R.; Normand, J.; Raghavachari, K.;; Rendell, A. B., J. C.; Iyengar, S. S.; Tomasi, J.; Cossi, M.; Rega,; N.; Millam, J. M. K., M.; Knox, J. E.; Cross, J. B.; Bakken, V.;; Adamo, C. J., J.; Gomperts, R.; Stratmann, R. E.; Yazyev, O.;; Austin, A. J. C., R.; Pomelli, C.; Ochterski, J. W.; Martin, R. L.;; Morokuma, K. Z., V. G.; Voth, G. A.; Salvador, P.;; Dannenberg, J. J. D., S.;Daniels,A.D.; Farkas,O.;; Foresman, J. B. O., J. V.; Cioslowski, J.; Fox, D. J. Gaussian 09,; revision B.01 or C.01; Gaussian, I. W., CT, 2009.
63. Zhao, Y. T., D. G. Acc. Chem. Res. 2008, 41, 157−167.
64. Yanai, T. T., D.; Handy, N. Chem. Phys. Lett. 2004, 393, 51− 57.
65. Dunning, T. H. H., P. J. Modern Theoretical Chemistry; Plenum: New York, 1976; Vol. 3. .
66. Hay, P. J.; Wadt, W. R., *J. Chem. Phys* **1985,** *82*, 299.
67. Wadt, W. R.; Hay, P. J., *J. Chem. Phys* **1985,** *82*, 284.
68. Hay, P. J. W., W. R. J. Chem. Phys. 1985, 82, 270.
69. Check, C. E. F., T. O.; Bailey, J. M.; Wright, B. J.; Gilbert, T. M.; Sunderlin, L. S. J. Phys. Chem. A 2001, 105, 8111. .
70. Dennington, R. K., T.; Millam, J. GaussView, version 5.0.8; Semichem Inc.: Shawnee Mission, KS, 2009. .
71. O'Boyle, N. M. T., A. L.; Langner, K. M. J. Comput. Chem. 2008, 29, 839−845. .
72. Tomasi, J. M., B.; Cammi, R. Chem. Rev. 2005, 105, 2999−3094.
73. (a) Becht, A.; Vogler, A., Photoredox reactions of lead(IV) and -(II) hydroxo complexes. *Inorg. Chem.* **1993,** *32* (13), 2835-2837; (b) Knor, G.; Vogler, A.; Roffia, S.; Paolucci, F.; Balzani, V., Switchable photoreduction pathways of antimony(V) tetraphenylporphyrin. A potential multielectron transfer photosensitizer. *Chem. Commun.* **1996,** *0* (14), 1643-1644; (c) Kohl, S. W.; Weiner, L.; Schwartsburd, L.; Konstantinovski, L.; Shimon, L. J. W.; Ben-David, Y.; Iron, M. A.; Milstein, D., Consecutive Thermal H2 and Light-Induced O2 Evolution from Water Promoted by a Metal Complex. *Science* **2009,** *324* (5923), 74-77; (d) Vogler, A.; Kunkely, H., Splitting of alkyl carbonates photocatalyzed by copper complexes as a model for an artificial photosynthesis. *Inorg. Chem. Commun.* **2011,** *14* (1), 96-98; (e) Petruzzella, E.; Margiotta, N.; Ravera, M.; Natile, G., NMR Investigation of the Spontaneous Thermal- and/or Photoinduced Reduction of trans Dihydroxido Pt(IV) Derivatives. *Inorg. Chem.* **2013,** *52* (5), 2393-2403.
74. *Yield (%) = 100*(moles of product/moles of **1**).*
75. Paulsen, P. J. C., W. D. Anal. Chem. 1963, 35, 1560. .
76. Cambridge Isotope Laboratories, I. C. I. L. T., MA, 2014; Vol. 2014, https://www.isotope.com/userfiles/files/assetLibrary/NMR_solvents_data_chart_ &_storage.pdf

77. Rieche, A., *Angew. Chem.* **1958,** *70*, 251.
78. Milas, N. A.; Golubovic, A., *J. Am. Chem. Soc.* **1959,** *81*, 6461.
79. Sashidhara, K. V.; Avula, S. R.; Ravithej Singh, L.; Palnati, G. R., *Tetrahedron Lett* **2012,** *53*, 4880.
80. (a) Gollnick, K.; Griesbeck, A., [4+2]-Cycloaddition von Singulett-Sauerstoff an 2,5-Dimethylfuran: Isolierung und Reaktionen des monomeren und dimeren Endoperoxids. *Angew. Chem.* **1983,** *95* (9), 751-751; (b) Kuo, Y.-H.; Shih, K.-S.; Lee, G.-H.; Wang, Y., Two Crystalline Dimeric Peroxides from Sensitized Photooxidation of 2,5-Dimethylfuran. *Heterocycles* **1988,** *27* (3), 599-603.
81. (a) Foote, C. S., Photosensitized oxygenations and the role of singlet oxygen. *Acc. Chem. Res.* **1968,** *1* (4), 104-110; (b) Clennan, E. L., New Mechanistic and Synthetic Aspects of Singlet Oxygen Chemistry. *Tetrahedron* **2000,** *56* (47), 9151-9179.
82. Kotani, H.; Ohkubo, K.; Fukuzumi, S., Photocatalytic Oxygenation of Anthracenes and Olefins with Dioxygen via Selective Radical Coupling Using 9-Mesityl-10-methylacridinium Ion as an Effective Electron-Transfer Photocatalyst. *J. Am. Chem. Soc.* **2004,** *126* (49), 15999-16006.
83. (a) Herzberg, G., *Spectra of Diatomic Molecules*. Van Nostrand Reinhold: New York, 1950; (b) Schweitzer, C.; Schmidt, R., Physical Mechanisms of Generation and Deactivation of Singlet Oxygen. *Chem. Rev.* **2003,** *103* (5), 1685-1758.
84. (a) Xu, X.; Muller, R. P.; Goddard, W. A., The gas phase reaction of singlet dioxygen with water: A water-catalyzed mechanism. *Proc. Natl. Acad. Sci.* **2002,** *99* (6), 3376-3381; (b) Cramer, C. J., *Essentials of Computational Chemistry: Theories and Models*. 2nd ed.; John Wiley & Sons: Chichester, 2004.
85. Martin, R. L.; Hay, P. J.; Pratt, L. R., Hydrolysis of Ferric Ion in Water and Conformational Equilibrium. *J. Phys. Chem. A* **1998,** *102* (20), 3565-3573.
86. Parreira, R. L. T.; Galembeck, S. r. E., Characterization of Hydrogen Bonds in the Interactions between the Hydroperoxyl Radical and Organic Acids. *J. Am. Chem. Soc.* **2003,** *125* (50), 15614-15622.
87. Xu, X.; Goddard, W. A., Peroxone chemistry: Formation of H2O3 and ring-(HO2)(HO3) from O3/H2O2. *Proc. Natl. Acad. Sci.* **2002,** *99* (24), 15308-15312.
88. Lawson, H. J.; Atwood, J. D., Iridium dioxygen complexes in the oxidation of substrates: kinetics, mechanism, and steric and electronic effects in the oxidation of carbon monoxide, carbon dioxide, triphenylphosphine, and sulfur dioxide by RIr(O2)(CO)L2 (R = methyl, phenyl, neopentyl; L = tri-p-tolylphosphine, triphenylphosphine, methyldiphenylphosphine, tri-p-anisylphosphine). *J. Am. Chem. Soc.* **1989,** *111* (16), 6223-6227.
89. Edwards, J. O.; Sauer, M. C. V., Reactions of acetone and hydrogen peroxide. I. Primary adduct. *J. Phys. Chem.* **1971,** *75* (19), 3004-3011.
90. Gollnick, K.; Griesbeck, A., [4+2]-Cycloaddition of Singlet Oxygen to 2,5-Dimethylfuran: Isolation and Reactions of the Monomeric and Dimeric Endoperoxides. *Angew. Chem., Int. Ed. Engl.* **1983,** *22* (9), 726-727.
91. Gollnick, K.; Griesbeck, A., *Angew. Chem. Int. Ed. Engl.* **1983,** *22*, 726.
92. (a) Weliange, N. M.; Sharp, P. R., Ethylene Oxidation by a Platinum(II) Hydroxo Complex. Insights into the Wacker Process. *Organometallics* **2012,** *31* (19), 6823-6833; (b) Weliange, N. M.; Szuromi, E.; Sharp, P. R., Proton-Catalyzed Oxo-Alkene Coupling: 2-Platinaoxetane Formation. *J. Am. Chem. Soc.* **2009,** *131* (25), 8736-8737; (c) Khusnutdinova, J. R.; Newman, L. L.; Zavalij, P. Y.; Lam, Y. F.; Vedernikov, A. N., Direct C(sp3)-O Reductive Elimination of Olefin Oxides from PtIV-Oxetanes Prepared by Aerobic Oxidation of PtII Olefin Derivatives (Olefin = cis-Cyclooctene, Norbornene). *J. Am. Chem. Soc.* **2008,** *130* (7), 2174 -2175; (d) Khusnutdinova, J. R.; Zavalij, P. Y.; Vedernikov, A. N., Facile Aerobic Oxidation of dpms-Platinum(II) Ethylene Complexes (dpms = di(2-pyridyl)methanesulfonate). *Organometallics* **2007,** *26* (9), 2402-2413.
93. (a) Ess, D. H.; Gunnoe, T. B.; Cundari, T. R.; Goddard, W. A.; Periana, R. A., Ligand Lone-Pair Influence on Hydrocarbon C,àíH Activation: A Computational Perspective,ñ≥. *Organometallics* **2010,** *29* (24), 6801-6815; (b) Bercaw, J. E.; Hazari, N.; Labinger, J. A., Activation of a C-H Bond in Indene by [(COD)Rh(Œº2-OH)]2,Ä†. *Organometallics* **2009,** *28* (18), 5489-5492; (c) Williams, T. J.; Caffyn, A. J. M.; Hazari, N.; Oblad, P. F.; Labinger, J. A.; Bercaw, J. E., C-H Bond Activation by Air-Stable [(Diimine)MII(m2-OH)]22+ Dimers (M = Pd, Pt). *J. Am. Chem. Soc.* **2008,** *130* (8), 2418-2419; (d) Bercaw, J. E.; Hazari, N.; Labinger, J. A.; Oblad, P. F., C-H Bond Activation by [{(Diimine)Pd(mu-OH)}2]2+ Dimers: Mechanism-Guided Catalytic Improvement. *Angew. Chem. Int. Ed.* **2008,** *47* (51), 9941-9943; (e) Hanson, S. K.; Heinekey, D. M.; Goldberg, K. I., C,àíH Bond Activation by Rhodium(I) Phenoxide and Acetate Complexes: Mechanism of H,àíD Exchange between Arenes and Water.

Organometallics **2008,** *27* (7), 1454-1463; (f) Kloek, S. M.; Heinekey, D. M.; Goldberg, K. I., C-H Bond Activation by Rhodium(I) Hydroxide and Phenoxide Complexes. *Angew. Chem. Int. Ed.* **2007,** *46* (25), 4736-4738; (g) Cundari, T. R.; Grimes, T. V.; Gunnoe, T. B., Activation of Carbon-Hydrogen Bonds via 1,2-Addition across M-X (X = OH or NH2) Bonds of d6 Transition Metals as a Potential Key Step in Hydrocarbon Functionalization: A Computational Study. *J. Am. Chem. Soc.* **2007,** *129* (43), 13172-13182.

94. (a) Barnett, S. M.; Goldberg, K. I.; Mayer, J. M., A soluble copper,Äibipyridine water-oxidation electrocatalyst. *Nat Chem* **2012,** *4* (6), 498-502; (b) Blakemore, J. D.; Schley, N. D.; Balcells, D.; Hull, J. F.; Olack, G. W.; Incarvito, C. D.; Eisenstein, O.; Brudvig, G. W.; Crabtree, R. H., Half-Sandwich Iridium Complexes for Homogeneous Water-Oxidation Catalysis. *J. Am. Chem. Soc.* **2010,** *132* (45), 16017-16029.

95. (a) Kessler, M.; Schüler, S.; Hollmann, D.; Klahn, M.; Beweries, T.; Spannenberg, A.; Brückner, A.; Rosenthal, U., Photoassisted Ti-O Activation in a Decamethyltitanocene Dihydroxido Complex: Insights into the Elemental Steps of Water Splitting. *Angew. Chem. Int. Ed.* **2012,** *51* (25), 6272-6275; (b) Kunkely, H.; Vogler, A., Water Splitting by Light with Osmocene as Photocatalyst. *Angew. Chem. Int. Ed.* **2009,** *48* (9), 1685-1687.

96. (a) Ramón, R. S.; Gaillard, S.; Poater, A.; Cavallo, L.; Slawin, A. M. Z.; Nolan, S. P., [{Au(IPr)}2(μ-OH)]X Complexes: Synthetic, Structural and Catalytic Studies. *Chem. Eur. J.* **2011,** *17* (4), 1238-1246; (b) Fulmer, G. R.; Muller, R. P.; Kemp, R. A.; Goldberg, K. I., Hydrogenolysis of Palladium(II) Hydroxide and Methoxide Pincer Complexes. *J. Am. Chem. Soc.* **2009,** *131* (4), 1346-1347; (c) Smythe, N. A.; Grice, K. A.; Williams, B. S.; Goldberg, K. I., Reductive Elimination and Dissociative beta-Hydride Abstraction from Pt(IV) Hydroxide and Methoxide Complexes. *Organometallics* **2009,** *28* (1), 277-288; (d) Khusnutdinova, J. R.; Zavalij, P. Y.; Vedernikov, A. N., C-O Coupling of LPtIVMe(OH)X Complexes in Water (X = 18OH, OH, OMe; L = di(2-pyridyl)methane sulfonate). *Organometallics* **2007,** *26* (14), 3466-3483; (e) Vedernikov, A. N.; Binfield, S. A.; Zavalij, P. Y.; Khusnutdinova, J. R., Stoichiometric Aerobic Pt(II)--Me Bond Cleavage in Aqueous Solutions to Produce Methanol and a Pt(II)-(OH) Complex. *J. Am. Chem. Soc.* **2006,** *128* (1), 82-83.

97. Garrou, P. E., ΔR Ring Contributions to 31P NMR Parameters of Transition-Metal-Phosphorus Chelate Complexes. *Chem. Rev.* **1981,** *81*, 229-266.

98. (a) Clark, H. C.; Goel, A. B.; Goel, R. G.; Goel, S., Preparation and characterization of platinum(II) complexes Pt(P-C)LX, where (P-C) is metalated tri-tert-butylphosphine. *Inorg. Chem.* **1980,** *19* (11), 3220-3225; (b) Thorn, D. L., Ligand Metalation in Triisopropylphosphine,àíPlatinum(II) Compounds,Ä†. *Organometallics* **1998,** *17* (3), 348-352; (c) Ingleson, M. J.; Mahon, M. F.; Weller, A. S., [PtMe(iPr3P)2]+: a Pt(II) complex with an agostic interaction that undergoes C-H activation. *Chemical Communications (Cambridge, United Kingdom)* **2004,** (21), 2398-2399; (d) Ghavale, N.; Wadawale, A.; Dey, S.; Jain, V. K., Synthesis, structures and spectroscopic properties of cyclometalated tri-tert-butylphosphine complexes of platinum(II). *J. Organomet. Chem.* **2010,** *695* (21), 2296-2304.

99. Wickramasinghe, L. A.; Sharp, P. R., Photoreduction of Pt(IV) Halo-Hydroxo Complexes: Possible Hypohalous Acid Elimination. *Inorg. Chem.* **2014,** *53* (3), 1430–1442.

100. Ghidiu, M. J.; Pistner, A. J.; Yap, G. P. A.; Lutterman, D. A.; Rosenthal, J., Thermal versus Photochemical Reductive Elimination of Aryl Chlorides from NHC,ÄìGold Complexes. *Organometallics* **2013,** *32* (18), 5026-5029.

101. (a) Johnson, P. M.; Albrecht, A. C., Assignment of Excited Electronic States of the Benzyl Radical by the Method of Three,ÄêStep Photoselection. *The Journal of Chemical Physics* **1968,** *48* (2), 851-865; (b) Devolder, P.; Dessaux, O.; Goudmand, P., Identification of chemiluminescent emitters observed during the reaction of active nitrogen with toluene at 77 K

Comptes Rendus des Seances de l'Academie des Sciences, Serie 2 **1981,** *292*, 717-720; (c) Uejoh, K., Fluorescence spectrum of the benzyl radical in methylcyclohexane at 4.2 K. *Spectrochimica Acta Part A: Molecular and Biomolecular Spectroscopy* **2004,** *60* (3), 595-602.

102. Crosby, S. H.; Thomas, H. R.; Clarkson, G. J.; Rourke, J. P., Concerted reductive coupling of an alkyl chloride at Pt(IV). *Chem Commun (Camb)* **2012,** *48* (46), 5775-7.

103. Feller, M.; Diskin-Posner, Y.; Leitus, G.; Shimon, L. J.; Milstein, D., Direct observation of reductive elimination of MeX (X = Cl, Br, I) from Rh(III) complexes: mechanistic insight and the importance of sterics. *J Am Chem Soc* **2013,** *135* (30), 11040-7.

VITA

Lasantha A Wickramasinghe is from Sri Lanka which is known as the pearl of Indian ocean. He grew up in Colombo, capitol of Sri Lanka. After finishing his high school in Mahanama College he enrolled in chemistry program in Institute of Chemistry Ceylon, where he obtained his BSc degree in chemistry. He later joined the doctoral program in the department of chemistry at the University of Missouri-Columbia. He worked under the guidance of Prof. Paul R Sharp. His graduate research has consisted of synthesis and photochemistry of platinum(IV) hydroxo complexes.